Diss. ETH NO. 23092

ON THE PREDICTION OF CONCRETE SPALLING UNDER FIRE

A thesis submitted to attain the degree of

DOCTOR OF SCIENCES of ETH ZURICH

(Dr. sc. ETH Zurich)

presented by

FANGXIA LU

MEng Bridge and Tunnel Eng, Tongji University

born on 22.06.1984

citizen of P.R. China

accepted on the recommendation of

Prof. Dr. M. Fontana, examiner

Prof. Dr. V. Kodur, co-examiner

Dr. D. Fernando, co-examiner

Prof. Dr. M. Knobloch, co-examiner

2015

Acknowledgements

I would like to thank all the people who have in some way contributed to the production of this thesis. Without the help and support of countless people in the last four years, I wouldn't finish my PhD.

My deepest gratitude is to my supervisor, Prof. Mario Fontana for giving me the opportunity to write this thesis in his group. I am so fortunate to have a supervisor who gave me the freedom to explore while provided the expert guidance and advice. His insightful comments kept me on the track. I appreciated his trust and patience throughout the project.

I would also like to thank my co-examiners, Prof. Venkatesh Kodur, Dr. Dilum Fernando and Prof. Markus Knobloch. Many comments and constructive criticisms from you are really helpful at different stages. Thanks to your knowledge and assistance I have finished the thesis successfully.

I am grateful to Prof. Andrea Frangi, Dr. Eike Klingsch and Heidi Honegger for the practical help and support. My acknowledgements also go to all the people who spent time in the lab with me, all the robust and friendly technicians in the structures laboratory at ETH: Patrick Morf, Dominik Werne, Thomas Jaggi, Christoph Gisler and Pius Herzog. Also to the graduate students contributed to the tests: Andreas Thürig and René Käßmann.

I also want to acknowledge my colleagues at IBK ETH and friends. Apart from concrete gray, you fill my study here with colors. Some special thanks to Andrew for proof-reading my thesis; Matthias for teaching me snowboard; Li (D-ARCH) for giving me a shelter when I was new here.

Finally, I want to thank my parents, I don't think you care about spalling of concrete, but you give me the everlasting support and love, your patience pays off. My daughter Litong, my wife Xi, it feels good to mention you in a dissertation, thank you for being there.

China Scholarship Council (CSC) is kindly acknowledged for the support of my PhD study at ETH Zurich.

Abstract

Concrete spalling induced by fire exposure is a major concern in the engineering community, especially explosive spalling, which may result in a reduction of cross section area and loading capacity. Therefore, as an important factor for fire resistance in concrete construction, concrete spalling must be evaluated. In this thesis, a spalling criterion has been proposed to predict explosive spalling of concrete and to evaluate protective methods. The proposed criterion is based on a combined stress mechanism, which includes both pore pressure and thermal stress.

To predict the pore pressure, the hot and residual permeability of concrete has been tested. The effects from temperature and moisture content on the permeability have been investigated. A permeability model has been developed and validated based on test results. Applying the permeability model in a thermo-hydro model, the pore pressure has been simulated. The model has been validated against the measured pore pressure reported in the literature and a good agreement has been achieved.

The combined effects from pore pressure and thermal stress have been considered in the spalling criterion. Fire tests on high performance concrete slabs have been simulated and the predicted spalling time and depth were close to the test results. The validated criterion has been applied to carry out parametric studies to quantify the effect of various factors on explosive spalling. The permeability limit for explosive spalling has been proposed to be 2×10^{-17} m^2 for exposure to the ISO standard fire. The influences from moisture content and heating rate have also been taken into account, the permeability limit changes with these factors.

To prevent explosive spalling, many protective methods have been tested. It has been shown that both insulating mortar and plates are feasible options. However, the thickness of insulating material must be determined according to the protection level, because fire tests have shown that insufficient thickness may induce deeper and more violent spalling. The proposed criterion can provide a guideline for the use of the insulating materials.

The use of polypropylene fibers (PP-fibers) has been studied by fire tests as well. The amount of 2 kg/m^3, which is recommended by Eurocode 2, has been proved effective in preventing explosive spalling, if a satisfactory geometry of the fibers is provided. With the help of the proposed permeability model, the effect from PP-fibers has been included in the spalling model and a reduced risk of spalling has been predicted. With respect to the type and amount of PP-fibers, an increasing factor has been used in the model to evaluate the added PP-fibers.

For the practical assessment of spalling, an evaluation strategy using the spalling criterion has been proposed. Tests are suggested to determine the input for evaluating the spalling risk and for protective methods. For external loads, some pilot investigations have been done and even contradictive results from various tests and literature could be explained by the spalling model. The spalling risk of loaded concrete elements can already be considered by the spalling model, however further validation tests are recommended.

Zusammenfassung

Abplatzen von Beton infolge Brandeinwirkung ist ein wesentliches Problem im Brandschutzingenieurwesen und kann zu einer bedeutenden Reduktion des Querschnitts und der Tragfähigkeit führen, vor allem wenn es explosionsartig eintritt. Das Abplatzen ist ein wesentlicher Bestandteil bei der Beurteilung des Brandwiderstandes von Stahlbetonbauteilen. In dieser Dissertation wird ein Kriterium eingeführt, das die Gefahr von explosivem Abplatzen abschätzt und auch Schutzmassnahmen berücksichtigt. Das Abplatzkriterium basiert auf einem überlagernden Spannungszustand, der sowohl den Porendruck als auch die temperaturinduzierten Spannungen berücksichtig.

Um den Porendruck zu bestimmen, wurde die Heiss- und Residualpermeabilität von Beton gemessen. Die Permeabilität von Beton wurde experimentell untersucht, insbesondere der Einfluss der Temperatur und des Feuchtegehaltes auf die Permeabilität. Ein Permeabilitätsmodell wurde entwickelt und mit den Versuchsergebnissen validiert. Das Permeabilitätsmodell wurde in das thermo-hydro Model integriert, um den Porendruck zu simulieren. Versuchsdaten und Daten aus der Literatur wurden verwendet, um das Modell zu validieren. Es wurde eine gute Übereinstimmung erreicht.

Die gemeinsamen Einflüsse des Porendrucks und der Temperaturspannung werden im Abplatzkriterium berücksichtigt. Das Modell kann den Abplatzzeitpunkt und die Abplatztiefe von durchgeführten Brandversuchen an hochfesten Betonplatten gut voraussagen. Anhand einer Parameterstudie wurde das validierte Kriterium angewandt, um den Effekt verschiedener Faktoren auf das explosive Abplatzen zu bestimmen. Als Grenzwert für die Gefahr von explosivem Abplatzen unter der ISO Normbrandkurve wird eine Permeabilität von $2x10^{-17}$ m^2 vorgeschlagen. Der Feuchtegehalt und die Aufheizgeschwindigkeit beeinflussen diesen Grenzwert.

Um explosives Abplatzen zu verhindern, wurden zahlreiche Schutzmassnahmen getestet. Isolierender Mörtel und Dämmschichtplatten sind beide machbaren Lösungen. Die Dicke der isolierenden Schicht muss anhand des Sicherheitsniveaus festgelegt werden, da ungenügende Dicken zu tieferem und aggressiverem Abplatzen führen. Das eingeführte Kriterium eignet sich grundsätzlich auch zur Beurteilung der Anwendung von isolierendem Material.

Die Verwendung von Polypropylenfasern (PP-Fasern) wurde ebenfalls anhand von Brandversuchen untersucht. Die gemäss Eurocode 2 vorgeschlagene Massendichte von 2 kg/m^3 PP-Fasern eignet sich, um explosives Abplatzen unter Versuchsbedingungen zu verhindern, sofern eine geeignete Faserform gewählt wird. Das Permeabilitätsmodell kann den Einfluss der PP-Fasern berücksichtigen und das Kriterium prognostiziert ein reduziertes Abplatzrisiko.

Eine Auswertungsmethode basierend auf dem Abplatzkriterium wird eingeführt, um das Abplatzverhalten anwendungsorientiert zu bestimmen. Versuche werden empfohlen um die notwendigen Eingangsparameter genauer zu bestimmen und die Abplatzgefahr sowie Schutzmassnahmen zuverlässiger zu evaluieren. Anhand des Abplatzkriteriums konnten Vorversuche mit belasteten Proben und sogar widersprüchliche Ergebnisse aus der Literatur erklärt werden Somit kann das Abplatzrisiko von belasteten Betonelementen mit dem Abplatzmodell bereits beurteilt werden. Weitere Validierungsversuche werden aber empfohlen.

Content

1. Introduction 1

1.1 General 1

1.2 Need for current work 2

1.3 Research objectives 2

1.4 Scope 3

2. State of the art review 5

2.1 General 5

2.1.1 Spalling of concrete at high temperatures 5

2.1.2 Fire spalling of concrete 5

2.1.3 Study on fire spalling of concrete 9

2.1.4 Types of concrete spalling 10

2.2 Concrete properties at elevated temperatures and their influence on spalling 11

2.2.1 Thermal properties of concrete at elevated temperatures 13

2.2.2 Physical properties of concrete at elevated temperatures 14

2.2.3 Mechanical properties of concrete at elevated temperatures 15

2.3 Mechanism of explosive spalling 19

2.3.1 Thermal stress spalling 20

2.3.2 Pore pressure spalling 22

2.3.3 Combined pore pressure and thermal stress spalling 23

2.3.4 Conclusions on mechanism of explosive spalling 25

2.4 Codes of Practice 26

2.5 Protective methods 27

2.6 Knowledge gaps 28

3. Thermo-hygro model 31

3.1 Introduction 31

3.2 Calculation model and governing equations 31

3.2.1 Heat transfer 32

3.2.2 Pore pressure calculation 34

3.3 Permeability test 40

3.3.1 Test methods 41

3.3.2 Comparison of the test methods 43

3.3.3 Permeability of concrete with different moisture content 44
3.3.4 Effects of fibers on the permeability of concrete 46
3.4 Permeability model 49
3.4.1 The effect of moisture content 50
3.4.2 The effect of PP-fibers 54
3.4.3 Discussion of the permeability model 57
3.5 Validation and parameter study 57
3.5.1 Predicted temperature development in concrete 58
3.5.2 Predicted pore pressure in concrete 58
3.5.3 Influence from moisture content on pore pressure 61
3.5.4 The effects of PP-fibers on pore pressure 62
3.6 Conclusions 65

4. Criterion for explosive spalling 67
4.1 Introduction 67
4.2 Governing equations 67
4.2.1 Biot's coefficient 68
4.2.2 Superposition of stresses 69
4.3 Validation 71
4.3.1 Explosive spalling of HPC 72
4.3.2 The role of external loads 74
4.4 The effects from permeability and moisture content on explosive spalling 76
4.5 The role of heating rate 77
4.5.1 The effects of heating rate on thermal stress 78
4.5.2 The effects of heating rate on pore pressure 79
4.5.3 The effects of heating rate on explosive spalling 80
4.6 The role of external loads 82
4.6.1 Permeability under external loads 83
4.6.2 Effects from external loads on explosive spalling 83
4.7 Conclusions 85

5. Protective methods and spalling risk evaluation 87
5.1 Introduction 87
5.2 Polypropylene fibers 87

5.2.1 Experimental investigation 88
5.2.2 Simulation by spalling criterion 89
5.2.3 Practical considerations 91
5.3 Protective mortar 93
5.3.1 Experimental investigation 93
5.3.2 Simulation by spalling criterion 95
5.3.3 Considerations on practical use 99
5.4 Protective plate 103
5.4.1 Prediction from spalling criterion 103
5.4.2 Experimental investigation 107
5.4.3 Consideration on practical use 110
5.5 Evaluation strategy 111
5.5.1 Only test at ambient temperature is possible 111
5.5.2 Test at high temperature is possible 112
5.5.3 Fire test is possible 112
5.6 Conclusions 112

6. Conclusions and prospects 115
6.1 General 115
6.2 Conclusions 115
6.3 Prospects 117

Appendix
A. Effects of moisture content on the permeability of concrete 119
B. Effects of fibers on the permeability of concrete 125
C. Effects of external loads on the permeability of concrete 130

Literature 133

1. Introduction

1.1 General

Spalling of concrete is not a new phenomenon, the first recorded observation can be traced back to middle 19th century (Barret 1854). When a concrete element is exposed to a fast heating regime, its surface often disintegrates due to the generated forces in concrete. This is referred as concrete spalling. In experiment and practice, concrete exhibits a range of different spalling forms. Based on the nature of occurrence and influence on structure, spalling of concrete is grouped into several categories (Khoury 2005). Among them, explosive spalling may induce the most serious influence on the structure. As the name suggests, this form of spalling is violent and mostly involves explosive failure of the concrete (Connolly 1995). Explosive spalling is characteristic with a large release of energy and an explosive noise. All forms of spalling may reduce the period of fire resistance. Explosive spalling induces a sudden decrease of cross section, which reduces the bearing capacity of the structural element. In addition, the protective concrete cover to the steel reinforcements is removed, as shown in Fig. 1.1. Since the yield strength of steel decreases heavily at high temperatures, the removal of a concrete layer may accelerate yielding of steel, therefore, explosive spalling may result in premature flexural failure of the concrete member. The consequences are related to the fire scenarios and external loads. The occurrence of concrete spalling, according to Ingberg et al. (1925), is also effected by the types of concrete.

Fig. 1.1 Explosive spalling of a concrete slab (Lu & Fontana 2015).

A review of investigations on concrete spalling (Chapter 2) has shown that modern concrete with higher density is more prone to explosive spalling, especially the high performance concrete (HPC). Despite the advantages such as high strength and good durability, the application of HPC has some disadvantages like explosive spalling in fire. Explosive spalling has become a major concern. Since most of the concrete structures have been constructed with ordinary Portland concrete (OPC) the risk of spalling is modest. The issues related to explosive spalling have not been fully investigated and no valid practical methods are available for fire safety design of concrete with a tendency to explosive spalling. With the increasing use of HPC in tunnels, offshore structures and high-rise buildings, it has become necessary to study the concrete spalling in fire to address these concerns in practice.

To improve the fire resistance of HPC, some investigations have been carried out and some methods have been proved capable of preventing explosive spalling. The addition of polypropylene fibers (PP-fibers) and insulating coatings are recommended. However, due to the lack of valid guidelines, the fire

safety design is very costly and uncertain because there are no generally applicable protective methods validated by fire tests. To facilitate the fire safety design, a study on the protective methods against explosive spalling is required, which must be based on spalling mechanisms.

1.2 Need for current work

The severity of explosive spalling has become more intense, since the introduction of dense (e.g. high performance) concrete. As a result, a lot of effort has been paid to study the nature of explosive spalling of concrete, especially in the last decades (see Chapter 2). The research focused on many fields, such as

- Investigation on spalling mechanism
- Measures to prevent spalling
- Moisture and pore pressure measurement
- Spalling assessment
- Numerical modeling for explosive spalling
- Fire safety design and test methods, etc.

Many factors have been found related to the occurrence of explosive spalling, e.g. permeability, moisture content, fire scenario, external load, etc. Mechanisms of explosive spalling based on pore pressure or thermal stress have been proposed. While these individual theories based on one of the two mechanisms could usually explain some observations in tests, they failed to consider the equally important role of the other mechanism. To date, the academics generally believe that explosive spalling is induced by the combined effects from both pore pressure and thermal stress, with this hypothesis, many of the contradictory characteristics of spalling that have been observed by researchers over the years can be comprehensively explained. However, the above mentioned hypothesis has not yet been considered in the risk analysis and the accuracy of spalling prediction is still difficult, because there is no valid framework to interpret explosive spalling behavior.

As for the protective methods, the proposed hypothesis can explain the benefits from the application of PP-fibers and insulating coatings. Yet the effectiveness of the method must be further validated by fire test, which are usually very costly. This research on explosive spalling aims also at facilitating fire safety design, by developing a valid verification method for practical concrete spalling prevention.

Based on the above hypothesis, a framework for predicting explosive spalling is developed. The mechanism of combined stresses from pore pressure and thermal stress will be used to develop a spalling model to predict the explosive spalling. A risk analysis and the evaluation of protective methods will be connected to the research on explosive spalling. The work reported in this dissertation will contribute to close the gap between theory and practice.

1.3 Research objectives

From the above sections, it is clear that there is a lack of a framework to investigate explosive spalling comprehensively and the research is not well related to the needs in practice. To address the knowledge gap the following items will be studied in this research project:

- A literature review on the spalling of concrete induced by fire. Relevant experimental and numerical studies will be covered to investigate the concrete properties at high temperature. In addition, the review will especially focus on the key factors, mechanisms and models for studying the stress states in concrete under fire.
- Tests on concrete permeability considering the influences from moisture content and PP-fibers. The test results will illustrate the change of concrete permeability at high temperatures. The effects from external loads on the permeability of concrete will be investigated by the permeability measurements under compressive stresses.
- Develop a permeability model based on the test results and a Thermo-Hydro model for predicting the pore pressure in concrete.
- Validate the proposed models by comparing against test results. Thereby, the pore pressure and moisture content will be taken into account in the spalling analysis framework.
- Undertake parametric studies on pore pressure in concrete. Many test observations related to pore pressure should be explained by the proposed models.
- Propose a spalling criterion based on the proposed spalling mechanism. The effects from pore pressure and thermal stress will be combined to evaluate the risk of explosive spalling. Measures to prevent spalling can be investigated in the framework as well.
- Validate the developed spalling model based on the spalling criterion against fire test on concrete slabs.
- Conduct parametric studies to quantify the influences of various factors on the explosive spalling of concrete. The risk of explosive spalling of concrete should be interpreted comprehensively and many factors described in Section 1.2 will be involved in developing a framework for spalling prediction.
- Undertake tests on concrete slabs with insulating plates according to the guidelines provided by the spalling model. An application of the proposed framework will be carried out.
- Propose an evaluation strategy according to the experimental conditions. The data from fire tests and parametric studies will be used for risk analysis and fire safety design.

1.4 Scope

This dissertation is presented in seven Chapters. The above research subjects are addressed by both experimental and numerical studies.

- Chapter 1 provides a general introduction. The background and the need for the current work are presented.
- Chapter 2 is a state-of-the-art review on the concrete spalling in fire. The concrete properties at elevated temperatures are summarized and the analytical models from codes and standards are discussed. Also the mechanisms of explosive spalling are reviewed.
- Chapter 3 presents the pore pressure analysis. The permeability of concrete has been measured for various concrete mixtures. A permeability model is proposed with respects to moisture content and the application of PP-fibers. The pore pressure is simulated by using a Thermo-Hydro model (TH-model).
- Chapter 4 is about the spalling criterion. The effects from both pore pressure and thermal stress have been combined by the proposed spalling mechanism. The influencing factors will be

considered by the spalling criterion. A spalling model will be proposed based on the spalling criterion. Explosive spalling can be predicted by the spalling model. The important factors to explosive spalling have been discussed in the framework.

- Chapter 5 shows the application of the spalling model. The risk analysis has been carried out under various fire scenarios. The protective methods, such as PP-fibers, protective mortar and protective plate have been investigated. An evaluation strategy has been introduced according to the experimental conditions.
- Chapter 6 consists of the main conclusions from the current study and the prospects for the further research.

2. State of the art review

2.1 General

2.1.1 Spalling of concrete at high temperatures

Concrete has been the most used building material in construction for a long time due to its wide applicability and low cost. The fire resistance of concrete elements is usually good and the penetration of heat is slow, because concrete has relatively high thermal capacity and low heat conductivity. Using modern concrete technology (admixtures, production processes, etc.), concrete strength is increasing and at the same time concrete is becoming more dense, especially when silica fume is used to increase the concrete performance. High performance concretes (HPC) are more and more used in high-rise buildings or tunnels. Apart from the advantages of high density (high strength and good durability), the elements of HPC have been seen to spall, leading to a reduced fire resistance. Spalling was reported as early as 1916, in the Far Rockaway fire in the United States (Woolson 1918). Fire spalling of concrete was considered as the cause for building collapse, despite the fact that the building was supposed to be a first class fire proof. Concerns were further driven by the knowledge that more and more HPC spalling is observed in practice and in tests (Kodur 2000), since Sönnerberg (1952) stated the implications of mechanical vibration of modern concrete on its fire spalling performance.

Results from a number of studies (Kodur 2013) have shown that there are marked differences between the properties of high performance concrete (HPC) and ordinary Portland concrete (OPC) at high temperatures. Fire spalling of concrete has been observed since the introduction of reinforced concrete, but its importance is raising due to the introduction of HPC and self-compacting concrete (SCC). After decades of study (Jansson 2013), the reliable prediction and prevention of spalling are still very difficult, because of the large number of factors involved and the high variability of the spalling behavior itself. Some practical spalling cases have supplied indications of influencing factors and a lot of effort was spent to study the phenomenon of spalling, when concrete is exposed to rapid heating in fire. Some of these cases and studies are reviewed in this chapter, to gain a better insight of the fire spalling of concrete.

2.1.2 Fire spalling of concrete

As more high performance concrete is used in structures especially for columns with high compression loads, severe fire spalling of concrete is more often observed during fire cases. The British Concrete Society Committee made an inquiry into Fire Resistance in 1984 and showed that fire spalling was involved in over 80% of the reported fire accidents in concrete structures (Malhotra 1984). Fire spalling of concrete will lead to a decrease of cross section, reducing the strength of a structure or member and will make most simplified existing design models (e.g. Eurocode 2) invalid. There have been particular cases in tunnels, where extensive damage led to very expensive repairs, drawing attention to spalling prediction and prevention. Several examples of severe spalling of HPC in tunnel fires summarized by Khoury (2000) have been listed in Table 2.1. Some other fire cases in real structures will be presented to learn from experiences of spalling in practice.

Table 2.1 Concrete damage in recent tunnel fires summarizes from the reports (Khoury 2000).

Tunnel	Concrete strength	Maximum temp (°C)	Fire duration (h)	Length affected	Segment depth affected
Great Belt (1994)	76 MPa, 28 day	800	7	16 segment rings (1.65 m long)	Up to 68% spalled in layers along 10 segments
Channel (1996)	110 MPa, mature	1100	9	500 m with 50 m severely affected by spalling	Up to 100% of segment thickness spalled showing grout
Mont Blanc (1999)	20 MPa	1000	50	900 m; tunnel crown most affected	Not reported

2.1.2.1 Great Belt tunnel 1994

On 11th June 1994, during the tunnel construction, the tunnel boring machine caught fire in the Great Belt Tunnel near Korsør, Denmark. According to the report by Tait & Höj (1996), the primary fuel was hydraulic oil from the tunnel boring machine. All of the crews were evacuated and by the time the fire brigade arrived, the fire was too intensive to be extinguished. The extreme fire lasted for 7 hours and the maximum temperature reached approx. 800 °C according to the report. The concrete included micro-silica, fly ash, and granite aggregate, with a 28-day strength of 76 MPa was found to have spalled seriously during the first 20 minutes of fire exposure. Up to 68% of the cross section of the 76 MPa (28 days) HPC was destroyed by spalling. In the segment that was affected most severely by the fire, only a third of the 400 mm thick cross-section remained.

To investigate the amount of fire spalling, fire tests were performed on two tunnel segments from the production. The result of the experiments showed that the degree of spalling was 140 mm, less than in the real fire of 227 mm. The original assessment that the spalling would only limited to 40 mm was incorrect. This significant fire incident showed the severe consequence of fire spalling and the difficulty in predicting spalling (Trafikministeriet 1995).

Fig. 2.1 Tunnel element from the Great Belt tunnel fire test at SP (Trafikministeriet 1995)

2.1.2.2 Channel Tunnel 1996

On 18th November 1996, a heavy goods carrier shuttle in the Channel Tunnel caught fire (Shuttleworth 1997), which led concerns into the effects of fire on concrete structures. The Channel Tunnel is a high speed railway tunnel crossing the English Channel. The mature strength (28 days) of concrete was 110 MPa (Khoury 2000). The fire lasted for about 9 hours, and was severe since the maximum temperature was estimated to be 1100 °C. The affected length was over 500 m owing to the fact that the fire spread from one truck to another, in which 46 m nearest to the fire source suffered most. In some areas during the fire, the whole concrete cross section of the 110 MPa HPC had spalled such that the grout was exposed. The tunnel would have collapsed if the fire occurred in another part of the tunnel. Firemen reported that on entering the fire zone in the Channel Tunnel, they were showered with small, hot pieces of concrete, which came from the explosive concrete spalling.

This accident in the Channel Tunnel led to expensive repair and the tunnel was closed for a total of six months. The damaged elements were replaced by 680 tons of plain shotcrete and 630 tons of fiber reinforced shotcrete.

Fig. 2.2 Damaged section in the Channel Tunnel (Shuttleworth 1997)

2.1.2.3 Mont Blanc Tunnel 1999

On 24th March 1999, a Belgian truck carrying flour and margarine caught fire in the tunnel and the caused damage to the tunnel vault. The damage to the concrete lining was attributed to the decreased strength of the concrete due to high temperature. Although the temperatures in the tunnel during the fire were estimated to be 1000 °C, and that the fire lasted for 50 hours, explosive spalling did not seem to have occurred (Faure 2007), which Abraham (2003) assumes can be explained by the high permeability of the concrete (low concrete strength). High permeability prevented high pore pressure inside concrete, which is treated as a trigger for explosive spalling (Bazant 2005). In Mont Blanc tunnel fire no spalling was observed and concrete remained in place. After over 50 hours of fire, many believed that all the concrete was totally destroyed, but the obtained profiles showed that only a few centimeters of concrete was burnt (Faure 2007).

After heating, the concrete appears as a very good isolating material, whose high void ratio (13%) is likely the reason for the good isolation. This shows the role that fire spalling of concrete plays in fire cases: without explosive spalling, concrete shows good performance under fire; but in the case of Channel

tunnel, spalling could induce collapsed of the whole structure. So spalling must be considered in the protection design.

Fig. 2.3 Consequences of the Mont Blanc tunnel fire (Faure 2007).

2.1.2.4 Wu-bridge's western approach span 2015

Apart from fires in tunnels, fire spalling of concrete is also observed in other structures. On 17th January 2015, plastic material stored under the approach span of Wu-bridge caught on fire (Wu Bridge fire report 2015). The Wu-bridge is a city highway bridge across the Grand Canal in city of Wuxi, China. The fire lasted for 3 hours, with over 20 m^2 lining on the bottom of the approach span spalled away, the depth of spalling was up to 50 mm, and the reinforcing bars were exposed with some even losing connection to the base concrete. The concrete strength was 50 MPa, some core samples were taken from the affected area. The load bearing capacity was not much reduced, according to the investigation report (2015).

Fire spalling has little effect on the safety of the structure for ordinary low dense (strength) concrete as the spalling is seldom more than slight surface flaking. However in the case of Wu Bridge, spalling happened to the concrete with 50 MPa, spalling areas were large and the cost of repair was high, although no collapse was observed. This shows the need for better investigation of spalling risk even for concrete with moderate strength.

Fig. 2.4 Damaged element in the Wu Bridge (2015)

The aforementioned fire cases of concrete structures have shown that the performance of HPC under fire is not ideal, as it can suffer from violent spalling (explosive spalling) and its damage extent is higher than that of OPC. Fire spalling is the main concern in using HPC in practice, and the fire cases of HPC with high or moderate strength have drawn attention to perform a fire spalling study. Further laboratory experiments have shown evidence of spalling in HPC when exposed to high temperatures and many factors are found to be influencing fire spalling of HPC (Klingsch 2014).

2.1.3 Study on fire spalling of concrete

Since the first recorded observation of fire spalling 150 years ago, a lot research has been reformed to study the mechanism of fire spalling of concrete (Jasson 2013). A brief review of some important research and investigations of fire spalling of HPC will be presented.

Ingberg et al. (1925) concluded from a large number of fire tests that concrete with high silica content was prone to spalling during fire exposure. This fire test program was the basis for the study of concrete with silica fume, i.e. modern HPC, which are prone to fire spalling. According to Ingberg et al., the reason for the behavior was the volume change of different aggregates and water evaporation.

Sundius (1931) studied a fire in a building, he found cracks parallel to the heated surface could lead to flaking. Based on the study, he drew the conclusion that the crack growth in the cement paste was induced by the expulsion of water. The heated water inside concrete will generate a high pore pressure, as one of the major influencing factors in fire spalling, the effect of moisture evaporation has been proven in later research by Shorter and Harmathy (1961).

Hasenjäger (1935) summarized the main factors of fire spalling of concrete in his PhD. thesis at the University of Braunschweig. Apart from other secondary aspects, thermal stress and pore pressure were clearly taken as main factors. According to Jansson (2013), these two important factors have been the subject of intense discussion by the scientific community of concrete spalling. But the result did not led to a development of model suitable for structural engineering.

Shorter and Harmathy (1961) brought forward the theory of moisture clog. According to this theory, the moisture will be driven by the pressure gradient to a saturated region inside the concrete, this region is the so called “moisture clog”. When the moisture clog is created, movement of steam will be restricted and will lead to high pore pressure. The moisture clog can be described by the difference in viscosity between vapor and liquid water and the effect will be further studied in Chapter 3 by introducing a new adapted permeability model.

Zhukov (1976) produced a theory based on concrete slab tests. One important conclusion was low water-cement (W/C) ratios could lead to higher spalling risk. Because concrete with high w/c ratios has higher porosities and permeability, is therefore less susceptible to spalling. This is similar to Malhotra’s (1984) observation. Zhukov’s superposition of stresses caused by thermal and external loads and by vapor pressure has great impact on the modeling of the spalling mechanism. The combined stress from pore pressure and thermal stress will be discussed and further used in the spalling criterion (see chapter 4).

Sertmehmetoglu (1977) measured the pore pressure, with the help of pressure transducers. The maximum pore pressure recorded in all of the tests was 2.1 MPa. This is less than the tensile strength of

concrete, even at high temperature, which was estimated to be around 3 MPa. Other tests results showed pore pressures of this magnitude as well, (e.g. Thelandersson 1974, Mindeguia 2010) showed that the peak pore pressure was also less than the tensile strength of concrete. Sertmehmetoglu's study indicated that pore pressure alone did not cause spalling. These results caused doubt on spalling mechanism that addressed spalling mere to pore pressure (Saito 1965).

Malhotra (1984) concluded from the practical experiences that poor concrete was superior to good concrete with regard to fire spalling. Dense concrete (good concrete) with low permeability could generate high steam pressure to induce spalling. Since then, the permeability of concrete has been taken into account in fire spalling study, especially when concerning the risk of HPC spalling that is characterized by high density and low permeability.

Hertz (1992) studied the concrete densified by silica fume under high temperature with regards to spalling. The results showed that concrete containing proportions of silica fume were more likely to spall, even when exposed to low heating rates. Most parameters are found to have the same qualitative influence on explosive spalling of concretes with and without silica fume. The risk of explosive spalling increases with increased moisture content, decreased permeability, decreased tensile strength, and increased heating rate.

Connolly (1995) categorized spalling into four groups, surface spalling, explosive spalling, aggregate spalling and corner spalling. Khoury (2005) had a similar categorization of spalling. He grouped spalling into six categories. Each category of spalling has its own causative factors, and many of these factors have contradictive influences on the different types of spalling. Explosive spalling is considered as the most serious form of spalling under fire, so the causative factors of explosive spalling will be studied in coming sections.

Klingsch (2014) concluded within his PhD thesis that the heating rate has an influence on spalling pattern, which cannot be explained by the existing models of pore pressure-induced explosive spalling. In his tests with linear heating (e.g. with constant heating rates), lower heating rates lead to spalling initiated from sections deeper inside the specimen, whilst higher heating rates lead to smaller concrete fragments after spalling. Polypropylene fibers (PP-fibers) could prevent explosive spalling, probably by accelerating the escape of moisture at high temperature, and the type and amount of PP-fibers is important for their efficiency.

2.1.4 Types of concrete spalling

In terms of different kinds of spalling, Gary (1916) has made first efforts to categorize spalling of concrete into four groups already in 1916. Over recent decades, two additional groups were described and defined by Khoury (2005) during his research on explosive spalling of concrete, he added post-cooling spalling and sloughing off spalling. He grouped spalling of concrete at high temperatures into six categories:

- Explosive spalling
- Aggregate spalling
- Surface spalling
- Corner spalling
- Post cooling spalling

- Sloughing off spalling

Concrete spalling can be categorized by other terms, e.g. surface and explosive spalling are violent, yet the corner spalling and slough off are non-violent. In a single fire case, several of these different types of spalling can occur at the same time; depending on the duration the concrete is exposed to high temperatures.

In some case, it is very difficult to distinguish between some of these types of spalling, especially between explosive and surface spalling. According to Khoury (2005), when exposed to fire, the explosive, surface and aggregate spalling normally occur as early as a few minutes into the fire exposure, while the other three types usually occur later after t = 30-90 min fire exposure.

Table 2.2 summarizes the different forms of spalling and their main characteristics, when exposed to ISO fire. These six categories are briefly described.

Table 2.2 Characteristics of the different forms of Spalling by Khoury (2005).

Spalling	Time of occurrence	Nature	Sound	Influence on structure	Governing factors leading to spalling
Explosive	7-30 min	Violent	Loud bang	Very serious	Material, structural /mechanical and temperature related
Aggregate	7-30 min	Violent	Cracking	Can be serious	Mainly material related
Surface	7-30 min	Splitting	Popping	Superficial	Mainly material related
Corner	30-90 min	Non-violent	None	Can be serious	Mainly structural /mechanical related
Post cooling	After cooling	Non-violent	None	Can be serious	Structural /mechanical and material related
Sloughing off	When concrete weakens	Non-violent	None	Can be serious	Mainly structural /mechanical related

Among these spalling forms, explosive spalling can result in the explosive removal of a concrete layer up to 100 mm. Because of its important influence on the structure, explosive spalling is considered as the most serious form of spalling. Especially HPC with silica fume can suffer from explosive spalling under high temperature, which can reduce the resistance of the structure, especially when the core of the section or the reinforcing bars are exposed to high temperature. So explosive spalling must be considered in the assessment of the fire safety of a structure especially with HPC. In the following sections, discussions will be mainly focused on the explosive spalling of high performance concrete with silica fume.

2.2 Concrete properties at elevated temperatures and their influence on spalling

The degradation of mechanical and physical properties of concrete is important, when it is exposed to elevated temperatures. The performance of concrete in fire becomes a complex process because of the moisture content in concrete, which will change its aggregate phase at high temperature. The free water held by capillarity behaves differently from absorbed water held by surfaces force (physically bounded water) and bound water held chemically (chemically bounded water). Furthermore, at elevated temperatures, the crystal structure of aggregates changes, or the weight of aggregates decreases. The

high thermal gradient in concrete induces expansion in the hot regions, or when restrained, leads to high thermal stress, which makes the performance of concrete even more complex.

Concrete is composed of graded fine and coarse aggregates, sand, cement, water and pores. The mechanical and transport properties of concrete are dependent on its moisture content. The loss of moisture is observed in tests, especially above 100 °C due to the phase change from liquid water to vapor. The weight loss of concrete with increasing temperature obtained by Noumowe (1996) is shown in Fig. 2.5. From 30°C to 600°C, in conjunction with evaporation, dehydration of the hardened cement paste (breakdown of gel) occurs. At 120°C the expulsion of water physically bound in the smaller pores or chemically combined, initiates and continues up to about 500°C where the process is essentially complete. In the temperature range from 450°C there is decomposition. From 450°C to 550°C there is decomposition of the portlandite. A further process of decomposition of the hardened cement paste takes place between 600°C and 700°C with the decomposition of the calcium-silicate hydrate phases. At this stage, the loss of weight is almost finished, no noticeable change of mass is observed in the tests (Harmathy 1973).

With the loss of weight the porosity of concrete increases when exposed to high temperature, as shown in Fig. 2.6. The porosity varied little till 120 °C, and increased with temperature particularly after 300°C and the pore size distribution was significantly modified, the number of larger pore sizes increased measurably. These processes are related to the change of thermal, physical and mechanical properties at high temperature. Thermal properties of concrete such as thermal conductivity and specific heat influence the temperature rise and distribution in concrete. Physical properties that influence the explosive spalling are density and permeability. The pore pressure as a trigger of spalling (Bazant 2005) in concrete is greatly influenced by permeability. Permeability is defined as temperature-dependent, it rises with temperature. It is influenced by moisture content as well (see chapter 3). Mechanical properties that determine the phenomenon of explosive spalling are strength, Young's modulus of concrete and fracture energy. All of the mentioned properties are a function of temperature and have to be properly accounted for studying explosive spalling of concrete. In this section, a review of concrete properties will be provided.

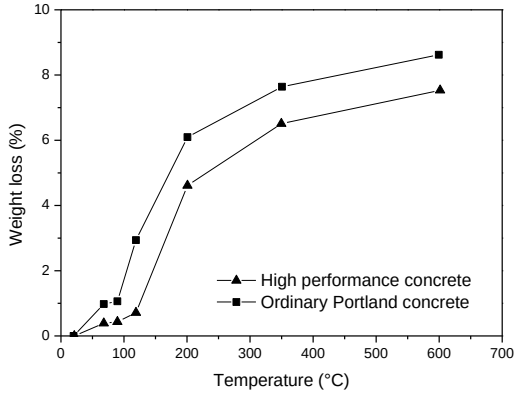

Fig. 2.5 Weight loss of concrete at high temperature (Noumowe 1996).

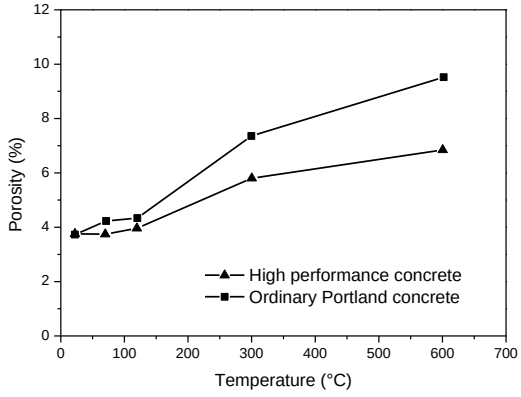

Fig. 2.6 The porosity of concrete at high temperature (Noumowe 1996).

2.2.1 Thermal properties of concrete at elevated temperatures

Thermal conductivity

Thermal conductivity is defined as the quantity of heat that passes per unit time through a plate of particular area and thickness when its opposite faces differ in temperature by one kelvin. As per Schneider (1982), thermal conductivity is mainly influenced by the moisture content and aggregate type. In can be seen from Fig. 2.7 that the thermal conductivity of concrete generally decreases with temperature. The presence of moisture will increase the thermal conductivity of concrete, thus the thermal gradients are lower at the early stages, and become higher when the heated surface is dried under high temperature. As per Saito (1965), this explains the increased susceptibility of concrete with high moisture content to spalling in terms of increased thermal gradients.

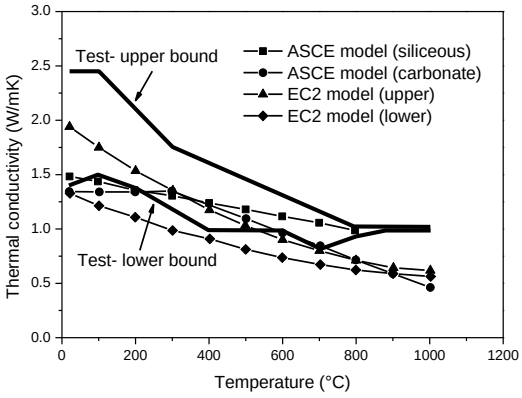

Fig. 2.7 Thermal conductivity of concrete at high temperature (Kodur 2014).

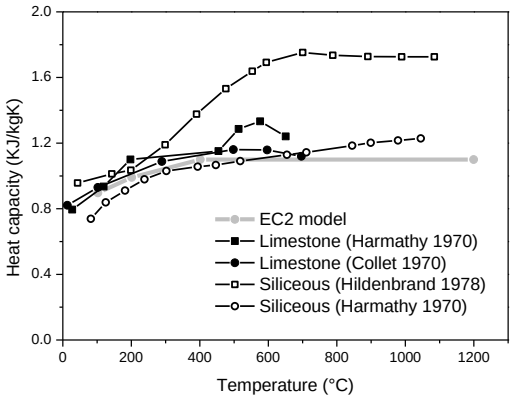

Fig. 2.8 Heat capacity of concrete at high temperature.

Heat capacity

Heat capacity describes the ratio of the amount of heat energy transferred to an object and the resulting increase in temperature of the object. Fig. 2.8 shows heat capacity of concrete with different kinds of aggregates and the constitutive model in Eurocode 2 (2004). It can be seen that the aggregate type has limited impact on the heat capacity of concrete. The Specific heat capacity is generally expressed as a function of temperature in the Eurocode 2, ignoring the impacts of aggregate type. According to the experimental studies by Kodur (2014), this Eurocode 2 constitutive model is valid for both OPC and HPC.

Weight loss

Weight loss is related to concrete properties at high temperatures and the weight loss is mainly determined by moisture transport. Test results have shown that high moisture transport reduces the risk of spalling (Klingsch 2014). According to Jansson (2013), the weight loss rate of concrete with PP-fibers is higher, and the anti-spalling function of added PP-fibers in concrete may be due to the modification of the moisture transport by increasing the permeability. This will be discussed in the permeability model in Chapter 3.

2.2.2 Physical properties of concrete at elevated temperatures

Density

According to the studies by Harmathy & Allen (1973), Hildenbrand & Peehs (1978) and Schneider (1982) the density of concrete depends on the moisture content for temperatures up to 150 °C. Fig 2.5 presents the effect of aggregate type on the density of concretes at high temperature. At temperatures from 150°C to 600°C (limestone decarbonation), the density of limestone concrete is relatively constant. Limestone decarbonation (between 600 °C and 900 °C) induces a further significant decrease in density of limestone concrete.

The density of siliceous concrete decreases with the loss of moisture content up to 700 °C, then experiences a sharper decrease with heating above 700°C, which was attributed by Schneider (1982) to the high thermal expansion of quartz. The constitutive model of concrete density in Eurocode 2 is also plotted in Fig. 2.9, the Eurocode 2 model does not specify the types of aggregates, and in general it agrees the change of all kinds of concrete up to 700 °C. It is commonly used for evaluating the density of concrete at high temperatures.

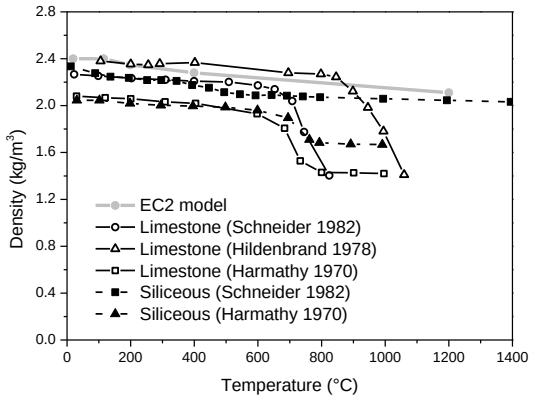

Fig. 2.9 Density of concrete at high temperature.

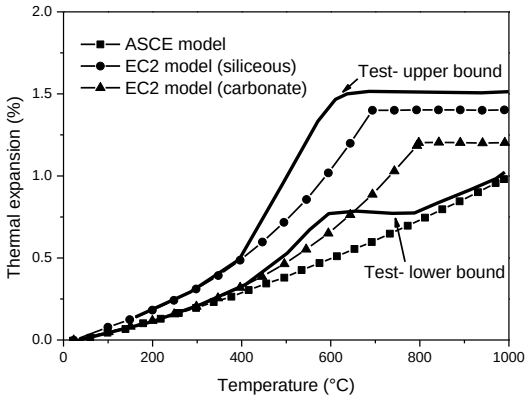

Fig. 2.10 Thermal linear expansion of concrete at high temperature (Kodur 2014).

Coefficient of thermal expansion

The coefficient of thermal expansion represents the volume change of a material due to temperature changes and is defined as the change in length of a material due to a unit (degree) change in temperature. This coefficient can be used as a measure for the thermal stress induced by temperature gradients. Data from the literature indicates that concrete's thermal expansion is a complicated process, because it is affected by the aggregate type and its composition, which have respective coefficients of thermal expansion. Results from the literature indicate that the main factor influencing the coefficient of thermal expansion is the aggregate type, the thermal expansion of siliceous aggregate concrete is greater than that of carbonate aggregate concrete. Fig. 2.10 shows the variation of coefficient of thermal expansion with temperature for siliceous concrete and carbonate concrete respectively according to Eurocode 2 (2004).

Permeability

Permeability is a measure of the ability of a porous material to allow fluids to pass through it. It is commonly used as the main indicator for the durability of concrete (a low permeability is beneficial). Referring to spalling, HPC is more vulnerable to explosive spalling when exposed to high temperature, because its low permeability, which results in a high build-up of pore pressure during heating (Klingsch 2014).

The permeability of concrete depends on porosity and pore characteristics such as pore size, orientation, connectivity, and size variation. In general, the permeability of concrete is assumed to increase with temperature and has been implemented in several models. The increasing trend of permeability is usually attributed to the evaporation of free water and the change of porous system (Gawin 1999). However, tests on the permeability of concrete at high temperature performed by Schneider (1989) showed a more complex pattern of permeability. As shown in Fig. 2.11, when the specimen was kept at each temperature for 10 hours, a significant dent in permeability within a temperature range of T = 150-250°C occurred; when the specimen was kept for 50 hours, such a dent disappeared. Jacob's (1994) study showed this can be attributed to the change of moisture content or degree of saturation as shown in Fig. 2.12. Tests results by Klingsch (2014) showed the dent in permeability of HPC was accompanied by a fast weight loss of concrete, which has been attributed to the dehydration of bounded water in concrete. The permeability of concrete is found to be influenced by the moisture content and the dent in permeability could be prevented by adding PP-fibers. As a protective method, PP-fibers prevent explosive spalling by increasing the permeability of HPC at high temperature. The permeability of concrete at high temperature will be further discussed in Chapter 3, where a model considering the dent and the influence of PP-fibers will be proposed.

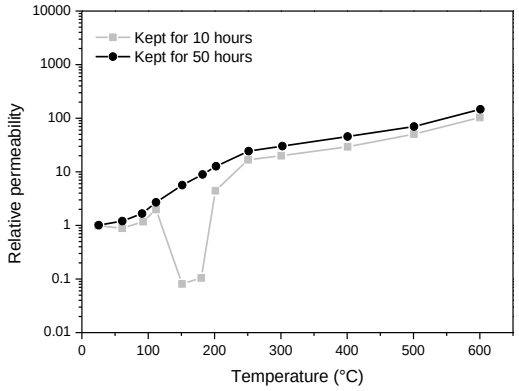

Fig. 2.11 Permeability of concrete after different conditioning time (Schneider 1989).

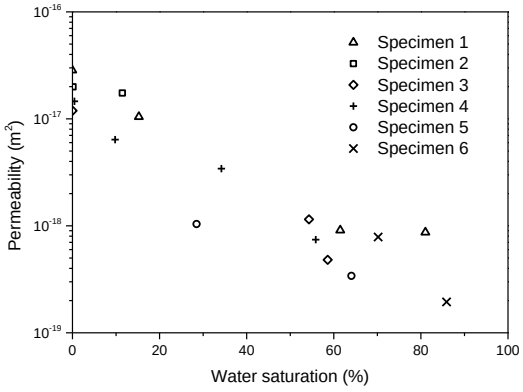

Fig. 2.12 Permeability of concrete as a function of the water saturation (Jacobs 1994).

2.2.3 Mechanical properties of concrete at elevated temperatures

Compressive strength

There is a big amount of high-temperature test data on the strength properties of HPC. The literature review shows that there is a large variation in the residual strength (at room temperature after cooling

down form a given maximal temperature) of concrete (Kodur 2014). Among the factors that directly affect compressive strength at elevated temperatures are the moisture content, the loading rate and the types of aggregates. The use of silica fume in HPC leads to significant variation in compressive strength of HPC in the temperature range of 200 °C to 500 °C; however, the test results on OPC show a smooth degradation throughout a 20-800 °C temperature range. Fig. 2.13 and Fig. 2.14 respectively illustrate the degradation of compressive strength ratio for OPC and HPC with different aggregate types at elevated temperatures.

According to Schneider (1982), the concrete compressive strength of OPC is marginally affected by temperatures up to 300 °C, which can be attributed to the thermal strain and the aggregate locking effect. At higher temperatures, micro-cracks and decomposition of cement result in the faster deterioration of compressive strength. On the other hand, the use of silica fume improves the compressive strength at ambient temperature, which may be attributed to a dense micro-structure. However, this dense micro-structure is highly impermeable and the low permeability leads a build-up of pore pressure at temperatures beyond 100 °C. This pore pressure results in the rapid development of micro-cracks in HPC, which is the main factor making the HPC more sensitive to temperatures up to 300 °C than OPC (Kodur 2014).

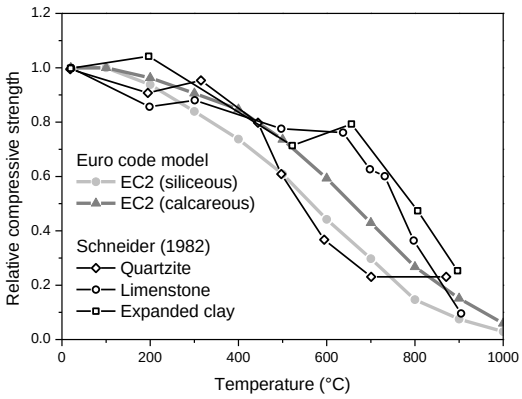

Fig. 2.13 Compressive strength of OPC at high temperature.

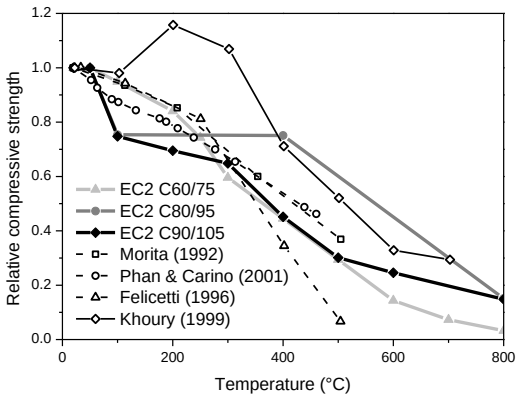

Fig. 2.14 Compressive strength of HPC at high temperature.

As shown in Fig. 2.13 and Fig. 2.14, Eurocode 2 (2004) suggests constitutive models for high temperature compressive strength of OPC and HPC respectively. According to the OPC curve, OPC with siliceous aggregate concrete shows lower strength than calcareous and lightweight OPC, which agrees with reported test results (Schneider 1982). In the case of HPC, the constitutive model predicts a rapid strength loss according to Kodur (2014), Eurocode 2 (2004) for Class 3 can be taken as conservative values for compressive strength variation with temperature.

Tensile strength

The tensile strength of concrete determines the ability of concrete to resist spalling and cracking. The tensile strength of concrete is much lower than its compressive strength, at ambient temperature the tensile strength is around 7-11% of the compressive strength (Schneider 1988). There is limited experimental data of tensile strength of concrete at high temperature available because of the

difficulties in the direct measurement of concrete's tensile strength. An indication of concrete's tensile strength can be obtained by the splitting-tension and flexure tests. Based on these methods, test results have shown that the effect of elevated temperature on tensile strength shows a similar trend to its effect on compressive strength, but tensile testing of concrete is more sensitive to deterioration at elevated temperature. At 400 °C, concrete exhibits only about 30 % of the initial tensile strength at ambient temperature.

The effect of elevated temperature on tensile strength of OPC and HPC has been investigated. Test results have shown that concretes with high strength experiences a faster loss of tensile strength at high temperature because of the development of higher pore pressure, which is attributed to the denser micro-structure of HPC. Fig. 2.15 shows tensile the strength of three types of concrete C40, C60 and C70 with 28-day compressive strengths of 42.5, 68.0, and 76.0 MPa, respectively, after temperature exposure up to 1000 °C. The results for the two higher strength concretes dropped more than that for OPC. Fig. 2.16 illustrates the variation of tensile strength ration of OPC and HPC as a function of temperature as reported in previous studies (Felicitti 1996) and in Eurocode 2 (2004). Generally, the constitutive model in Eurocode 2 agrees well with the experimental results and can be taken as valid for OPC and HPC, although it underestimates the sharp decrease of HPC for temperatures under 200 °C.

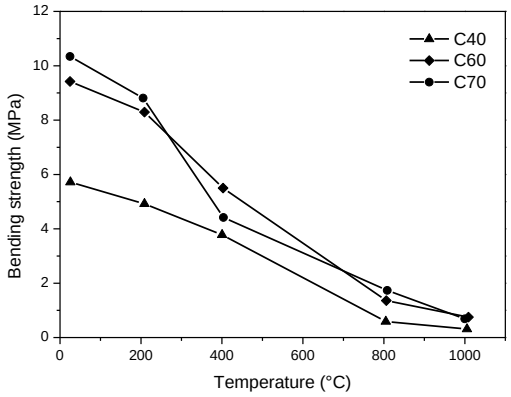

Fig. 2.15 Tensile strength of concrete at high temperature measured by bending test (Li et al. 2004)

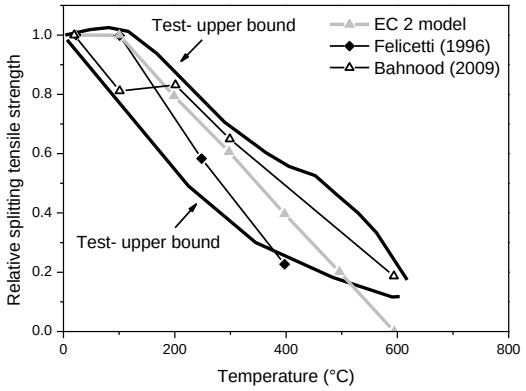

Fig. 2.16 Relative tensile strength of concrete at high temperature (Kodur 2014).

Modulus of elasticity

The modulus of elasticity for concrete is a measure of its stiffness or resistance to deformation. The concrete's stress-strain relation is nonlinear, so the modulus of elasticity varies over a wide range. Main variables affecting the concrete's modulus of elasticity are the water-cement ratio, the age of concrete and the amount and type of aggregate. As shown in Fig. 2.17, experimental tests by Schneider (1982) indicate the significant influence of the aggregate type on the modulus degradation. Results show that the elastic modulus for concrete decreases with increasing temperature. As per Zhang & Bicanic (2002), the degradation of the modulus of elasticity is associated with the loss of evaporable water for temperatures below 300 °C, further degradation at higher temperature is a result from the decomposition of concrete constituents. Fig. 2.18 illustrates the degradation of OPC and HPC, the results

indicate that the strength of concrete has limited effect on the modulus-temperature response when the modulus of elasticity is normalized with respect to the ambient temperature results.

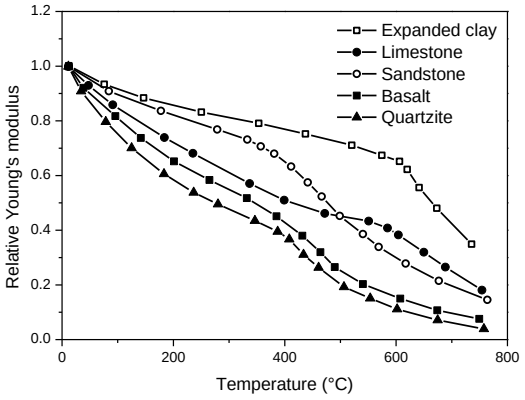

Fig. 2.17 Decrease of Young's modulus of concrete at high temperatures (Schneider 1982).

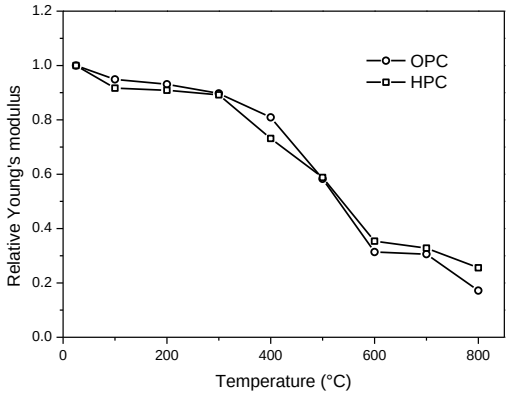

Fig. 2.18 Decrease of Young's modulus of OPC and HPC at high temperatures (Castillo 1990).

Biot's coefficient

Biot's coefficient defines the fraction of pore pressure transferred to the total stress and was first introduced by Biot (1941) based on the effective stress concept by Terzaghi (1925). As a fluid saturated porous media, concrete's damage behavior coupling with moisture and pore pressure can be described using the Biot's coefficient. Test results (Klimentos 1998 & Chen 2009) have shown that the Biot's coefficient is a complex function of porosity, permeability, pore-size distribution, overburden and confining stress, which means that it is not a constant. Biot refined the effective pressure coefficient to be in the range from porosity of concrete to 1. Equations 2.1 and 2.2 give the expression for the effective stress, which was suggested by Geertsma (1957) and Skempton (1960). These are exact and can be considered as fundamental laws for strain in poroelastic systems.

$$\hat{\sigma}_{ij} = \sigma_{ij} - bP_{\mathrm{p}}\delta_{ij} \qquad 2.1$$

$$b = 1-(K_b / K_a) \qquad 2.2$$

Where σ_{ij} denotes the applied stress (measured positive in tension), P_{p} is the pore fluid pressure, δ_{ij} is the Kronecker delta, b is Biot's parameter, K_{b} is the skeleton bulk modulus and K_{s} is the solid matrix bulk modulus. Ulm (2004) estimated the poroelastic properties of concrete, the results showed that the base Biot's coefficient was between 0.61 and 0.71 for concrete at ambient temperature. Chen (2009) investigated the effect of heat treatment on the poroelastic properties and the results showed that Biot's coefficient approaches 1 when exposed to high temperature. These results show that to predict explosive spalling of concrete, the commonly used porosity of concrete is far lower than the real fraction of pore pressure that transferred to the matrix, as per Ulm is larger than twice the porosity. In Chapter 4, Biot's coefficient will be discussed in detail as a parameter in a spalling criterion, to predict the explosive spalling of HPC.

Fracture energy

Fracture energy G_f has been proven to be useful for modeling the fracture behavior, it can be defined as the total energy dissipated over a unit crack area. The fracture energy can be obtained from the area under a strain stress curve by three-point bending tests of a notched beam. Zhang (2001) studied the hot and residual fracture energy of concrete, the results show that, for the hot concrete, fracture energy G_f undergoes a decrease-increase process with temperature as shown in Fig. 2.19. From 20 °C to 150 °C, the fracture energy G_f decreases mainly due to dehydration. At higher temperature, the concrete becomes ductile, hence more energy would be consumed to break the concrete element. On the other hand, the increase of residual fracture energy is attributed to the rehydration of cement. Higher heating temperature induces micro-cracks and dehydration, making the concrete more brittle and so the fracture energy decreases.

Bazant (1988) investigated the influence of moisture content on fracture energy. The results showed that with higher moisture concrete, the fracture energy of concrete decreased faster than for pre-dried concrete. This can be attributed to the high humidity as well. For the explosive spalling, the humidity is relatively higher in the spalling front because of the moisture clog, which makes HPC prone to explosive spalling as well.

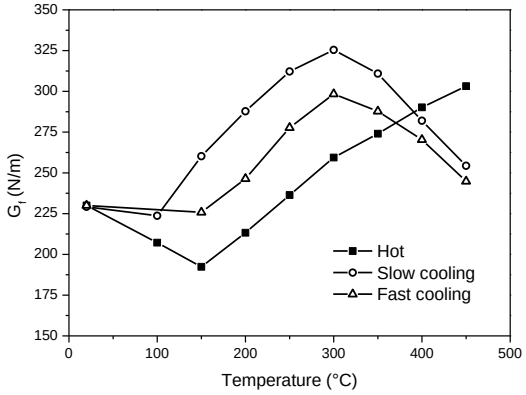

Fig. 2.19 Hot- and residual fracture energy of concrete (Zhang & Bicanic 2001).

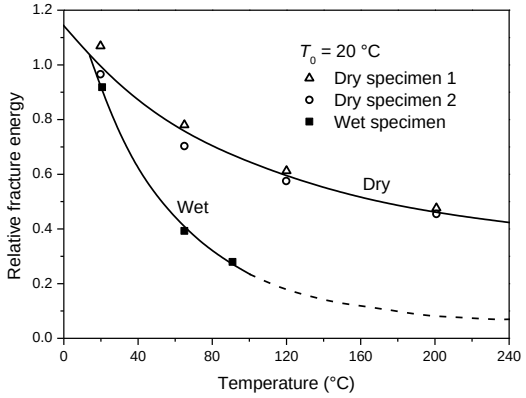

Fig. 2.20 Relative fracture energy at high temperature (Bazant & Prat 1988).

2.3 Mechanism of explosive spalling

From the previous review of the mentioned fire cases and the experimental tests, fire spalling is considered as one of the most harmful damages to HPC. Among others, explosive spalling is the most serious form of spalling due to heat exposure, therefore, since decades, efforts have been made to investigate the mechanism of explosive spalling and many spalling mechanisms and theories can be found in the literatures. This section will provide a summary and assessment of the spalling mechanism. The assessment will be based on the spalling observations from a literature review and from experiments made at ETH Zürich.

Since Hassenjäger (1935), many experimental studies have been performed to investigate the different influencing factors on explosive spalling. Despite the complexity, the influencing factors are generally agreed to be:

i. Heating rate
ii. Constraint / section size and shape
iii. Thermally induced stresses
iv. Permeability
v. Moisture content

Under high temperatures a few processes will take place inside the concrete, such as the release of bounded water, evaporation of water and the generalization of thermal gradients. Hence, the internal stresses in concrete are built up with a superposition of the pore pressure and the thermal gradient induced thermal stress. The influencing factors of explosive spalling (i - iii) are from the effects of thermal stress, and factors (iv - v) are related to the pore pressure. In this way, these factors can be assorted into two categories:

i. Thermal stress spalling.
ii. Pore pressure spalling.

Most of the proposed mechanisms of explosive spalling are filed under one or two of the categories. The review of mechanisms of explosive spalling will also be grouped according to the categories.

2.3.1 Thermal stress spalling

The theory of thermal spalling attributes the cause of explosive spalling to the temperature gradient in the concrete, which is recommended by some researchers (Saito 1965, Dougill 1972). When heated, thermal gradients in concrete will cause thermal stress because the expansion of the hotter parts is constrained by the cooler parts of the section. The hotter thin layer surface will expand more than the interior cooler region. As a self-equilibrating stress state, the heated surface will be in compression while the inner part will be in tension.

Saito (1965) proposed the hypotheses that spalling is the consequence of compression failure at the heated surface of concrete. This hypothesis supposes that spalling occurred when the thermal stress induced by the thermal gradient exceeded the temperature dependent compressive strength of concrete. He calculated the compressive stresses across the concrete section using an elastic analysis, the thermal stress changes with the heating time. At the early stage, the thermal stress increases with time till some point after heating, from which the stresses start to decrease.

Fig. 2.21 shows the change of thermal gradient with heating time. Saito found that under a standard BS 476 fire test, the thermal stress reached the maximum value normally within 30 minutes and then decreased with the thermal gradient descent. In this mechanism, the spalling is supposed to occur in the first 30 minutes under a standard BS 476 fire, otherwise the concrete can sustain the maximum thermal stress and the risk of spalling will be low. This theory agreed with some experimental test results and also has been confirmed by other tests by England (1971). Although the theory of thermal stress spalling was improved by Dougill (1972) to consider the thickness of the concrete member, it still cannot explain several observations in tests and the difference in spalling sensitivity between OPC and HPC.

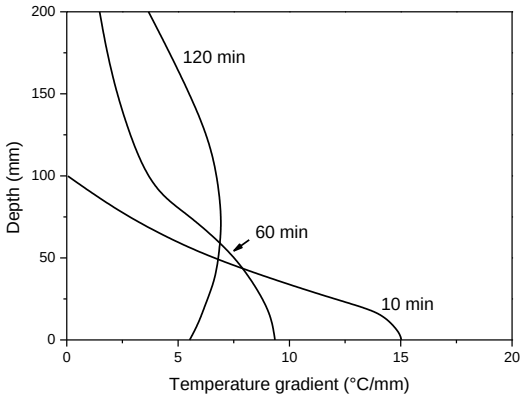

Fig. 2.21 Thermal gradient with depth during heating time (Saito 1965).

Klingsch (2013) reported explosive spalling in HPC with low thermal stress, when the specimen was heated under a low heating rate. Fig. 2.22 shows the measured temperatures in different positions. It can be seen that the thermal gradient was very small, so no high thermal stress would be induced. However, spalling occurred when the specimens were heated to 300 °C, as shown in Fig. 2.23. This observed spalling cannot be attributed to thermal stress. Additionally, the thermal stress spalling theory fails to explain the role of moisture content. Test results have shown that with low moisture content the concretes are less susceptible to spalling. As for the water-cured specimens, the theory would suggest that the likelihood of spalling is reduced, which is opposite to the observations.

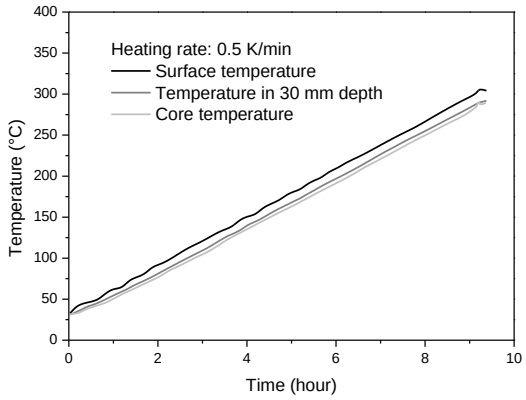

Fig. 2.22 Temperature measured at the surface, in 30 mm depth and in the core for the specimen that failed by explosive spalling (Klingsch 2013).

Fig. 2.23 Specimen (cylinder d=150mm, L=300mm) before and after the test with a low heating rate of 0.5 K/min (Klingsch 2013).

2.3.2 Pore pressure spalling

Test results have shown that the spalling is related to moisture content, several possible mechanism have been proposed based on the build-up of pore pressures during heating. The pore pressure drives off water from concrete as seen in Fig. 2.24, and imposes the bursting stress on the concrete. Meyer-Ottens (1972) proposed that a comparison of the bursting stress against the tensile strength of concrete could be a measure of the susceptibility to spalling. In this way, some test results can be explained and the higher risk of spalling in HPC can be attributed to its lower permeability compared to OPC, because the low permeability results in higher pore pressure in concrete during heating. The effects of PP-fibers against spalling can be considered as well: the pore pressure is reduced during heating by the melting of PP-fibers, which can increases the permeability.

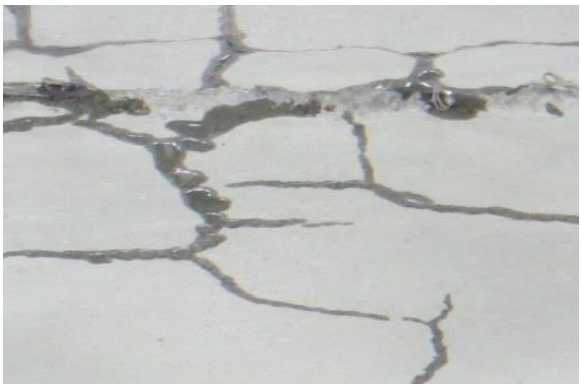

Fig. 2.24 Driven off water on the unheated side of a spalled element.

As hydration product, concrete contains chemical bounded water, free and adsorbed water in the pore. Akhtaruzzaman and Sullivan (1970) have shown that on the heating of concrete, the free water was removed at 105 °C and the adsorbed water started to loss from 175 °C. The quantity of moisture of a cement paste is related to the pore pressure. To evaluate the bursting stresses from pore pressure, many methods to calculate the pore pressure are developed. Meyer-Ottens (1972) produced an analytical model which can explain some observations in the tests. Bazant and Thonguthai (1979) proposed numerical solutions, using a finite element technique. The predicted pore pressures were comparable to direct pore pressure measurements. Dwaikat and Kodur (2009) modelled the development of pore

pressure using a hydrothermal model, the spalling is predicted when the pore pressure exceeds the tensile strength. The model explains the observed influence of permeability and tensile strength.

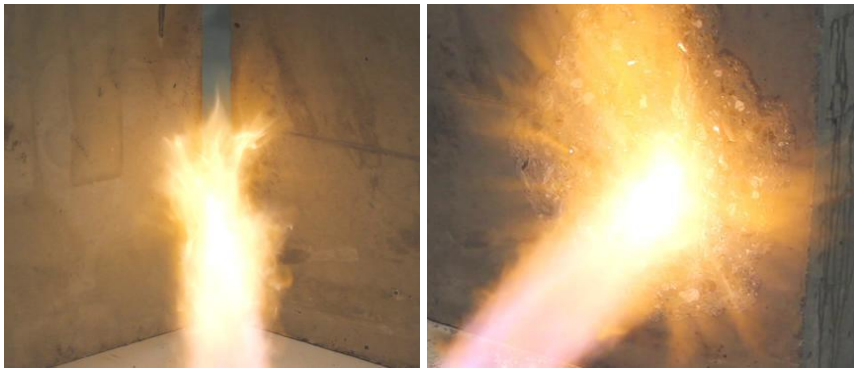

Fig. 2.25 Heating of the corners and center of the specimens (Jansson and Boström 2012).

However, the pore pressure spalling theory fails to explain some experimental observations. Jansson and Boström (2012) illustrated the influence of restraint on spalling, as shown in Fig. 2.25. The concrete slab did not spall when heated at the corners for 10 minutes. On the other hand, violent spalling occurred to the same slab when the specimen was heated in the center by the same flame. This showed that the restrain form is an important factor in spalling which can lead to various distribution of thermal stress in the specimen. In addition, according to Bazant (1979), pore pressures exceeding 2 MPa have never been measured, i.e. no pore pressures close to the tensile strength of the material have been measured during experiments. So the pore pressure alone is not the only cause of spalling. The spalling must be driven by an additional supply of energy together with the pore pressure. The pore pressure however cannot be neglected, because tests have shown that the spalling is related to moisture content and the effects of PP-fibers which reduce the pore pressure. In this context, explosive spalling of concrete cannot be explained by pore pressure development alone, but to predict spalling, the evaluation of pore pressure should be taken into account.

2.3.3 Combined pore pressure and thermal stress spalling

Thelandersson (1974) and Zhukov (1976) pointed out that the spalling is caused by the combined influence of pore pressure and compressive stresses in the restrained heated region. Zhukov proposed that the stresses in the heated concrete superimpose upon each other and when the combined stress exceeds the material strength of concrete, the pore pressure and thermal stress will lead to spalling. The stresses induced by heating on a loaded slab are listed in Table 2.3. In this theory the effects of pore pressure, constrain condition, heating rate etc. are included, as shown in Fig. 2.26.

Table 2.3 Stresses acting on a slab heated on one face (after Zhukov, 1976).

Direction	Description	Acting stresses
x-direction	Perpendicular to heated surface	Pore pressure σ_p (tensile)
y-direction	External loads, parallel to surface with loads	Pore pressure σ_p (tensile) Thermal stress σ_t (compressive) External loads σ_l (compressive)
z-direction	Parallel to heated surface without loads	Pore pressure σ_p (tensile) Thermal stress σ_t (compressive)

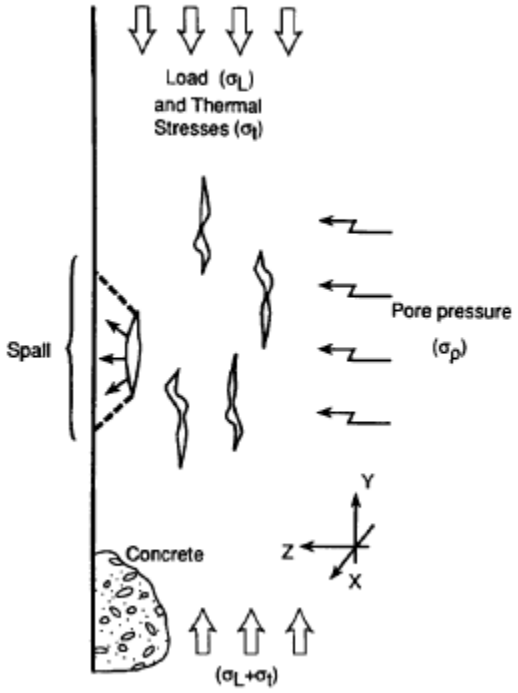

Fig. 2.26 Stresses acting in heated concrete (after Zhukov, 1976).

Zhukov used basic elastic theory to quantify the total strain in the x-direction ε_x as:

$$\varepsilon_x = \frac{1}{E}\left[\sigma_{\mathrm{p}} - v(\sigma_{\mathrm{l}} + 2\sigma_{\mathrm{t}})\right] \qquad 2.3$$

The strain energy density in the x-direction W_x, is the area under the stress-strain curve (taken as linear) and is given by:

$$w_{\mathrm{p}} = \frac{1}{2}\sigma_{\mathrm{p}}\varepsilon_x \qquad 2.4$$

The strain energy necessary to cause spalling $W_{spalling}$ is suggested by Zhukov as:

$$w_{\mathrm{spalling}} = \frac{1}{2} f_t \frac{f_t}{E} \qquad 2.5$$

If w_p exceeds $w_{spalling}$, spalling will be predicted. Where f_t is the tensile strength of concrete. If the Young's modulus is assumed the same, Equation 2.4 and Equation 2.5 can be compared and then spalling occurs when:

$$f_{\mathrm{t}}^2 = \sigma_{\mathrm{p}}^2 - v\sigma_{\mathrm{p}}(\sigma_{\mathrm{l}} + 2\sigma_{\mathrm{t}}) \qquad 2.6$$

It can be seen from Equation 2.6 that the pore pressure is an important factor for spalling, when the pore pressure is low, the concrete is less susceptible to spalling. On the other hand, explosive spalling is not purely a result of pore pressure, in Equation 2.6 the thermal stress and external loads work as another supply of energy. This mechanism agrees well with many experimental observations on

explosive spalling including the cases reported in Section 2.3.1 and 2.3.2, the spalling occurred when the combined stresses exceeded the strength of concrete.

Klingsch (2013) reported the effects of heating rates on explosive spalling, the high heating rate leads to higher risk of spalling. According to the combined stresses spalling theory, the thermal stress is higher during the faster heating, so the spalling is more likely to occur. In addition, Fig. 2.27 shows the different patterns of the spalled concrete in tests of concrete cylinders under various heating rates. Lower heating rates lead to spalling initiated from deeper sections with a single loud bang, higher heating rates lead to shallow spalled fragments with continuous popping. In the framework of combined stresses spalling theory, this observation correlates well with the different predicted spalling thickness of spalling under low and high heating rates.

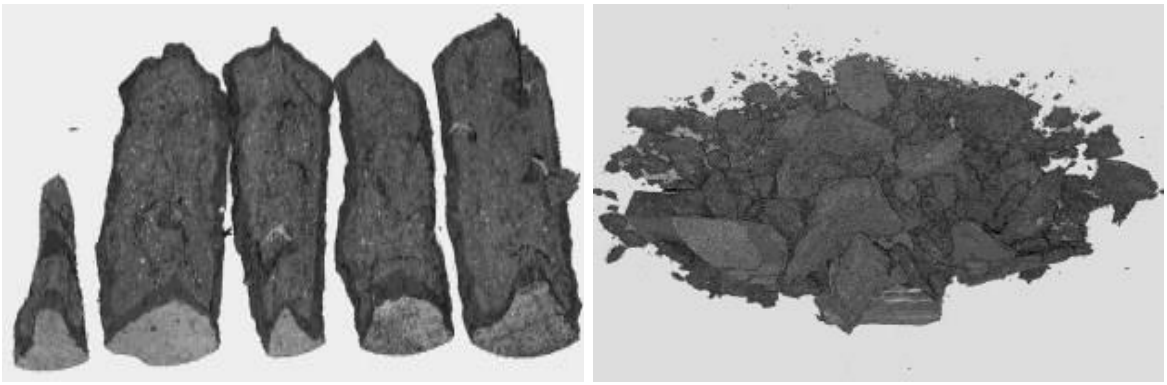

a) under low heating rates b) under high heating rates

Fig. 2.27 Stresses acting in heated concrete (Klingsch, 2013).

However, Zhukov assumed that the fraction of pore pressure was totally transferred to the total stress, i.e. the Biot's coefficient is 1.0. As discussed in Section 2.2.2, this assumption may overestimate the effects of pore pressure. This could be the reason that Zhukov (1994) suggested explosive spalling appeared likely in most situations, which is generally not the case. The lack of practical methods to evaluate the pore pressure makes a practical approach difficult. An engineering model based on these explanations is not yet available. Despite the limitations, the spalling theory of combined stress after Zhukov (1976) is useful and will be taken further in Chapter 4 to develop a spalling criterion.

2.3.4 Conclusions on mechanism of explosive spalling

The proposed mechanisms of explosive spalling are grouped in thermal stress spalling and pore pressure spalling. Based on the literature review and the results from tests, spalling cannot be purely a result of pore pressure or thermal stress. It is widely agreed that both thermal stress and pore pressure need be present for spalling to occur (Connolly 1995).

The combined pore pressure and thermal stress spalling theory after Zhukov is adopted and will be refined to develop a model for the prediction of explosive spalling. The effects of PP-fibers and protective lining will be considered as well. The modeling of pore pressure will be shown in Chapter 3, a spalling criterion is proposed in Chapter 4, and the modeling of spalling will be validated against test results in Chapter 5.

2.4 Codes of Practice

To guide practical design, fire resistances models for concrete elements are included in building codes and national standards. These codes and standards provide guidelines mainly based on fire tests. They do not give information or models for the prediction of explosive spalling or contain only warnings. For the use of HPC, the prescriptive approaches give therefore limited information on the fire behavior.

In the U.S., the ACI 216R Guides for Determining the Fire Endurance of Concrete Elements is the only standard-related document that contains information on properties of concrete at high temperature. However, HPC is not concerned especially with regard to the aspect of spalling. Like most codes ACI 216.1 standard specifies concrete cover thickness and minimum sectional dimensions to consider the fire resistance, but the effects from spalling to increase the collapse risk is not included.

In the Eurocode 1992-1-2 (2004), the use of HPC with a class in compressive strength of C55/67 to C80/95 is allowed, if the amount of silica fume does not exceed 6.0 % of the total mass of the dense concrete mixes HPC. However, tests by Klingsch (2013) have shown that spalling occurred even with a significantly lower content of silica fume. For higher grade C80/95 to C90/105 according to EN 1992-1-2, four methods are given to prevent concrete from explosive spalling:

Method A: Use of a secondary reinforcement mesh with a concrete cover of 15 mm. The reinforcement mesh should have a maximum spacing of 50 mm with reinforcement bars having a minimum diameter of 2.0 mm. No specification regarding the anchoring of this reinforcement is given.

Method B: Use of a concrete mix that does not have a tendency to explosive spalling at high temperatures as proved by tests or experience. No specification of testing or experience is mentioned.

Method C: Protective layers for which it is demonstrated that no spalling of concrete occurs under fire exposure. No specification of the design or verification of the thermal barrier is provided.

Method D: Include in the concrete mix more than 2 kg/m^3 of monofilament propylene fibers. No specification of the geometry or chemistry of the fibers is given.

Our tests have shown, that method B, C and D may be successful if correctly applied. However, the reproducibility of some of the methods is not obvious.

Until recently, the fire resistance evaluation of concrete elements is based mainly on tables and a prescriptive approach, but it is difficult to apply to get a performance based rational engineering approach because of missing data and a comprehensive spalling model. As for the HPC, which are more prone to spalling, the existing fire resistance provisions are not applicable if spalling cannot be excluded.

Some countries have considered the performance-based design, which provides cost-effective fire designs. A lot of experiments have been performed, and some mechanisms have been proposed to include the explosive spalling in fire resistance evaluation. However, as for explosive spalling of HPC, the lack of a validated numerical models and reliable data are the major obstacle for undertaking performance based fire design.

2.5 Protective methods

When the tendency to explosive spalling cannot be ruled out at high temperatures, some protective methods should be applied to the HPC. As mentioned earlier, Eurocode 2 (2004) suggests two methods against explosive spalling in HPC: protective layers and monofilament propylene fibers. Test results have shown that these methods are capable of preventing spalling.

According to Klingsch (2013), PP fibers minimize the risk of explosive spalling and avoid spalling or reduce the amount of concrete spalled from the specimen. It should be noted that the amount and the length and diameter of PP-fiber have a significant influence on explosive spalling. The Eurocode 2 recommended 2 kg/m^3 of propylene fibers does not consider the type and geometers of the fibers. Apart from fire tests, to date, no other method is validated to experiment the effects of various amount and type of PP-fibers.

Fig. 2.28 Slab with PP-fibers after 10 min ISO-fire exposure (Klingsch 2013).

As for the protective layers, Klingsch (2013) has shown that protective mortar can postpone or prevent spalling. In the tests, explosive spalling was observed in a HPC slab after 15 minutes of ISO exposure. Fig. 2.29 shows that with 10 mm of protective lining the HPC is protected for 119 minutes, and with 20 mm the spalling was prevented for 120 minutes. The protection of 10 mm postponed the occurrence of spalling but spalled with a single bang and a depth of spalling of was up to 63 mm. For insufficiently insulated specimen the risk is important, should be evaluated in advance.

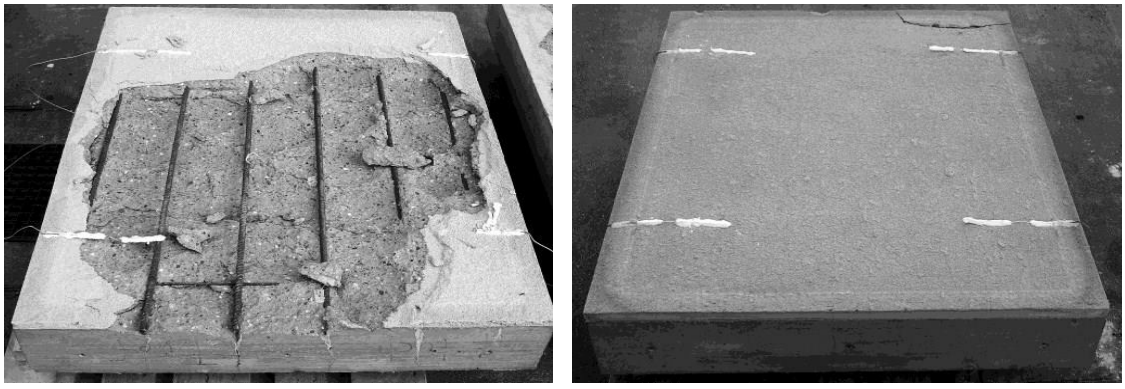

a) 10 mm protective lining. b) 20 mm protective lining.

Fig. 2.29 Slab with protective lining after ISO-fire exposure (Klingsch 2013).

The protective plates have been invested as well (Lu & Fontana 2015), as shown in Fig. 2.30. Test result has indicated that the protective mortar can prevent explosive spalling in HPC (see Fig. 2.31), when sufficient thickness was applied. Similar to the Protective mortar, insufficient protection must be avoided. Because if the explosive spalling is not prevented, the postponed spalling can be more severe. Therefore, there is a practical need for an evaluation method in fire safety design.

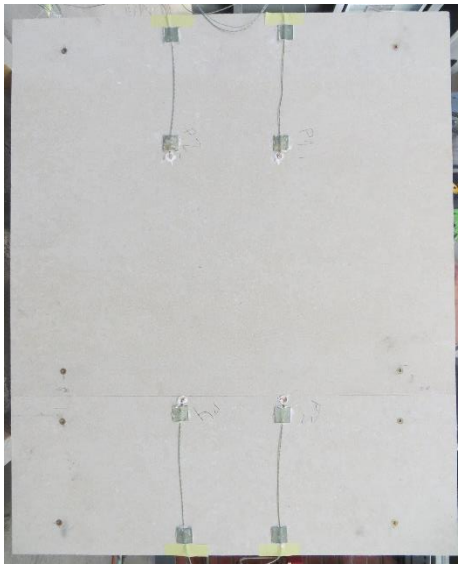

Fig. 2.30 HPC slab with protective plates.

Fig. 2.31 HPC with 18 mm of protective plate after 120 minutes of ISO-fire exposure.

There is limited information on methods to prevent spalling. Although much effort has been paid to investigate the effects of PP-fibers and protective lining, the protective methods still have to be validated by fire resistance tests. Because of the unavailability of validated numerical models, fire safe design is very costly.

2.6 Knowledge gaps

Explosive spalling in fire is one of the major concerns especially in the use of HPC and much experimental research has been performed to investigate the governing factors. Despite many discrepancies and contradictions in the observed effects, the high pore pressure in HPC during heating is widely considered as one important reason why HPC is more susceptible to spalling than OPC. From the preceding state-of-the-art review, it is clear that explosive spalling is not purely a result of pore pressure and that the thermal stress and external stress also influence the susceptibility to spalling.

To predict explosive spalling and to evaluate the effects of protective methods, a detailed study and analysis is required considering permeability, moisture content, heating rate, external loading and other features such as the use of PP-fibers and protective linings. Based on the experimental observations and the theoretical models, a detailed numerical model needs to be developed which is capable of accounting for all of these factors and must be the focus of future work. Such a model will facilitate the fire safety design and provide guidelines for further experiments. Following are some of the tasks to close the current knowledge gaps on prediction of explosive spalling and the protective methods:

1. A reliable Thermo-hydro model is to be developed for the prediction of pore pressure in concrete. The effect of moisture content and PP-fibers should be considered. This requires experimental studies on the permeability of concrete, the measurement of permeability of HPC with various types and amounts of PP-fibers will be carried out.
2. A spalling model based on the spalling criterion for prediction will be proposed. From the previous review of spalling mechanisms, such a criterion must use a combined stress approach and should account for pore pressure, thermal stress and external loads. The spalling model will be validated against test results, spalling time and depth will be compared to the test results.
3. Parametric studies will be performed using the validated spalling model. The influence of moisture content, heating rate, external loads, concrete strength and permeability on explosive spalling will be studied. Some contradictive observations in tests will also be discussed in this framework.
4. Using the validated spalling model, the use of protective methods will be evaluated. And a guideline for using PP-fibers will be proposed with respect to the type and amount of fibers. The spalling model should be able to quantify the thickness of protective linings for various design scenarios, based on the thermal properties of the insulation material and the properties of the concrete. The numerical spalling model based on the spalling criterion will facilitate fire safety design of concrete structures considering spalling.

3. Thermo-hydro Model

3.1 Introduction

A review of literature reported in Chapter 2 has concluded that the pore pressure is one of the most influential factors for concrete spalling in fire. The mechanism based on combined action of thermal stress and pore pressure by Zhukov, suggests that stresses resulting from pore pressure can be superimposed with other induced stresses such as thermal stress and external loads. The combined stresses can result in explosive spalling during heating if the resistance limit of concrete is exceeded. In this framework, pore pressure acts as the trigger of spalling, so the evaluation of pore pressure has an important role in predicting explosive spalling of dense concrete (e.g. HPC) in fire. This chapter describes a numerical Thermo-hydro model for the calculation of pore pressure developed within the concrete.

To simulate the pore pressure, the concrete is treated as a porous material. In general, the concrete material can be modeled as three phases, solid, liquid and gaseous, and accordingly three components: the solid matrix, water and vapor. Based on the liquid-vapor equilibrium, the heat and mass transfer process in concrete can be calculated by a previously developed theory based on the thermo-dynamic properties of water (Bazant 1979). Due to the complexity of the problem and the fact that explosive spalling occurs usually perpendicular to the heating surface, the current simulation is in one-dimensional or axisymmetric geometry. For this purpose, the heat transfer is simulated in the one-dimensional concrete section, the temperature distribution will serve as input for the pore pressure simulation. A one-dimensional Thermo-hydro model (TH-model) is employed to calculate the pore pressure inside the concrete. The governing equations will be given in following Section 3.2.

As shown in Chapter 2, permeability is the dominating factor for the pore pressure in concrete and increases generally with temperature. However, some test results have shown a significant drop in permeability in the temperature range from 150 °C to 250 °C. To study the effect of temperatures on permeability, some permeability measurements were carried out. In addition, the influence from PP-fibers on permeability has been investigated, as shown in Section 3.3. Using these test results, a permeability model is proposed in Section 3.4. The proposed permeability model considers the moisture content and effects of PP-fibers. It can be seen that besides the added amount of PP-fibers, their geometry influences the permeability as well. Using this permeability model, the TH-model was validated against the pore pressure measured in tests, and the results have been validated against test results.

Using the validated TH-model, the effect of parameters such as moisture content and addition of PP-fibers was examined (Section 3.5). The parameter studies were aimed at investigating the main factors governing the pore pressure and validating the selected spalling mechanism. Full details are presented in this chapter.

3.2 Calculation model and governing equations

The moisture in concrete evaporates during heating, the generated high pore pressure will drive the air and water vapor to flow and mass diffusion of water vapor enhances the evaporation rates as well. The whole process can be described in three basic mechanisms: heat conduction in the cross section, the diffusion of the gaseous components and the pressure driven convective flow governed by Darcy's law (Sahota 1979). Most of the heat and mass transfer models take the similar assumptions of moisture migration, according to Fick's second law with concentration-dependent diffusion coefficient (Harmathy 1969, 1971). The

properties of concrete with respect to the transfer of moisture at high temperature is very complex, for practical purpose the calculation of pore pressure are mainly based on simplified methods (Bazant 1978).

The proposed Thermo-hydro model treats the governing heat and mass transfer equations similar to the considerations by Dwaikat and Kodur (2009), air and water vapor are regarded as ideal gases, so that Darcy's law holds for the gases. The model discretizes the concrete section into a number of elements and calculates the pore pressure in concrete exposed to fire, and the calculations are carried out at time steps (discrete-time). At each time step, thermal-hydro analysis is performed in two steps; heat transfer and pore pressure calculations. The following governing equations and boundary conditions describe the whole calculation scheme.

3.2.1 Heat transfer

The first step is to obtain the temperature distribution in the concrete section. In a one-dimensional case, the heat transfer is the only axis and there is no heat escape from the sides (perfect insulation). According to Fourier's law of heat conduction, for a one-dimensional element with constraint section, as shown in Fig. 3.1, Dwaikat and Kodur (2009) suggested the governing heat transfer equation:

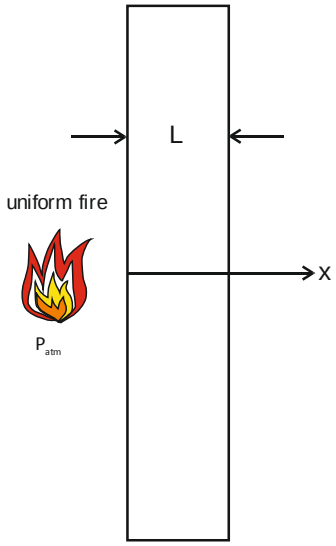

Fig. 3.1 Plane geometry.

$$\frac{\partial(k(x)\partial T/\partial x)}{\partial x}+Q=c_{\rho}\rho\frac{\partial T}{\partial t} \qquad 3.1$$

Where k is the thermal conductivity, c_p the specific heat, ρ the density of concrete, T the temperature in Kelvin, t the time in second and Q the heat source.

The boundary conditions (BC) for fire-exposure boundary are prescribed as:

$$k\frac{\partial T}{\partial x}=-h_{\mathrm{f}}\left(T-T_{\mathrm{BCf}}\right) \qquad 3.2$$

The heat flux at the unexposed boundary is given by:

$$k\frac{\partial T}{\partial x} = -h_{\mathrm{c}}(T - T_{\mathrm{BC0}}) \tag{3.3}$$

Where h_f is the transfer coefficient of the fire exposure side and h_c is the heat transfer coefficients of the unexposed side. T_{BCf} and T_{BC0} are the boundary temperatures of the fire exposure side and the unexposed side. Heat transfer coefficients h_f of 25 W/m^{2}K and h_c of 9 W/m^{2}K are suggested by Dwaikat and Kodur according to Eurocode 2.

The thermal conductivity in W/m/K is taken as the upper limit according to Eurocode 2:

$$k = 2 - 0.2451\frac{\theta}{100} + 0.0107\left(\frac{\theta}{100}\right)^2 \tag{3.4}$$

The density of concrete varies with temperature due to the water loss as defined by Eurocode 2:

$$\rho = \begin{cases} \rho_{\mathrm{con}}(20°\mathrm{C}) & 20°\mathrm{C} \le \theta \le 115°\mathrm{C} \\ \rho_{\mathrm{con}}(20°\mathrm{C})\left(1 - 0.02\dfrac{(\theta - 115)}{85}\right) & 115°\mathrm{C} < \theta \le 100°\mathrm{C} \\ \rho_{\mathrm{con}}(20°\mathrm{C})\left(0.98 - 0.03\dfrac{(\theta - 200)}{200}\right) & 200°\mathrm{C} < \theta \le 400°\mathrm{C} \\ \rho_{\mathrm{con}}(20°\mathrm{C})\left(0.95 - 0.07\dfrac{(\theta - 400)}{800}\right) & 400°\mathrm{C} < \theta \le 1200°\mathrm{C} \end{cases} \tag{3.5}$$

Where θ is the concrete temperature in Celsius and ρ_{con}(20 °C) is the density of concrete at 20 °C.

The specific heat of dry concrete is suggested in Eurocode 2 in J/kg/K by:

$$c_{\mathrm{p}} = \begin{cases} 900 & 20\ ^o\mathrm{C} \le \theta \le 100\ ^o\mathrm{C} \\ 900 + \theta - 100 & 100\ ^o\mathrm{C} < \theta \le 200\ ^o\mathrm{C} \\ 1000 + \dfrac{\theta - 200}{2} & 200\ ^o\mathrm{C} < \theta \le 400\ ^o\mathrm{C} \\ 1100 & 400\ ^o\mathrm{C} < \theta \le 1200\ ^o\mathrm{C} \end{cases} \tag{3.6}$$

Where θ is the concrete temperature in Celsius. The moisture content is considered by a simplified increase in in the heat capacity with a linear interpolation as shown in Fig. 3.2. In calculation, the specific heat will be determined by the local moisture content. The effect of vaporization will be considered and the temperature plateau is simulated. The validation will be shown in Section 3.5.1.

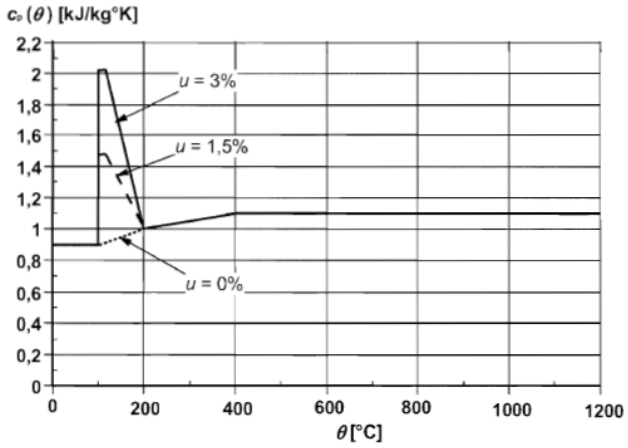

Fig. 3.2 Specific heat, $c_p(\theta)$, as a function of temperature at 3 different moisture contents (Eurocode 2).

The heat source in Equation 3.1 considers the radiation energy on the heated surface of concrete. The radiation heat transfer can be calculated by Stefan-Boltzmann's law:

$$Q = -\varepsilon\sigma_b T^4 \tag{3.7}$$

Where T is the surface temperature of concrete in Kelvin, σ_b is the Stefan-Boltzmann's constant equal to 5.67×10^{-8} W/m^2/K^4, ε is the emission rate of concrete. Since the emissivity of concrete takes as 0.88-0.93 in the design standard (Incropera and Dewitt 2002), ε is selected as 0.88 in this model.

To get a reliable simulation of temperatures in concrete, the model is validated against the measurement of temperatures in Section 3.5. The simulated temperature distribution is used to calculate the pore pressure in the concrete.

3.2.2 Pore pressure calculation

The coupled moisture and heat transfer in concrete is known as irreversible thermodynamics, Bazant (1979) suggested that the transfer relation can be simplified as:

$$J = -\lambda \mathrm{grad} P_v \tag{3.8}$$

Where J is the mass flux to the gradient of pore pressure P_v. Equation 3.8 is the same as Darcy's law and λ can be taken as Darcy's coefficient. Darcy's law is normally applicable to saturated porous material, based on test data. As for the non-saturated mass transfer in concrete, Bazant (1979) suggested that Equation 3.8 can be extended to simulate the moisture and heat transfer, when P is taken as the pore pressure P_v, rather than the liquid (capillary) pressure. Using the pore pressure P_v as the driving force of the moisture transfer. The dehydrated water released into the pores during heating will be reflected in the conservation of mass. In this way, the coupled moisture and heat transfer in concrete are governed by four principles, as Dwaikat and Kodur (2009) proposed, namely:

- Conservation of mass for liquid water,
- Ideal gas law,
- The total volume of all components in a unit volume,
- Conservation of mass for water vapor.

3.2.2.1 Conservation of mass for liquid water

The moisture in the forms of evaporated water, liquid water and the dehydrated water in concrete is described by the conservation of mass of unit volume:

$$m_E = m_{LW0} - m_L + m_D \tag{3.9}$$

Differentiating with respect to time,

$$\frac{dm_E}{dt} = -\frac{dm_L}{dt} + \frac{dm_D}{dt} \tag{3.10}$$

According to the chain rule, Equation 3.10 can be written as

$$\frac{dm_E}{dt} = -\frac{dm_L}{dP_V}\frac{dP_V}{dt} - \frac{dm_L}{dT}\frac{dT}{dt} + \frac{dm_D}{dT}\frac{dT}{dt} \tag{3.11}$$

Where m_E is the evaporate water mass, m_{LW0} is the initial mass of liquid water, m_L denotes the mass of liquid water, m_D is the mass of liquid water that formed due to dehydration, T is the temperature and t represents time.

3.2.2.2 Ideal gas law

Water vapor is considered as an ideal gas, which is valid for most engineering applications (Harmathy 1969). The ideas gas law relates the pressure, temperature and volume, for water vapor it can be expressed as:

$$P_V V_V = n_V R T \tag{3.12}$$

In which $n_V = \frac{m_V}{M}$,

Hence,

$$P_V = \frac{R}{M}\frac{m_V T}{V_V} \tag{3.13}$$

Differentiating with respect to time,

$$\frac{dP_V}{dt} = \frac{R}{M}\left(\frac{V_V(dm_V/dt) + m_V V_V(dT/dt) - m_V T(dV_V/dt)}{V_v^2}\right) \tag{3.14}$$

Rearranging Equation 3.14:

$$\frac{dm_V}{dt} = \frac{V_V M}{RT}\frac{dP_V}{dt} - \frac{m_V}{T}\frac{dT}{dt} + \frac{m_V}{V_V}\frac{dV_V}{dt} \tag{3.15}$$

Where m_V is the mass of water vapor, R is the gas constant equal to 8.31446 J/mol/K, n_V the number of moles of water vapor, M the molar mass of water, V_V the volume of water vapor and T is the temperature in Kelvin.

3.2.2.3 Conservation of volume for all components

For a unit volume of concrete, the sum of the volume fractions of all phases equals unity, the conservation of volume can be expressed as:

$$V_{\mathrm{V}} + V_{\mathrm{L}} + (V_{\mathrm{S0}} - V_{\mathrm{D}}) = 1 \tag{3.16}$$

Rearranging Equation 3.16 gives:

$$V_{\mathrm{V}} = 1 - V_{\mathrm{L}} - (V_{\mathrm{S0}} - V_{\mathrm{D}}) \tag{3.17}$$

Where V_{L} is the volume fraction of liquid water, V_{S0} is the initial volume fraction of solid, V_{D} the volume fraction of dehydrated liquid water and ρ_{L} represents the density of liquid water.

Using the volume-mass-density relationship, Equation 3.17 changes to:

$$V_{\mathrm{V}} = 1 - \frac{m_{\mathrm{L}}}{\rho_{\mathrm{L}}} - (V_{\mathrm{S0}} - \frac{m_{\mathrm{D}}}{\rho_{\mathrm{L}}}) \tag{3.18}$$

Differentiating both sides of Equation 3.18 with respect to time, the following equation will be obtained:

$$\frac{dV_{\mathrm{V}}}{dt} = \frac{1}{\rho_{\mathrm{L}}}\left(\frac{dm_{\mathrm{D}}}{dt} - \frac{dm_{\mathrm{L}}}{dt}\right) - \frac{1}{\rho_{\mathrm{L}}^2}\frac{d\rho_{\mathrm{L}}}{dT}\frac{dT}{dt}(m_{\mathrm{D}} - m_{\mathrm{L}}) \tag{3.19}$$

Substituting Equation 3.10 into Equation 3.19 results in:

$$\frac{dV_{\mathrm{V}}}{dt} = \frac{1}{\rho_{L}}\left(\frac{dm_{\mathrm{E}}}{dt}\right) - \frac{1}{\rho_{\mathrm{L}}^2}\frac{d\rho_{\mathrm{L}}}{dT}\frac{dT}{dt}(m_{\mathrm{D}} - m_{\mathrm{L}}) \tag{3.20}$$

By substituting Equation 3.20 in Equation 3.15, the following equation can be obtained:

$$\frac{dm_{\mathrm{V}}}{dt} = \frac{V_{\mathrm{V}}M}{RT}\frac{dP_{\mathrm{V}}}{dt} - \frac{m_{\mathrm{V}}}{T}\frac{dT}{dt} + \frac{m_{\mathrm{V}}}{V_{\mathrm{V}}\rho_{\mathrm{L}}}\left(\frac{dm_{\mathrm{E}}}{dt} - \frac{1}{\rho_{\mathrm{L}}}\frac{d\rho_{\mathrm{L}}}{dT}\frac{dT}{dt}(m_{\mathrm{D}} - m_{\mathrm{L}})\right) \tag{3.21}$$

3.2.2.4 Conservation of mass of water vapor

As Bazant (1979) proposed the basic theory is simplified by applying Darcy's law for the moisture transfer, and the dehydrated water in concrete must be reflected in the condition of conservation of water vapor. The following equation can be obtained for one-dimensional problems:

$$\frac{dm_{\mathrm{V}}}{dt} = -\frac{dJ}{dx} + \frac{dm_{\mathrm{E}}}{dt} \tag{3.22}$$

In which J is the mass flux of moisture as a linear combination of the gradient of pore pressure P_v. Bazant proposed that J can be reflected in this simplified model as Equation 3.8, for the one-dimensional problem, the relation can be expressed as:

$$J = -\lambda(\frac{\mathrm{d}P_v}{dx}) \tag{3.23}$$

Based on the mass flux relationship, Equation 3.22 can be written as:

$$\frac{dm_V}{dt} = -\frac{d(\lambda \frac{dP_V}{dx})}{dx} + \frac{dm_E}{dt} \tag{3.33}$$

Darcy's coefficient λ can be written as:

$$\lambda = m_V \frac{k_T}{\mu_V} \tag{3.34}$$

Where k_T is the permeability of concrete at temperature T, and μ_V the dynamic viscosity of water vapor. In Equation 3.34, Darcy's coefficient λ is computed by the viscosity of water vapor, although mass transfer is considered driven by the pore pressure, the existence of liquid water can still influence the flow. The observation in the permeability tests shows that the effects of liquid water should be considered, details will be discussed further in Section 3.4.

Substituting λ in Equation 3.34, Equation 3.33 can be written as:

$$\frac{dm_V}{dt} = \frac{d\left(\left(m_V \frac{k_T}{\mu_V}\right)\frac{dP_V}{dx}\right)}{dx} + \frac{dm_E}{dt} \tag{3.35}$$

By substituting Equation 3.21, Equation 3.35 can be written as:

$$\frac{V_V M}{RT}\frac{dP_V}{dt} - \frac{m_V}{T}\frac{dT}{dt} + \frac{m_V}{V_V \rho_L}\left(\frac{dm_E}{dt} - \frac{1}{\rho_L}\frac{d\rho_L}{dT}\frac{dT}{dt}(m_D - m_L)\right) = \frac{d\left(\left(m_V \frac{k_T}{\mu_V}\right)\frac{dP_V}{dx}\right)}{dx} + \frac{dm_E}{dt} \tag{3.36}$$

Hence, the governing differential equation for pore pressure is given by:

$$\frac{V_V M}{RT}\frac{dP_V}{dt} = \frac{d\left(\left(m_V \frac{k_T}{\mu_V}\right)\frac{dP_V}{dx}\right)}{dx} + (1 - \frac{m_V}{V_V \rho_L})\frac{dm_E}{dt} + \frac{m_V}{T}\frac{dT}{dt} + \frac{m_V}{V_V \rho_L^2}\frac{d\rho_L}{dT}\frac{dT}{dt}(m_D - m_L) \tag{3.37}$$

Using Equation 3.11, Equation 3.37 can be written as:

$$\begin{aligned}\frac{V_V M}{RT}\frac{dP_V}{dt} = {} & \frac{d\left(\left(m_V \frac{k_T}{\mu_V}\right)\frac{dP_V}{dx}\right)}{dx} + (1 - \frac{m_V}{V_V \rho_L})(-\frac{dm_L}{dP_V}\frac{dP_V}{dt} - \frac{dm_L}{dT}\frac{dT}{dt} + \frac{dm_D}{dT}\frac{dT}{dt}) \\ & + \frac{m_V}{T}\frac{dT}{dt} + \frac{m_V}{V_V \rho_L^2}\frac{d\rho_L}{dT}\frac{dT}{dt}(m_D - m_L)\end{aligned} \tag{3.38}$$

Rearranging Equation 3.38 gives:

$$\begin{aligned}&\left((1 - \frac{m_V}{V_V \rho_L})\frac{dm_L}{dP_V} + \frac{V_V M}{RT}\right)\frac{dP_V}{dt} \\ &= \frac{d\left(\left(m_V \frac{k_T}{\mu_V}\right)\frac{dP_V}{dx}\right)}{dx} + \left((1 - \frac{m_V}{V_V \rho_L})(-\frac{dm_L}{dT} + \frac{dm_D}{dT}) + \frac{m_V}{T} + \frac{m_V}{V_V \rho_L^2}\frac{d\rho_L}{dT}(m_D - m_L)\right)\frac{dT}{dt}\end{aligned} \tag{3.39}$$

Equation 3.39 can be simplified by introducing three parameters, A, B, and C as follows:

$$A\frac{dP_V}{dt} = \frac{d}{dx}B\frac{dP_V}{dx} + C \tag{3.40}$$

Where

$$A = \left((1 - \frac{m_V}{V_V \rho_L}) \frac{dm_L}{dP_V} + \frac{V_V M}{RT} \right)$$

$$B = m_V \frac{k_T}{\mu_V}$$

$$C = \left((1 - \frac{m_V}{V_V \rho_L})(-\frac{dm_L}{dT} + \frac{dm_D}{dT}) + \frac{m_V}{T} + \frac{m_V}{V_V \rho_L^2} \frac{d\rho_L}{dT} (m_D - m_L) \right) \frac{dT}{dt}$$

3.2.2.5 Initial state and boundary conditions

The initial pore pressure P_{V0} is given by

$$P_{V0} = \phi P_{S0} \tag{3.41}$$

Where Φ is the initial relative humidity in the concrete and P_{S0} the initial saturation pressure, which can be computed based on the initial temperature of concrete.

As for the boundary conditions, on the surface of concrete, the vapor pressure is assumed fixed and equal to initial pore pressure P_{V0}, due to the lack of information on the changes in the surrounding environment during heating.

3.2.2.6 Constitutive relationships

Bazant and Thouguthai (1978) developed the semi empirical isotherms to predict the liquid water inside the concrete, which was described as a function of pore pressure and temperature. The main assumption in isotherms made by Bazant (1979) is that water in concrete is capillary water (adsorbed water is ignored). Bazant has showed that the adsorbed water significantly decreases at elevated temperatures and thus capillary water becomes the dominant state of water in HPC. The relationship of pore pressure, water content and temperature must further be given for unsaturated concrete, Bazant (1979) proposed coefficients for liquid water inside the concrete based on the best fit of test results. The method was presented by Dwaikat and Kodur (2009), the mass of liquid water can be given as:

$$m_L = \begin{cases} \rho_c \left(\frac{m_0 P_V}{\rho_c P_S}\right)^{1/m(T)} & , \frac{P_V}{P_S} \le 0.96 \\ m_{0.96} + (\frac{P_V}{P_S} - 0.96)\frac{m_{1.04} - m_{0.96}}{0.08} & , 0.96 < \frac{P_V}{P_S} < 1.04 \\ m_{1.04}\left(1 + 0.12(\frac{P_V}{P_S} - 1.04)\right) & , \frac{P_V}{P_S} \ge 1.04 \end{cases} \tag{3.42}$$

When (P_V/P_S) exceeds 100 %, the case represents the condensation of water vapor. According to Bazant's isotherms, the mass of liquid water m_L exceeds the saturation mass of liquid water m_{L0} at room

temperature when the relative humidity exceeds 100 %, because of the condensation of water vapor transferred to the high pressure region. The increase in pressure is associated with an increase in concrete porosity due to elastic deformation and cracking. This provides more space for the increase in the mass of liquid water at room temperature, so the mass of liquid water m_L will increase further with P_V.

Different from Dwaikat's consideration, the liquid water transfer is considered by the change of mass of liquid water m_L to the gradient of pore pressure P_v. The liquid water change will be transferred to the bordering elements. Differentiating Equation 3.42 with respects to pore pressure and time can be given as:

$$\frac{dm_L}{dP_V}=\begin{cases}\dfrac{m_0}{m(T)P_S}\left(\dfrac{m_0P_V}{\rho_cP_S}\right)^{1/m(T)-1} & ,\dfrac{P_V}{P_S}\le 0.96\\ \dfrac{m_{1.04}-m_{0.96}}{0.08} & ,0.96<\dfrac{P_V}{P_S}<1.04\\ 0.12\dfrac{m_{1.04}}{P_S} & ,\dfrac{P_V}{P_S}\ge 1.04\end{cases} \tag{3.43}$$

$$\frac{dm_L}{dT}=\begin{cases}-m_L\left(\dfrac{\dfrac{dm(T)}{dT}}{m(T)^2}\ln\left(\dfrac{m_0P_V}{\rho_cP_S}\right)+\dfrac{\dfrac{dP_S}{dT}}{m(T)P_S}\right) & ,\dfrac{P_V}{P_S}\le 0.96\\ \dfrac{dm_{0.96}}{dT}-\dfrac{P_V\dfrac{dP_S}{dT}}{P_S^2}\left(\dfrac{m_{1.04}-m_{0.96}}{0.08}\right)+\mathrm{X} & ,0.96<\dfrac{P_V}{P_S}<1.04\\ \dfrac{dm_{1.04}}{dT}\left(1+0.12\left(\dfrac{P_V}{P_S}-1.04\right)\right)-0.12\dfrac{m_{1.04}P_V\dfrac{dP_S}{dT}}{P_S^2} & ,\dfrac{P_V}{P_S}\ge 1.04\end{cases} \tag{3.44}$$

Where ρ_c is the mass of cement per unit volume of concrete and P_S the saturation pressure. Some terms above are given by the following equations:

$$m(T)=1.04-\frac{(T+10)^2}{22.3(T_0+10)^2+(T+10)^2} \tag{3.45}$$

$$m_{0.96}=\rho_c\left(0.96\frac{m_0}{\rho_c}\right)^{1/m(T)} \tag{3.46}$$

$$m_{1.04}=m_0+m_D \tag{3.47}$$

$$\frac{dm(T)}{dT}=-\frac{2(T+10)(22.3(T_0+10)^2+(T+10)^2)-2(T+10)^3}{22.3(T_0+10)^2+(T+10)^2} \tag{3.48}$$

$$\frac{dm_{0.96}}{dT}=-m_{0.96}\frac{\ln\left(0.96\dfrac{m_0}{\rho_c}\right)\dfrac{dm(T)}{dT}}{(m(T))^2} \tag{3.49}$$

$$\frac{dm_{1.04}}{dT}=\frac{(m_0/\rho_L)}{(1-V_{S0})}\frac{d\rho_L}{dT}+\frac{dm_D}{dT} \tag{3.50}$$

$$X = \left(\frac{P_V}{P_S} - 0.96\right)\left(\frac{\frac{dm_{1.04}}{dT} - \frac{dm_{0.96}}{dT}}{0.08}\right) \quad 3.51$$

In reality, the concrete is not always saturated, especially the pre-dried specimens and the concrete elements in practice. The dehydrated water m_D is not always enough to fill the concrete, even when liquid transfer is considered, and the saturation assumption may overestimate the total moisture content in concrete. Thus, in calculation, the moisture concentration is not considered as mass of water for saturation. The m_0 will be determined by the actual moisture content at initial temperature T_0.

The transition region in Equation 3.43 is restricted to 0.96 and 1.04, which leaves room for a smooth transition between saturated and non-saturated regimes. As validated by test results, the transition has been assumed as straight lines connecting the values of (P_V/P_S) = 0.96 and 1.04 at the temperature T. So Equation 3.43 holds for semi-saturated as well.

Two types of water; namely, evaporable and non-evaporable water, are present in cement paste. Evaporable water is lost when cement paste is oven-dried at 110 °C, while non-evaporable is lost during the dehydration process at higher temperature. As shown in Equation 3.9, the liquid water formed due to dehydration influences the evaporated water during heating. Dehydration of cement paste is a complex phenomenon that depends on many factors including temperature and chemical composition of the cement paste itself. Even to date, such phenomenon is not completely understood. The amount of non-evaporable water, which is chemically bound with cement, increases with the degree of hydration of the concrete mix. Thus for spalling predictions, according to Dwaikat, it would be conservative to assume that the concrete is fully hydrated. In the TH-model, dehydration of cement paste is considered based on the simplified approach by Bazant and Kaplan (1996). In this approach (where concrete is assumed to be fully hydrated at room temperature) the mass of dehydrated water, m_D, can be given as:

$$m_D = \begin{cases} 0 & ,T \le 100°C \\ 0.04\rho_c \dfrac{T-100}{100} & ,100°C < T \le 700°C \\ 0.24\rho_c & ,T > 700°C \end{cases} \quad 3.52$$

The proposed Thermo-dydro model describes the heat and mass transfer in a simplified method after Bazant. Darcy's law is acceptable to extend to non-saturated concrete if the permeability is not regarded as a property of the porous medium alone but as a factor that depends also on some characteristics of the fluid (Harmathy 1969). To propose a valid permeability model that accounts for the moisture content and the adding of PP-fibers, some tests are carried out at ETH Zürich (Klingsch 2013). Based on the test data, a permeability model will be proposed for the TH-model.

3.3 Permeability test

In the experimental study of explosive spalling, concrete is treated as a porous medium. The permeability is an important property for the porous medium, which describes the conductivity of concrete with respect to fluid (vapor or liquid) flow. Experiments and numerical studies have shown that the low permeability of HPC makes it more susceptible to explosive spalling (Khoury 2000, Klingsch 2014). To study the explosive spalling, various experimental studies have been carried out and the test results have shown that the

permeability of concrete varies with temperature and pore pressure. In addition, Jacobs (1994) and Harmathy (1969) indicated that the permeability is significantly influenced by moisture content. As discussed above, the moisture content is critical in the TH-model simplified by Bazant, because the characteristics of the fluid influence the mass transfer. Another important aspect from the viewpoint of explosive spalling is the addition of PP-fibers, which increase the permeability above the melting point. These effects should be investigated to predict the permeability of concrete at high temperature. Therefore, a program of experimental work was performed to study the influencing factors on permeability and to provide input for a permeability model (Section 3.5).

The permeability of concrete was measured both in the residual state and at elevated temperatures. For the residual permeability, the Torrent permeability tester was used (Proceq co. 2007), which can determine the vapor permeability very quick and reliable. Nevertheless, it is important to measure the material properties directly at elevated temperatures. Moreover, the comparison of the test results is critical for assessing two methods.

The effects of temperature, moisture content, the type and amount of PP-fibers are studied. The experimental work will be discussed in following sections, Table 3.1 presents a summary of test carried out for various targets.

Table 3.1 Summary of permeability tests.

Test	Group of tests	Target	Section
Hot and residual permeability of HPC	2 mixtures with PP-fibers	Effects from temperatures measured by two test methods.	3.3.1
Residual permeability of OPC and HPC with various moisture contents.	18 (3 mixtures, 6 pre-drying periods)	Effects from moisture content on the permeability of concrete.	3.3.3
Residual permeability of HPC with various types and amounts of PP-fibers.	8 mixtures with or without PP-fibers	Effects of fibers on the permeability of concrete	3.3.4

3.3.1 Test methods

3.3.1.1 Hot permeability

To measure the permeability at high temperature, a test setup was developed at ETH Zürich as shown in Fig. 3.3. A smooth concrete disk was put between the two lids and sealed with silicone, leakage openings are applied in the upper and lower lid. In case of any leakage due to insufficient sealing or decomposition of the silicone, the test can be stopped manually. The permeability was determined by inserting compressed air into the upper lid and the volume of air penetrated via the concrete disk was measured for a period of time.

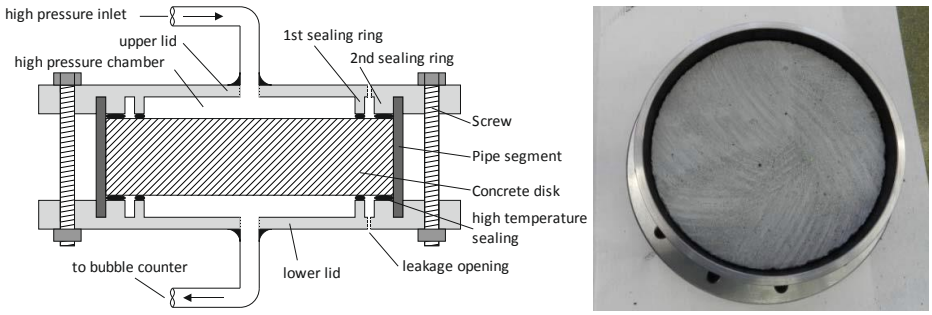

Fig. 3.3 Setup to measure the gas flow of a specimen.

The specimen with the lids was placed into an electric furnace and heated to desired temperature levels. After conditioning time, compressed air with different pressure levels was compressed through the concrete disk. The volume of air penetrated through the concrete was measured with a bubble counter. The hot permeability of the concrete specimen can be computed according to Darcy´s law, as given in the following equation:

$$k_T = \frac{Q\eta l}{A \bullet \Delta P} \qquad 3.53$$

Where k_T is the permeability based on the gas viscosity, Q the volume of flow through the concrete during unit time, η the dynamic viscosity of air, l the thickness of the concrete disc, A the cross section of the concrete disc and ΔP difference in pressure.

The entire test setup is shown in Fig. 3.4. The specimen was heated and compressed in the furnace, the permeability was measured directly at elevated temperature and the test results will be compared with the residual permeability measured with Torrent method after cooling (Section 3.3.1.2).

Fig. 3.4 Furnace including permeability testing device.

3.3.1.2 Residual permeability

As for the residual permeability, the permeability of concrete was analyzed after cooling from high temperatures according to the Torrent method, as shown in Fig. 3.5.

Fig. 3.5 Residual permeability measuring device according to the Torrent method.

The permeability is measured by placing a low pressure cap onto one concrete disk and outgassing this cap. The permeability is then determined by measuring the pressure difference and the measured flow of air between both chambers. The measured permeability is displayed directly on the device. The calculation of the gas permeability is based on the following equation (Torrent 2006):

$$k_T = \left(\frac{V_V}{A}\right)^2 \frac{\eta}{2\varepsilon P_a} \left(\frac{\ln\left(\frac{P_a + P}{P_a - P}\frac{P_a - P_0}{P_a + P_0}\right)}{\sqrt{t} - \sqrt{t_0}} \right)^2 \qquad 3.54$$

Where k_T is the permeability based on the gas viscosity, V_c the volume of the inner testing chamber, A the cross section area of the inner testing chamber. The dynamic viscosity of air η is taken as 2.0×10^{-5} Ns/m^2 at 20 °C, ε the estimated porosity of the concrete taken as 0.15, P_a the ambient air pressure taken as 96 kPa. P_0 is the pressure at the beginning of the test in the inner testing chamber, P the pressure in the inner testing chamber at time t, t_0 the time at the beginning of testing and t the time at the end of testing.

The specimens were heated in the furnace and measured after the surface temperature was lower than 100 °C to protect the sealing rings of the device. In addition, the mass loss of the specimen was measured. After each measurement, the specimen was heated to the next temperature level.

3.3.2 Comparison of the test methods

The above-mentioned test methods were used to study the effects of temperature on permeability of concrete. To validate the methods, the results from the hot and residual permeability were compared. Residual permeability of various mixtures of HPC was measured by Torrent method, however, only limited test data of hot permeability were available for use. To compare with the residual permeability, two mixtures were chosen, as listed in Table 3.2, both contained Type 2 PP-fibers, which had a length of l = 6 mm and a diameter of $\varnothing$ = 18 µm.

Table 3.2 Mixtures of studied concrete for comparing hot and residual permeability.

Components	Units	M1P1	M1P2
Cement CEM I 52.5 R	kg/m^3	832	
Quartz sand H31	kg/m^3	975	
Micro silica	kg/m^3	135	
Quartz powder W3	kg/m^3	207	
Water	kg/m^3	166	
Superplasticizer (BASF Glenium ACE)	kg/m^3	29.4	
Steel fibers	kg/m^3	192	
PP-fibers (Type 2)	kg/m^3	1	2
W/C ratio	-	0.20	

The pressure level for hot permeability was chosen as 10 bar according to Klingsch (2015), and the pumped low pressure for Torrent method was fixed to 1 bar. In the experiments, the cylinders disks were cut from the cylinder with a thickness of 40 mm. The disks were polished both ends and dried at a temperature of 105 °C to a constant mass.

The permeability of M1P1 and M1P2 measured by two methods is shown in Fig. 3.6. It can be seen that the permeability increases generally with temperature; however, a drop is observed by both methods. This is attributed to the moisture content: in the temperature range from 105 °C to 250 °C, the moisture content will change due to the dehydration. Similar results were reported by Schneider (1989), in addition, Schneider showed that when the specimens were kept 50 hours at high temperature, the drop would disappear. This should be taken into account in the permeability model; details will be discussed in the next section. Both methods have shown that with more PP-fibers, the permeability will increase faster at high temperature, but at room temperature, the adding of PP-fibers does not lead to a significant change of initial permeability.

Between the two methods, at 105 °C, no differences in permeability were noticed. At higher temperature, the hot permeability is slightly higher than the residual permeability, because of the high pressure used in the hot tests. At 250 °C, the difference between the two methods was smaller. The hot permeability is too high to be measurable above 275°C. The difference in permeability is mainly in the drop range, because the higher pressure level in the hot permeability method results in a faster drying of moisture.

In general, the permeability measured by the two methods is comparable, the permeability of concrete increases with temperature. Both methods indicated the drop in permeability was related to the change of moisture content. The comparison validates the use of the Torrent method to study the influence of temperature on permeability. The difference between the two methods is mainly in the temperature range of permeability drop, due to the different pressure level. The Torrent method gives lower measured residual permeability than the hot permeability. Due to uncertainties and effort of the hot permeability measurement, the easily applicable Torrent method will be chosen to study the effects of moisture content and the type and amount of PP-fibers.

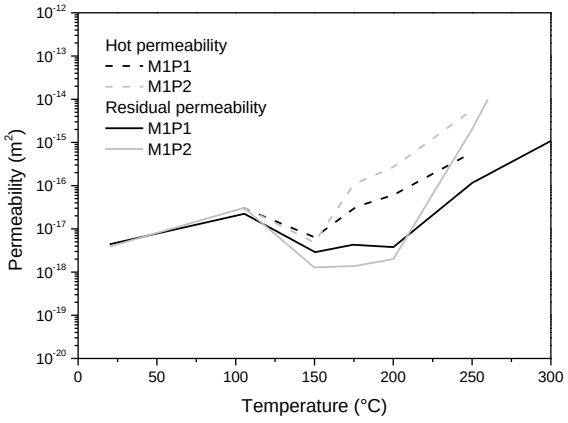

Fig. 3.6 Hot and residual permeability of concrete in comparison.

3.3.3 Permeability of concrete with different moisture content

Test results by Schneider (1989) have shown that permeability varied with the duration the specimens were kept at high temperature. After a long conditioning time, the permeability increased with temperature; however, when the specimen was kept shortly at high temperature, a dent was observed as shown in Fig. 3.6. The pattern of permeability is according to the tests related to the moisture content (Lu 2013). A long

conditioning time results in lower moisture content, the moisture flow is governed by vapor, the concrete is more permeable for vapor, because vapor viscosity is lower than that of liquid water. Tests by Jacobs (1994) showed as well that the permeability is dependent on the moisture content. But currently, no experiment has been performed to quantify the permeability of concrete in function of moisture content. To study the effect of moisture content, a series of permeability measurement has been carried out, the permeability of OPC (OPC_1), HPC (HPC_1) and HPC with PP-fibers (HPC_1_P2) were measured. Details are listed in Appendix A.

It is known that at room temperature, the permeability of concrete increases with the decrease of moisture content. This has been observed by Jacobs (1994) as well. At high temperature, the permeability of concrete is also influenced by the moisture content. With low moisture content, the permeability increases modestly and smoothly. With high moisture content, the permeability increases generally with temperature, yet drop and sudden increase of permeability were observed. Apart from the increase with temperature and pore pressure, the drop or decrease of permeability in some temperature ranges were correlated to the mass loss of the specimen, i.e. the change of moisture content.

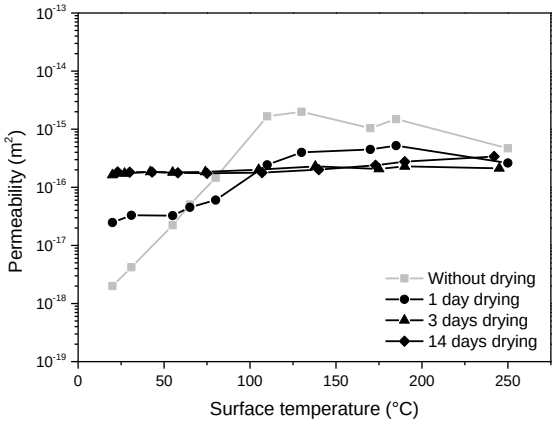

Fig. 3.7 Permeability of OPC_1 dried for various periods of time.

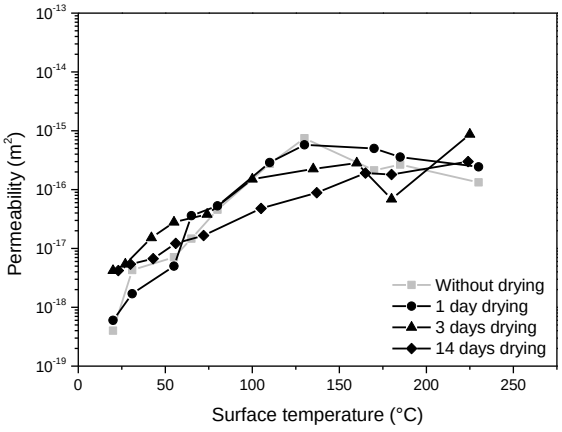

Fig. 3.8 Permeability of HPC_1 dried for various periods of time.

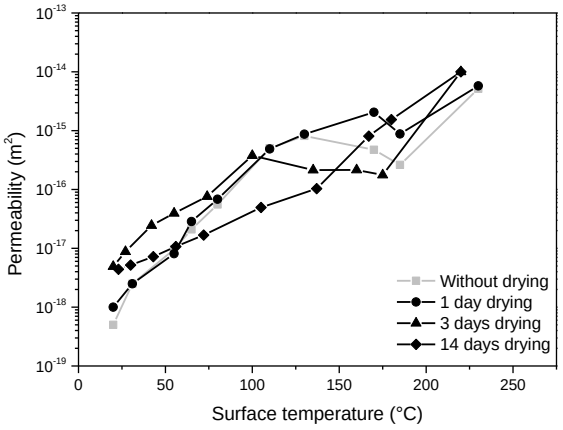

Fig. 3.9 Permeability of HPC_1_P2 dried for various periods of time.

For OPC, with high moisture content, the permeability increases significantly with temperature, and the drop in permeability can be observed. When it is pre-dried for more than three days, the permeability is almost constant as shown in Fig. 3.7. On the other hand, the permeability of HPC increases more significantly with temperature as shown in Fig. 3.8. Even after long pre-drying, the permeability of HPC is still influenced by the moisture content, because a lot of water is dehydrated at high temperatures. Fig. 3.9 shows the results of HPC with 2 kg/m^3 Type 2 PP-fibers. Above the melting point of the PP-fibers (160-170 °C) the permeability of HPC_1_P2 increases more significantly than that without PP-fibers. In addition, the moisture content influenced the effects from PP-fibers on permeability, with high moisture content the increase of permeability was slightly offset by the drop of permeability induced by the dehydrated water.

Permeability is related to temperature, pore pressure and moisture content. The effects of moisture content, such as the initial permeability and the drop during heating, must be taken into account in the permeability model. Based on the test results, a permeability model has been proposed in Section 3.4, which involves the temperature, pore pressure and moisture content. The effects of PP-fibers should be further studied with respect to the type and amount of fibers. To get a uniform temperature in the concrete in further tests, the specimen for residual method should be kept at least 1 hour in the furnace.

3.3.4 Effects of fibers on the permeability of concrete

Adding PP-fibers to HPC can prevent explosive spalling of concrete. It is a recommended protective method in Eurocode 2. As shown in the previous section, PP-fibers can increase permeability by melting at about 160-170 °C, as a result, the high pore pressure during heating can be relieved. Klingsch (2014) has reported that PP-fibers can reduce the risk of concrete spalling in fire, and that the type and amount of PP-fibers can influence their effect as protective method. However, no comprehensive permeability tests have been performed to study the effects from type and amount of PP-fibers. Therefore, tests on the permeability of concrete with various type and amount of PP-fibers was carried out, the results of these tests are taken as input for the permeability model, which is discussed in Section 3.4. To study the effects of fibers on the permeability of concrete, three types of PP-fibers with various amounts were added to the concrete HPC_1, the mixtures V2-V8 with various PP-fibers recipes were measured, and details are given in Appendix B.

From the test results of permeability with various types and amounts of PP-fibers, it can be seen that the permeability was increased by PP-fibers in the temperature range from 150 °C to 175 °C, corresponding to the melting point of PP-fibers. Using the environmental scanning electron microscope (ESEM), the change of PP-fibers with temperature is illustrated in Fig. 3.10 a) shows the PP-fibers in concrete at room temperature, the fibers were seen bounded to the concrete. b) shows the PP-fibers in concrete after being heated to 175 °C, some channels were built by the melting of PP-fibers, the melted fibers left some dark marks. After heating to 225 °C as shown in c), channels with the diameters of PP-fibers were observed, the fibers melt and flared away in the concrete. Considering the increasing temperature of permeability, the change of permeability is attributed to the channels from melting of PP-fibers. As shown by the permeability measurement, the effect starts from the melting point of PP-fibers.

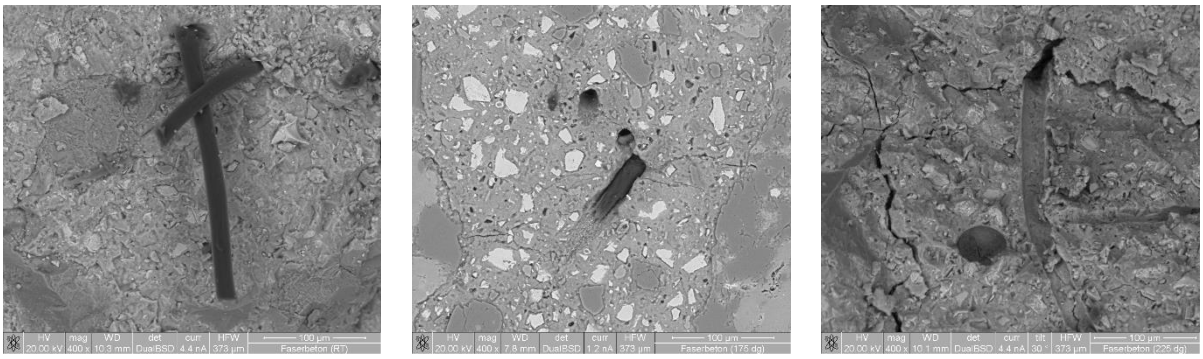

a) Without heating. b) Heated to 175 °C. c) Heated to 225 °C.

Fig. 3.10 ESEM observation on PP-fibers.

The amount of PP-fibers has a positive effect on the increase of permeability. The permeability measurements showed that the permeability of concrete increased more in the specimens with higher amounts of PP-fibers. With 1 kg/m^3 of PP-fibers, the permeability increase was modest, compared to that with 2 or 3 kg/m^3 of PP-fibers.

Together with the amount, the type of PP-fibers plays a role as well. With the amount of 1 kg/m^3, Type 2 (V5) increased the permeability faster than Type 1 (V2), as presented in Fig. 3.11. Above the melting point, 1 kg/m^3 of Type 2 increased the permeability and the drop due to moisture was prevented. On the other hand, the melting of Type 1 PP-fibers resulted in an increase of permeability as well, but the modest increase was not enough to accelerate the drying of water. The decrease of mass of V2 shown in Fig. 3.30 was slower, in the same temperature range, a drop in permeability was observed in the V2. With 1 kg/m^3, Type 2 presented better effects than Type 1.

With higher amounts, as shown in Fig. 3.13 and Fig. 3.15, the type of PP-fibers has little influence on the permeability. The permeability increased similarly with 2 kg/m^3 of all three types of PP-fibers, as well as the case of 3 kg/m^3 of Type 1 and Type 2. It can be concluded that the number of fibers is the decisive factor. With 1 kg/m^3 of thick PP-fibers (Type 1), the number of fibers, i.e. the channels, was not enough to increase the permeability. With 2 kg/m^3 and above, the number of the thick PP-fibers should be enough to prevent the drop of permeability as well, so no significant difference was noticed. In addition, with the amount of 2 kg/m^3, the effect seems independent of the type of PP-fibers, so this recommended amount by Eurocode 2 is reasonable. Although some test results (Yermak 2015) have shown that some certain types of PP-fibers are capable of preventing spalling with an amount less than 2 kg/m^3, however, due to the lack of a validated permeability model, these mixtures must be validated by experiment. To simplify the evaluation

of the use of PP-fibers, a permeability model considering the amount of PP-fibers will be proposed in the next section.

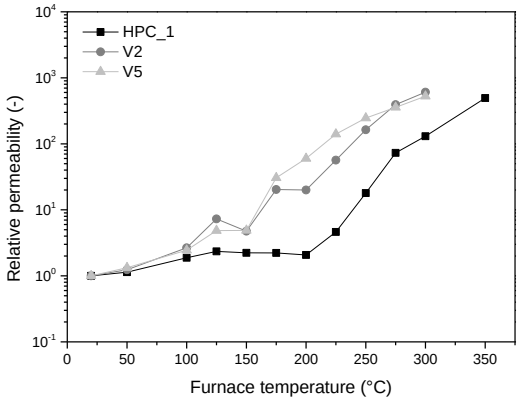

Fig. 3.11 Relative permeability of HPC_1, V2 and V5.

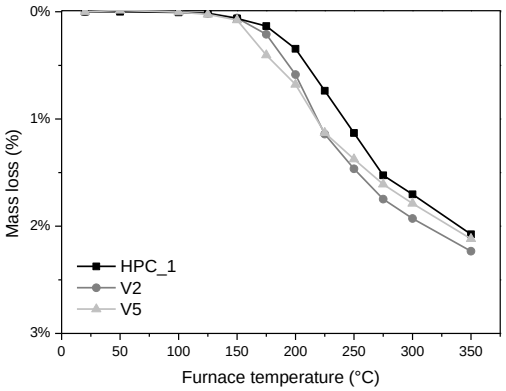

Fig. 3.12 Mass loss of HPC_1, V2 and V5.

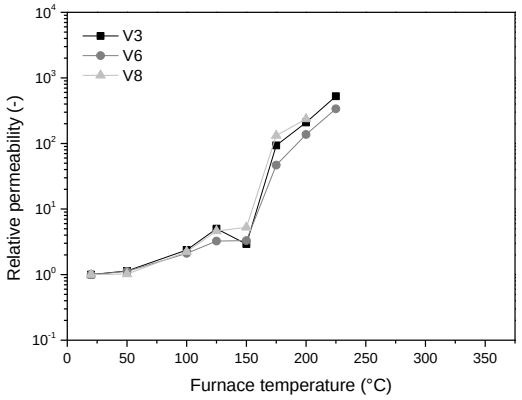

Fig. 3.13 Relative permeability of V3, V6 and V8.

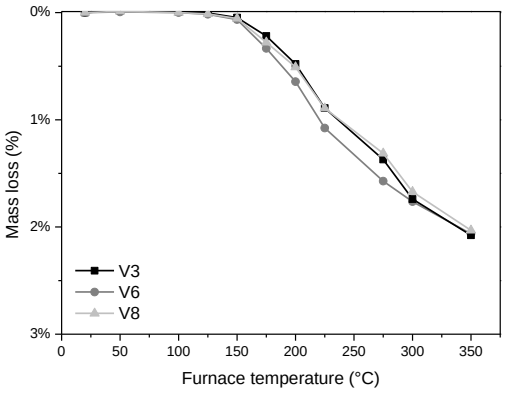

Fig. 3.14 Mass loss of V3, V6 and V8.

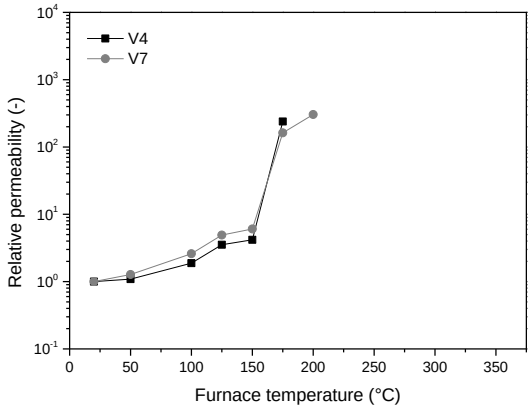

Fig. 3.15 Relative permeability of V4 and V7.

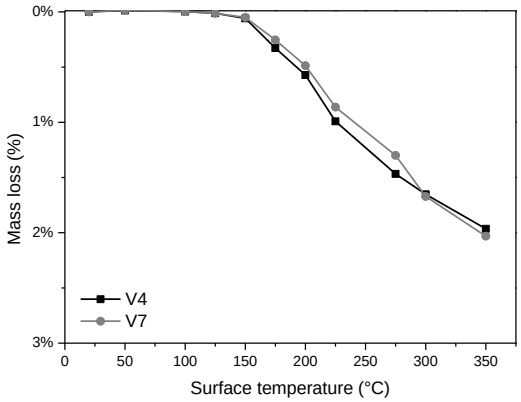

Fig. 3.16 Mass loss of V4 and V7.

The development of permeability at high temperature is influenced by moisture content as well, especially the drop of permeability. As shown in Fig. 3.11 and Fig. 3.12, the drop of permeability was accompanied with slower decrease of mass, namely higher moisture content. If the drying of dehydrated water is slow, a moisture clog can form. In the high moisture content zone, the permeability can be reduced according to the test results (Jacobs 1994). This could be the reason of the drop of permeability observed in the tests. Accordingly, the disappearance of the permeability drop (Schneider 1989) can be explained as well: the long conditioning time of 50 hours was enough for the dehydrated water to escape from the specimen, no moisture clog reduced the permeability any further. The increased permeability by Type 2 PP-fibers was high enough to prevent moisture clog, so no further drop was observed. On the other hand, with 1 kg/m^3 of Type 1 PP-fibers, with less number of channels, the V2 specimen had higher moisture content in the temperature range of 150 °C to 200 °C, as shown in Fig. 3.12, the permeability was influenced significantly by the moisture content, the drop was not prevented. As a result, the use of PP-fibers to increase permeability should consider the negative effect of moisture clog. To simulate the pore pressure, the moisture content should be taken into account in the permeability model. Details will be discussed in the Section 3.4.

3.4 Permeability model

Permeability is defined as the property that governs the rate of flow of a fluid in a porous solid. Test results (Schneider 1989) have shown that the permeability of concrete varies significantly with temperature and pore pressure. Therefore, the permeability model is usually taken as a function of pore pressure and temperature, for example the following model proposed by Gawin (1999) based on the test results conducted by Schneider and Herbst (1989):

$$k_{\mathrm{T}} = k_0 \times 10^{C_{\mathrm{T}}(T-T_0)} \left(\frac{P_{\mathrm{V}}}{P_0} \right)^{C_P} \tag{3.55}$$

Where k_{T} is the permeability of concrete at temperature T, k_0 is the initial permeability of concrete at initial temperature T_0 under initial pressure P_0 (taken as ambient pressure 101 kPa), P_{V} the pore pressure, C_{T} and C_{P} are constants for the effects of temperature and pore pressure.

According to the model, the permeability of concrete will increase with temperature and pore pressure. However, the observed drop as shown in Fig. 3.20 in the temperature range from 150 °C to 250 °C is not considered in Gawin's Model (Equation 3.55). Without considering the drop, the permeability is over-estimated in this temperature range, accordingly the pore pressure will be under-estimated. On the other hand, the effects of moisture content on permeability shown in the last section are not involved in the current model either. To predict the pore pressure reliably, a valid permeability model should be developed considering the test observations.

In this section, based on the permeability measurement of non-pre-dried and pre-dried specimens, a permeability model is proposed in this section. The observed drop of permeability and the influence from moisture content are included in the proposed model. As for the use of PP-fibers, the proposed model is modified to predict the change of permeability of concrete with PP-fibers.

3.4.1 The effect of moisture content

The permeability of concrete increases with temperature as shown in Fig. 3.17 by Schneider (1989). Apart from the general trend, a significant drop in permeability observed in the temperature range from 150°C to 250 °C is not negligible. The research by Jacobs (1994) has shown that the permeability of concrete decreases with the moisture content. In the temperature range above 110 °C, the water in concrete will increase due to the dehydration, and the dehydrated water will dry at high temperature. The existence of the dehydrated water coincides with the drop of permeability. Moreover, Schneider reported that, if the same specimen was kept for 50 hours at high temperature, the drop disappeared. It can be assumed that the absence of the drop was caused by the drying of the dehydrated water, the increased moisture content due to dehydration was offset by the long conditioning time. As a result, the observed drop of permeability will be related to the change of moisture content at high temperature.

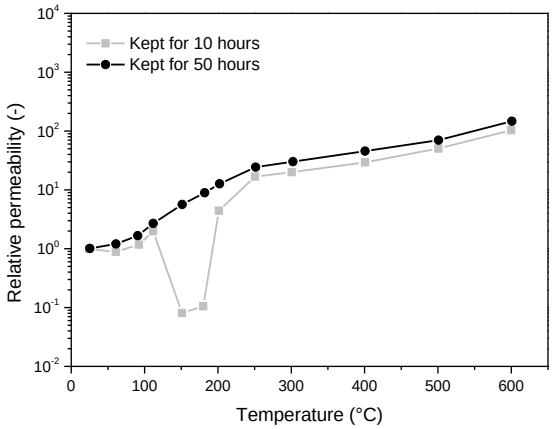

Fig. 3.17 Permeability of concrete after different conditioning times (Schneider 1989).

The influence of moisture content on the permeability of concrete is shown in Fig. 3.18. Jacobs measured the permeability of various concrete specimens with different moisture content. It can be seen that the permeability decreases with the moisture content (water saturation). Based on the simplified approach by Bazant and Kaplan (1996), Darcy's law as given in Equation 3.34 is extended to the mix fluid of vapor and water. If the water saturation is zero, the flow is governed by the vapor, then the viscosity is the viscosity of vapor; if the water saturation is 100 %, then the flow is governed the dynamic viscosity of water. Taken as the boundary condition, using the interpolation of viscosity, the parameters for Darcy's law can be given as:

$$k_{\mathrm{T}} = \begin{cases} k_0 \times 10^{C_{\mathrm{T}}(T_{\mathrm{M}}-T_0)} & ,P_{\mathrm{VM}} < P_0 \\ k_0 \times 10^{C_{\mathrm{T}}(T_{\mathrm{M}}-T_0)} \left(\dfrac{P_{\mathrm{VM}}}{P_0}\right)^{C_P} & ,P_{\mathrm{VM}} > P_0 \end{cases} \tag{3.56}$$

$$\mu = (1-w)\mu_{\mathrm{V}} + w\mu_{\mathrm{L}} \tag{3.57}$$

Where w is the level of saturation, calculated by $(V_{\mathrm{D}}+V_{\mathrm{L}})/(1-V_{\mathrm{S0}}+V_{\mathrm{D}})$, V_{L} the volume fraction of liquid water, V_{S0} the initial volume fraction of solid and V_{D} the volume fraction of dehydrated liquid water. The temperature T_{M} and pore pressure P_{VM} are the maximum values in the entire heating process. Because the permeability of concrete remains high after cooling from high temperature (Bosnjak & Ozbolt 2013), the effect is determined by the heating history. In Equation 3.56, the effect from pore pressure is considered

only above the ambient pressure P_0, in the lower range the permeability will not be increased by the pore pressure. Dwaikat and Kodur (2009) proposed that C_T be taken as 0.0025 based on the test results. In Equation 3.57, μ_v is the dynamic viscosity of vapor and μ_L the dynamic viscosity of water.

Using the form of Darcy's law per Equation 3.34, with the μ as the dynamic viscosity of vapor, the permeability model can be rearranged as following:

$$k_T = \begin{cases} \dfrac{k_0 \times 10^{C_T (T_M - T_0)}}{(1-w) + w\dfrac{\mu_L}{\mu_V}} & ,P_{VM} < P_0 \\ \dfrac{k_0 \times 10^{C_T (T_M - T_0)} \left(P_{VM}/P_0\right)^{C_P}}{(1-w) + w\dfrac{\mu_L}{\mu_V}} & ,P_{VM} > P_0 \end{cases} \quad 3.58$$

In this way, the moisture content is considered in the change of permeability. The model is compared to the test results by Jacobs (1994). Shown in Fig. 3.18, at ambient temperature, without the change of temperature and pore pressure, the predicted permeability change with the saturation agrees well with the test results.

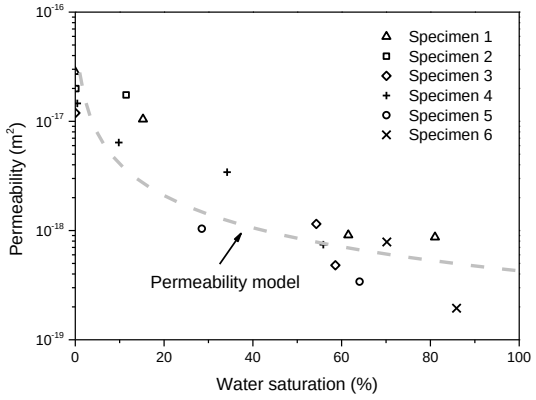

Fig. 3.18 Comparison of predicted and measured permeability of concrete by Jacobs (1994).

At high temperature, the dynamic viscosity of vapor μ_v and the dynamic viscosity of water μ_L are given as following:

$$\mu_V = \mu_{V0} + a_V (T - T_0) \quad 3.59$$

$$\mu_L = 0.6612 \times (T - T_0)^{a_L} \quad 3.60$$

Where $\mu_{v0} = 8.85\times10^{-6}$ Pa S, $a_v = 3.53\times10^{-6}$ Pa S/K and $a_L = -1.562$.

To further validate the permeability model at high temperature, the proposed permeability model is applied in the TH-model. According to Equation 3.58, the permeability changes with the temperature, pore pressure and moisture content. The heating process is set the same as in the permeability test, using the same heating rate. The predicted permeability from the model is compared with the measured permeability as shown in Fig. 3.19-Fig. 3.22.

After pre-drying at 105 °C for 25 days, the saturation level was low, the initial saturation mass of liquid water m_0 in TH-model was taken as 0.5 kg, the measured mass change of HPC_1 at 125 °C. It can be seen in Fig. 3.19, with low moisture content, the predicted initial permeability at ambient temperature is similar to the measured value. Considering the effect of dehydrated water, the drop of permeability can be predicted as well. The temperature range of the drop agrees well with the test result, approximately from 125 °C to 225 °C. The measured permeability rises faster above the range and the predicted result follows the pattern, because the moisture clog dries at high temperature. At higher temperatures, the model predicts lower permeability than the test measurements. This conservative result is acceptable for the interest of explosive spalling, which occurs usually under 300 °C (Klingsch 2014).

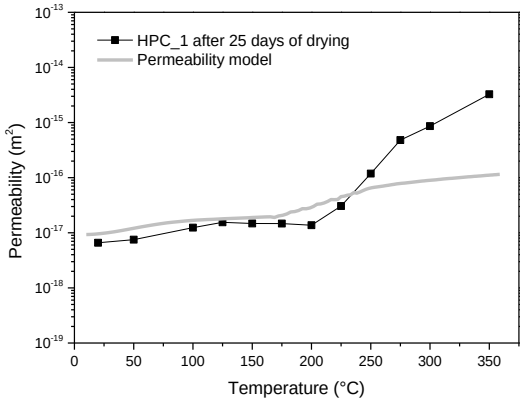

Fig. 3.19 Comparison of predicted and measured permeability of HPC_1 after 25 days of drying.

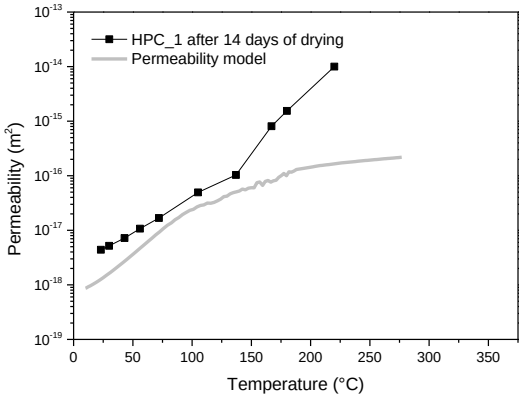

Fig. 3.20 Comparison of predicted and measured permeability of HPC_1 after 14 days of drying.

As for the case of 14-day pre-dried HPC, the predicted permeability with 25 kg/m^3 of initial liquid water is compared to the test result, as shown in Fig. 3.20.

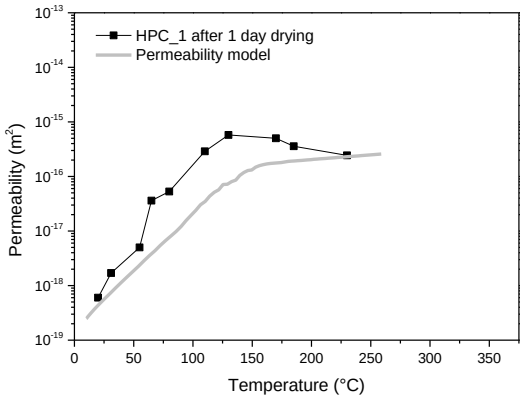

Fig. 3.21 Comparison of predicted and measured permeability of HPC_1 after 1 day of drying.

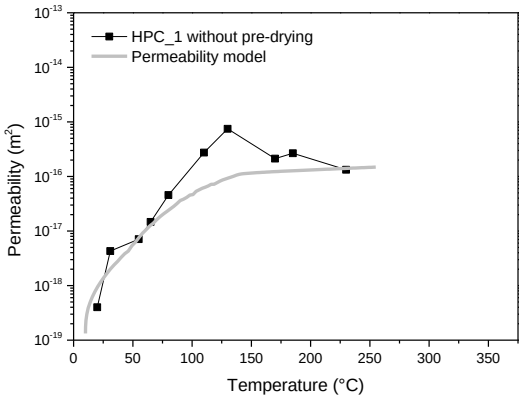

Fig. 3.22 Comparison of predicted and measured permeability of HPC_1 without pre-drying.

The initial permeability at ambient temperature is higher with lower moisture content, which can be considered by the permeability model. A slight drop of permeability is observed both in the predicted and measured results. At higher temperature, the permeability model provides conservative result: the predicted permeability does not rise so significantly as the test result. In general, the permeability considers the effect from pre-drying. The drop due to the change of moisture content is taken into account as well.

With higher initial moisture content, the change of permeability was studied as well. The 1-day pre-dried specimen contained about 4 % (100 kg/m^3) of initial liquid water according to the mass loss in the test. The predicted permeability of the specimen after 1 day drying is shown in Fig. 3.21. As for the specimen without pre-drying, the predicted permeability is shown in Fig. 3.22, which lost about 5% of liquid water by mass after it was heated to 125 °C. It can be seen that with high initial moisture content, lower initial permeability was predicted by the permeability model, which is also observed in the tests. However, the drying rate was predicted lower than that of test results and more moisture was in the simulated specimen. Therefore, the permeability was predicted lower than the test result at the beginning of heating. At high temperatures, the dehydrated water in concrete increased the moisture content of the tested specimens and a decrease of permeability has been induced. Due to the drop of permeability, the predicted values were also close to the measured permeability at high temperatures. In general, it can be concluded that the permeability model is capable of representing the change of permeability with respect to moisture contents.

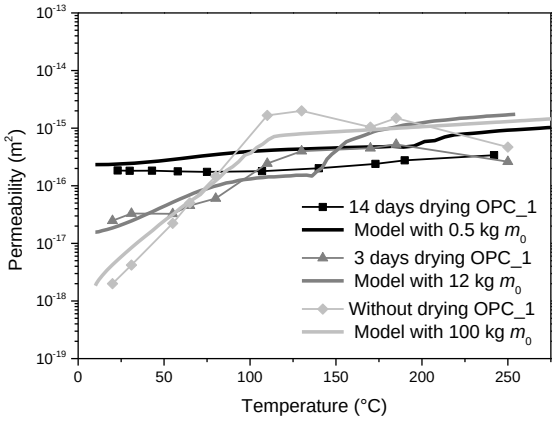

Fig. 3.23 Comparison of predicted and measured permeability of OPC_1.

Similarly, the model is used for OPC_1 with various moisture contents. As shown in Fig. 3.23, the modeled permeability is compared with the previously reported test results. It can be seen that the effects from moisture content, temperature and pore pressure were considered. The permeability model is capable of predicting the permeability of OPC as well. The more significant change of initial permeability with the moisture content than HPC was well predicted.

In general, the permeability from the model agrees well with the test results, the various changes of permeability in different temperature ranges are predicted. At ambient temperature, the predicted initial permeability changes with the moisture content. At higher temperatures, the drop of permeability is considered as well, with respect to the moisture due to dehydration. The proposed permeability model is useful to consider the change of permeability of concrete at high temperature and will be used in the TH-

model. The TH-model using the proposed permeability model will be validated by comparing the predicted and measured pore pressure. Details will be presented in Section 3.5.

3.4.2 The effect of PP-fibers

Polypropylene fibers (PP-fibers) have been recommended by Eurocode 2 as a protective method against explosive spalling of concrete. Test results have shown the effectiveness of the method as well (Klingsch 2014). However, the use of PP-fibers in concrete to prevent spalling must be validated by experiment, due to the lack of a valid model to consider the effects. To simplify the evaluation of the use of PP-fibers, the permeability model will be modified to involve the effect from PP-fibers, based on the permeability tests presented in Section 3.3.

The melting of PP-fibers will take place in a temperature range from 160 °C to 170 °C, which will increase the permeability of concrete. The used PP-fibers supplied by Bekaert® have a melting point of 165 °C. According to the test results, above the melting point, the permeability increased significantly up to 250 °C. The increase effect can be considered by introducing an increasing factor $\alpha_{\kappa,T}$ to the permeability model. Below the melting point of PP-fibers, the permeability is given as in Equation 3.57. In the temperature range of 165 °C to 250 °C, the permeability increases progressively according to the increasing factor. Above 250 °C, the permeability will be increased by the increasing factor. The modified model can be written as:

$$k_{T,P} = \begin{cases} k_T & ,T \le 165\ °C \\ k_T \times \left(1 + (a_{T,P} - 1)\dfrac{T - 165}{85}\right) & ,165\ °C \le T < 250 \\ k_T \times a_{T,P} & ,T \ge 250\ °C \end{cases} \qquad 3.61$$

Where k_T is the permeability given in Equation 3.57. For simplicity, in the current stage the $\alpha_{\kappa,T}$ is assumed as a constant to be determined by the type and amount of the used PP-fibers.

To validate the model considering the effect of PP-fibers, the measured permeability of HPC with Type 2 PP-fibers reported in Section 3.3 is used. To fit the test result of permeability, an increasing factor of 10 has been selected for V5 with 1 kg/m^3 of PP-fibers. For higher amounts of PP-fibers, the increasing factors are selected to be 20 and 30 for V6, V7 with 2 kg/m^3 and 3 kg/m^3 of PP-fibers respectively. As the next step, the modified permeability model is applied in the TH-model. The predicted permeability from the model is compared with the measured permeability as shown in Fig. 3.24-Fig. 3.26.

With 1 kg/m^3 of Type 2 PP-fibers, the permeability of V5 increased by the melting of PP-fibers. The predicted permeability from the model with an increasing factor of 10 is compared with the test results in Fig. 3.24. It can be seen that the effect from PP-fibers at the melting point was simulated, the predicted permeability increased approximately to the level of the measured result at high temperature. The dehydrated water led to a slight drop under the melting point as observed in test. With the permeability considering the moisture content, the pattern of permeability was well simulated. The constant increasing factor considers the change in the temperature range of 165 °C to 250 °C, the progressive increase agrees well with the test result.

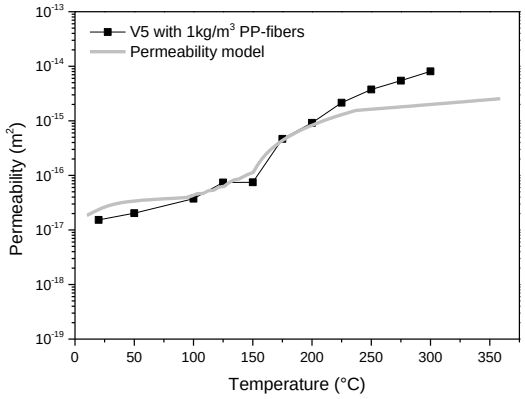

Fig. 3.24 Comparison of predicted and measured permeability of V5 (with 1 kg/m^3 of Type 2 PP-fibers).

The permeability of V6 increased more significantly than that of V5, because of the higher amount of PP-fibers. Therefore, the increasing factor in the permeability model was taken as 20 for 2 kg/m^3 of Type 2 PP-fibers. The predicted result is compared with the test result in Fig. 3.25. The permeability reached the measurement range at about 250 °C and the model at same temperature predicted increase from PP-fibers. It can be seen that the permeability model with an increasing factor of 20 simulates the general permeability change of V6.

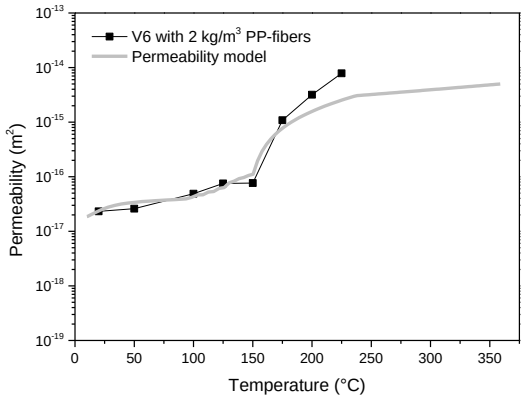

Fig. 3.25 Comparison of predicted and measured permeability of V6 (with 2 kg/m^3 of Type 2 PP-fibers).

As for V7 with 3 kg/m^3 of Type 2 PP-fibers, the increasing factor of 30 is selected for the simulation using the permeability model. Fig. 3.26 shows the predicted and the measured permeability. At 225 °C, the measurement range of the Torrent permeability tester was met, so the permeability was at least 1×10^{-14} m^2. The predicted permeability increased to the magnitude above the melting point. At high temperature, the modified model seems to underestimate the permeability of V7, because of the conservative permeability model.

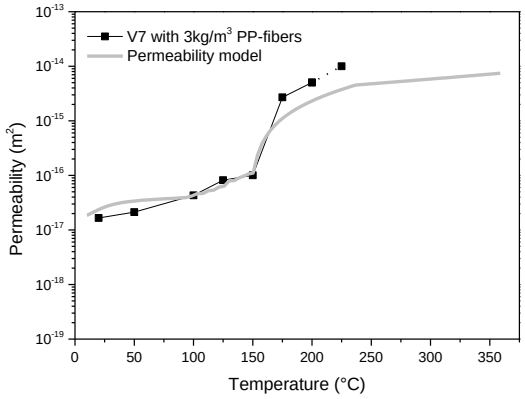

Fig. 3.26 Comparison of predicted and measured permeability of V7 (with 3 kg/m^3 of Type 2 PP-fibers).

To further validate the increasing factor for the permeability model, the permeability of a denser HPC M1 (Klingsch 2015) was predicted. The M1 had a 28-day strength of 150 MPa and contained the same amount of Type 2 PP-fibers as V6 and the increasing factor for PP-fibers was still taken as 20. As shown in Fig. 3.27, in the denser HPC with initial permeability of the 3×10^{-18} m^2, the predicted permeability agrees with the measured trend, the increased level above the melting point was well predicted. Therefore, the constant increasing factor is acceptable to simulate the change of permeability of another HPC with the same recipe of PP-fibers as well.

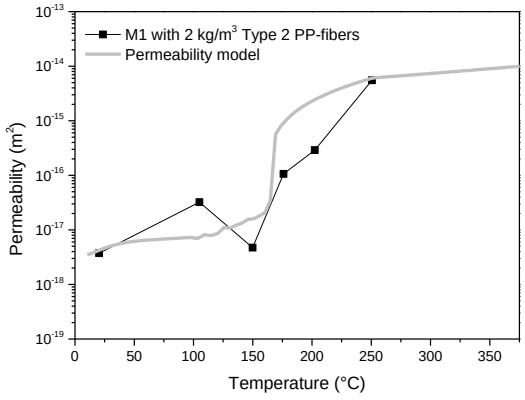

Fig. 3.27 Comparison of predicted and measured permeability of M1 by Klingsch (2014).

It can be seen from the comparisons, that the constant increasing factor is effective in predicting the change of permeability. The permeability is increased by the PP-fibers in the temperature range of 165 °C (melting point) to 250 °C. The modified model considers the change progressively. Based on the existing test result, for concretes with amounts of 1, 2 and 3 kg/m^3 of Type 2 PP-fibers, the increasing factors can be taken as 10, 20 and 30. All the predicted permeability agrees well with the test results. For 2 kg/m^3 of Type 2 PP-fibers, the increasing factor 20 is also fit for other mixtures. It can be assumed that the increasing factor is dependent on the recipe of PP-fibers. The increasing factor should be further studied with respect to various type and amount of PP-fibers in different concretes.

3.4.3 Discussion of the permeability model

The permeability of concrete is an important factor in the susceptibility to explosive spalling. To evaluate the risk of spalling, the change of permeability at high temperature must be considered. Test results have shown that the permeability increases with temperature and pore pressure. Furthermore, the presented test results in Section 3.3 emphasize the role of moisture content. The proposed permeability model involves all of the three factors and the predicted permeability agreed generally well with the measurements.

The use of PP-fibers can increase the permeability above the melting point of the fibers. The proposed permeability model predicts an increase of permeability above 165 °C. The effects from different amount of PP-fibers were involved using increasing factors. The constant factor works well according to the comparison to test results. As for Type 2 PP-fibers, the increasing factors are recommended for different amounts.

To evaluate the change of permeability, the Torrent permeability tester provides the initial permeability at ambient temperature. The proposed permeability model predicts the change of permeability at high temperature. The use of PP-fibers can be considered according to the type and amount. The predicted permeability agrees well with the test results and can be used in the TH-model. When it is possible to measure the permeability of the specimen at high temperature, the increasing factor for PP-fibers can be determined by the test result and the predicted permeability can be validated.

As the next step, the proposed permeability model was applied in the TH-model. To validate the TH-model, the simulated pore pressure was compared with the measured values, with respect to permeability and moisture content. The validation will be presented in the next section.

3.5 Validation and parameter study

The validation of the proposed model is established by comparing the model predicted temperature and pore pressure with measured values. The temperatures from the model were compared with the test results at different locations. Due to the practical difficulties in measuring the pore pressure, there are limited test results for the validation of the TH-model. The main concern is that cracks in specimen lead to a leaking of the pressure. The measured pore pressure is usually lower than the true value. Therefore, the predicted values were compared to the peak values measured at different positions in the test. Both OPC and HPC are discussed to illustrate the effects from permeability on pore pressure.

Based on the validated model, two more parameters studied are moisture content and PP-fibers. The consideration from the permeability model provides a quantitative insight into the relationship that might exist between these parameters and pore pressures.

The material properties of concrete vary within their domain at high temperatures. As discussed in Chapter 2, due to the complexity, it is not possible to get the exact high temperature properties of concrete. Hence the proposed high temperature property relations in codes and standards are used. Details are presented in this section.

3.5.1 Predicted temperature development in concrete

To validate the proposed model, the simulation of heat transfer was carried out according to Equation 3.1 on the concrete slab used by Kalifa (2001). The heating rate to the 120 mm thick slab was 5 °C/s in the first 2 minutes and then the temperature was kept at 600 °C. As shown in Fig. 3.2, the specific heat of concrete is determined by the moisture content of 3.0 % and the increase of specific heat due to the vaporization is taken into account.

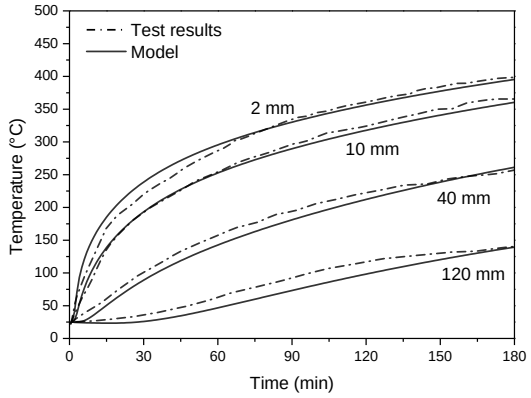

Fig. 3.28 Comparison of measured and predicted temperature for the slab tested by Kalifa (2001).

The temperatures measured at four locations in the slab were compared with the predicted values. As shown in Fig. 3.28, the predicted and the measured temperatures agreed well. At depths of 40 mm and 120 mm, both predicted and measured temperatures increase slower, which is usually mentioned as moisture clog due to vaporization of water. The simulation of the moisture clog is in close agreement with the test results thanks to the specific heat of concrete according to the moisture content. This slower temperature increase due to vaporization results in a greater thermal gradient, which will increase the risk of spalling. The effects of thermal gradient and heating rate will be discussed in Chapter 4 using the spalling model.

The measurements of temperature in concrete by Mindeguia (2010) have shown that the temperature developments vary little among different types of concrete mixture. Therefore, the proposed high temperature properties of concrete in Eurocode 2 can be used to simulate the development of temperature inside concrete.

3.5.2 Predicted pore pressure in concrete

The pore pressure simulation was carried out for the mixtures used by Mindeguia (2010), as listed in Table 3.3. The properties of concrete used in the TH-model are determined according to the mixtures. To validate the pore pressure calculation, the predicted results will be compared against the measured value. To avoid the effect from the pore pressure leaking in the test, the validation is carried out by comparing the peak pressure measured in the test with the simulated pore pressure at the same depth.

Table 3.3 Mixtures of studied concrete by Mindeguia (2010).

Components	Units	B325	B450
Cement CEM I 52.5R	kg/m^3	325	450
Siliceous 10/20 gravel	kg/m^3	960	960
Siliceous 5/10 gravel	kg/m^3	89	89
Siliceous 0/5 sand	kg/m^3	740	740
Water	kg/m^3	202	160
W/C ratio	-	0.62	0.36
28 day compressive strength	MPa	35	62
Permeability	m^2	1.5×10^{-16}	1.2×10^{-18}
Initial free water content	%	3.8	3.2

The measurement was conducted using the radiation heater. The temperature rapidly reached 600 °C (after around 5min) and then remained constant for 6 hours. The heating rate was simulated in the validated model for temperature. The measured and predicted temperatures are shown in Fig. 3.29, the close agreement validated the result from the model and the pore pressure was predicted based on this.

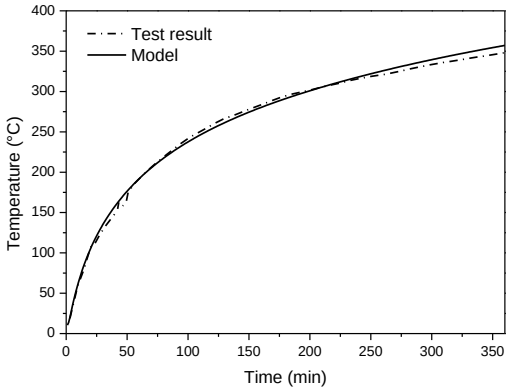

Fig. 3.29 Comparison of measured and predicted temperature at a depth of 10 mm for the slab tested by Mindeguia (2010).

As for the OPC B325, the initial permeability was 1.5×10^{-16} m^2 and the peak pore pressure measured in the test was 0.24 MPa at the depth of 20 mm. In the model the initial permeability, moisture content and cement content are taken as listed in Table 3.3. The predicted and measured pore pressures at 20 mm are presented together with saturating vapor pressure curve (P_{VS}) in Fig. 3.30. It can be seen that both predicted and measured pore pressures are under the theoretical boundary saturating vapor pressure curve and the predicted pore pressure at depth agrees well with the measured value. In the OPC case, the model is validated by the agreement of both the trend and the peak value of pore pressure.

The pore pressure at other depths in the specimen is shown in Fig. 3.31. The pore pressure increases with the exposure to heat. In the shallow region, the pore pressure increases earlier and the peak pore pressure is not as high as in the deeper region. The higher pore pressure in the deep region has been observed in test (Kalifa 2001) and was attributed to the higher moisture content due to the migration of vapor and liquid water. This effect has been considered in the model by involving the liquid water migration and the effect is shown by the predicted pore pressures at 10 mm, 20mm and 30 mm.

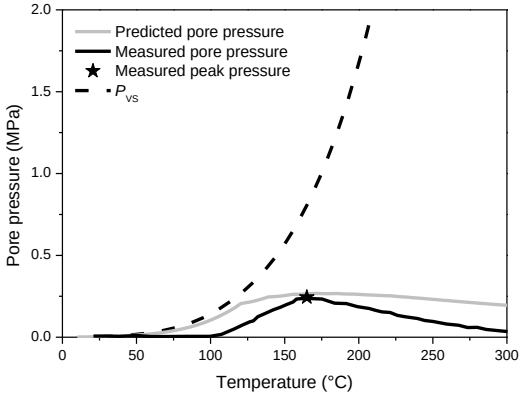

Fig. 3.30 Comparison of measured and predicted pore pressure at 20 mm in OPC.

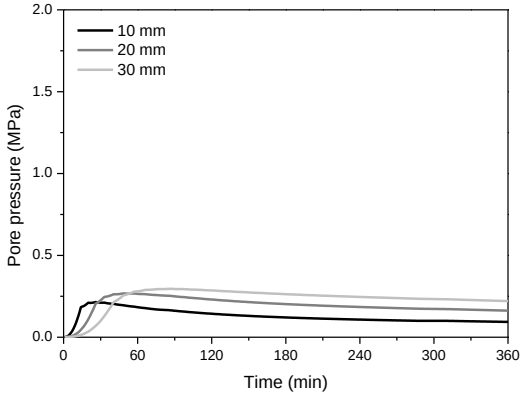

Fig. 3.31 Predicted pore pressures at different depth in the OPC (B325).

During heating, the pore pressure in HPC is higher due to the low permeability. The B450 with the strength of 62 MPa is tested in the same scenario as B325. The low permeability resulted in high pore pressure, the measured value at 10 mm was slightly higher than 1.0 MPa. The calculation was carried out and the results are shown in Fig. 3.32 and Fig. 3.33. It can be seen that the peak pore pressures from the model and test results agreed well, the predicted peak pore pressure at 10 mm was 1.06 MPa. In the test, the peak pore pressure at 10 mm was measured close to the saturating vapor pressure curve, which indicated that the local moisture content was still high before the pore pressure dropped. Considering the sharp drop of pore pressure and the local temperature decrease, it can be concluded that the pore pressure was reduced by leaking. The pore pressure measurement at deeper depth was also influenced by leaking, because at other locations the measured pore pressures were significantly lower. Yet the model predicted higher pore pressure in the deeper region as shown in Fig. 3.33. The peak value at 30 mm was about 1.5 MPa. The influence of low permeability of HPC is considered, pore pressure was predicted higher than that in OPC.

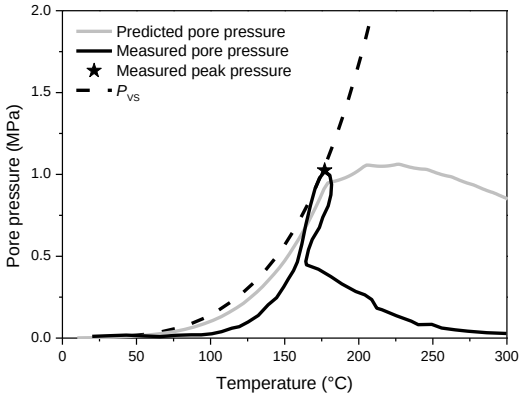

Fig. 3.32 Comparison of measured and predicted pore pressure at 10 mm in HPC.

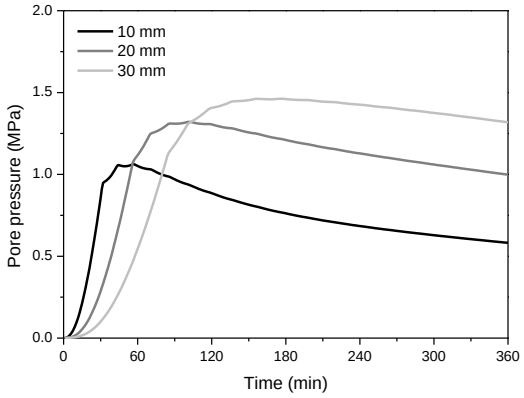

Fig. 3.33 Predicted pore pressures at different depth in the OPC (B450).

The simulations of both OPC and HPC have been carried out to validate the model. The predicted pore pressures were compared with the measured peak pressure and good agreements were achieved. However,

the measured pore pressure by Mindeguia (2010) did not show clear tendency of the pore pressure at various depths and it was because of the leaking of pore pressure. The practical difficulties limited the validation of the model against more test results. The validation has shown that the TH-model with the proposed permeability model is capable of predicting the pore pressure with good accuracy and the influence from permeability is taken into account, the pore pressure in HPC is predicted to be higher due to its lower permeability comparing to OPC. Using the proposed permeability model, the role of moisture content will be discussed in next section.

3.5.3 Influence from moisture content on pore pressure

To analyse the effect of moisture content, the pore pressures was simulated using the TH-model according to the permeability of concrete with different moisture contents. The permeability was calculated using the model as discussed in Section 3.4 and the simulation agrees well with the test results. The predicted pore pressures of pre-dried OPC_1 and HPC_1 were carried out according to ISO standard fire curve and compared against the specimens without pre-drying.

For OPC_1, based on the test results of 14 day pre-dried and non-pre-dried permeability, the predicted permeability of OPC_1 with 0.5 kg/m^3 and 100 kg/m^3 are shown in Fig. 3.34. The proposed model considered the lower initial permeability due to higher moisture content and at high temperature, the permeability in the wet specimens increased fast due to the decrease of moisture content. Using the TH-model, the predicted pore pressures with high and low moisture content are shown in Fig. 3.35. It can be seen that higher moisture content leads to higher pore pressure and the effect is more significant in the shallow region. In the deep region, the moisture content during heat will be increased by the moisture migration, so the difference of pore pressure from pre-drying was less in the deep region. The effect of moisture disappeared with heating, as the difference of moisture content will be offset by the heating. With lower initial permeability, the pore pressure in wet specimen was predicted higher. The higher pore pressure increased the permeability significantly.

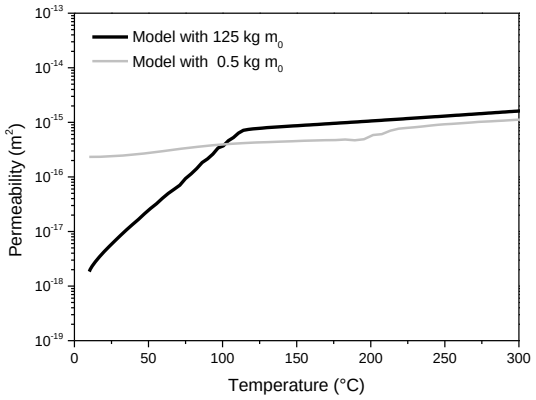

Fig. 3.34 Predicted permeability of OPC_1 with different moisture content.

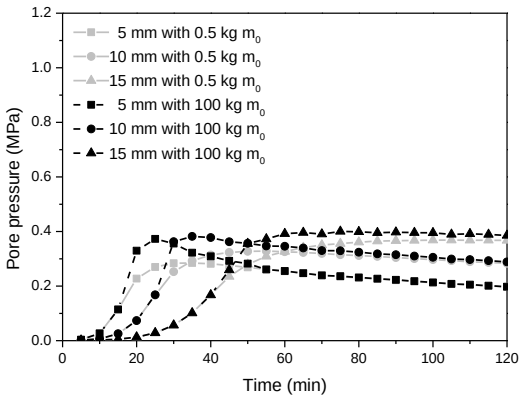

Fig. 3.35 Predicted pore pressure of OPC_1.

Above 105 °C, the permeability in the wet specimen was higher than the dried one as shown in Fig. 3.34. When the moisture content was similar in both specimens and the permeability in the wet specimen was slightly higher, no higher pore pressure in the non-pre-dried OPC was predicted at higher temperature.

For HPC, the pore pressure in the 25 day pre-dried specimen was predicted. The drying in HPC was slower than OPC because of the low permeability, after longer time the initial moisture content was reduced to the same level 0.5 kg/m^3 as the 14 day pre-dried OPC. In practice, due to the low drying rate in HPC, the moisture content will not change much when exposed to air. In the pore pressure simulation, similar results as in OPC are obtained, as shown in Fig. 3.37. The initial high moisture content led to higher pore pressure, especially in the shallow region. At high temperature, the permeability increased more in the wet specimen and the effect from different moisture content is also limited. No significant difference of pore pressure was noticed in the region deeper than 10 mm.

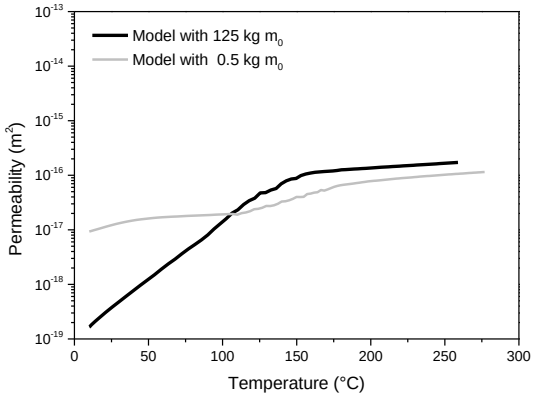

Fig. 3.36 Predicted permeability of HPC_1 with different moisture content.

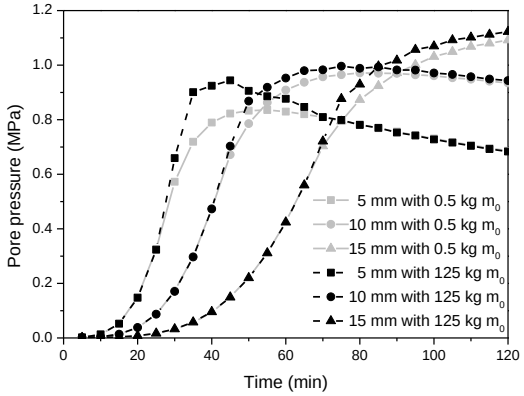

Fig. 3.37 Predicted pore pressure of HPC_1.

The effect from moisture content on pore pressure is calculated by the TH-model, the increase of pore pressure by high moisture content was limited, especially in the deep section. This is attributed to the fact that at high temperature, the moisture content is related to dehydration of water and the influence from initial moisture content is offset by the moisture migration, especially in the deep region of concrete. Experiments have shown that moisture content has some influence on spalling, e.g. the water-cured specimen showed higher susceptibility to explosive spalling (Akhtarruzaman & Sullivan 1970). The reason may not be limited purely to the minor change of pore pressure. The effect from moisture content on explosive spalling will be discussed further in Chapter 4, together with the thermal stress in the framework of spalling criterion.

3.5.4 The effects of PP-fibers on pore pressure

The use of PP-fibers can prevent explosive spalling of HPC (Klingsch 2013). The effect is mainly attributed to the reduction of pore pressure by the increased permeability (Bošnjak & Ožbolt 2013). As described in Section 3.4.2, the modified permeability model involves the effect from PP-fibers on permeability. Using the TH-model, the pore pressure of HPC with Type 2 PP-fibers will be predicted. To illustrate the effects, the

predicted pore pressure of HPC_1 without PP-fibers will be compared to the other pore pressures reduced by different amount of Type 2 PP-fibers.

The modified permeability model is applied in the TH-model to simulate the change of permeability of HPC with PP-fibers. Fig. 3.38 shows the predicted permeability of V5 with 1 kg/m^3 PP-fibers and HPC_1 without PP-fibers. The simulated permeability with increasing factor 10 for 1 kg/m^3 PP-fibers agrees with the permeability of V5 measured by Torrent tester. With the increasing factor, the predicted permeability increase of V5 is noticeable above the melting point. The pore pressure is reduced by the permeability increase as shown in Fig. 3.39. Below the melting point, no difference was noticed, and the pore pressure in V5 at various depths increased with temperature as HPC_1. When the melting point was achieved, the permeability from the model increased by the increasing factor. Then higher pore pressures were prevented in the whole section and in the deeper region. The peak value of pore pressure was limited to under 0.6 MPa. With 1 kg/m^3 PP-fibers, the effect was already significant. The use of PP-fibers to prevent spalling can be explained by the decrease of pore pressure.

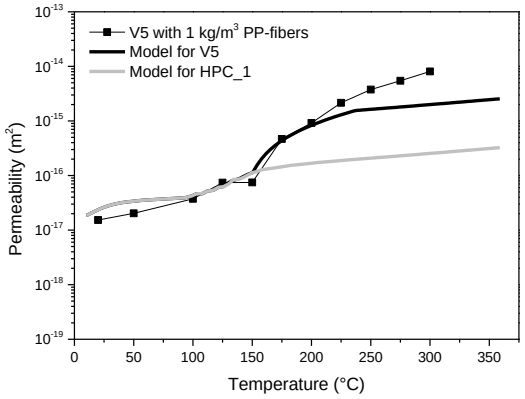

Fig. 3.38 Comparison of predicted permeability of V5 and HPC_1 with the test result.

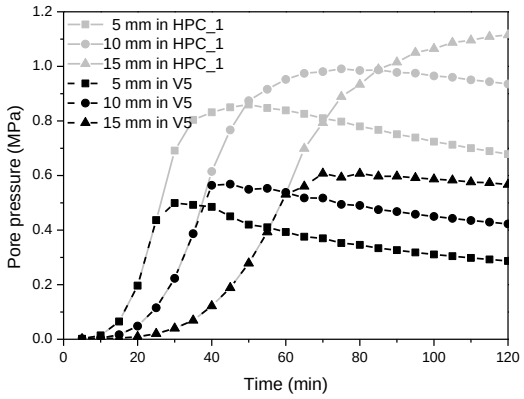

Fig. 3.39 Predicted pore pressure of V5 (with 1 kg/m^3 of PP-fibers) and HPC_1

With higher amount PP-fibers, the increasing factors for V6 and V7 are 20 and 30. The permeability model achieved an overall agreement with the test results as shown in Fig. 3.40 and Fig. 3.42. Compared to the HPC_1, the permeability increased more by the greater increasing factors. As for the reduction of pore pressure, the results from TH-model are presented in Fig. 3.41 and Fig. 3.43. It can be seen that the pore pressures in V6 and V7 were further lower than that in HPC_1. The effect from higher amount of PP-fibers is involved in the simulation. The difference between V6 and V7 was not significant.

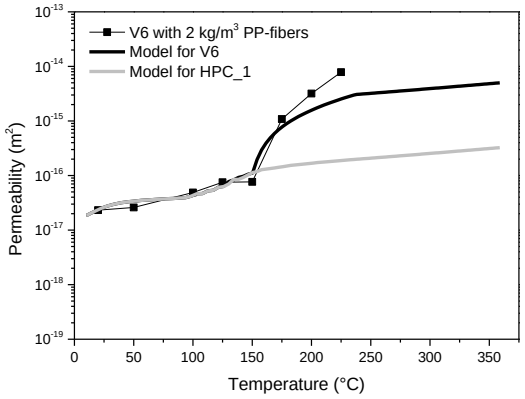

Fig. 3.40 Comparison of predicted permeability of V6 and HPC_1 with the test result.

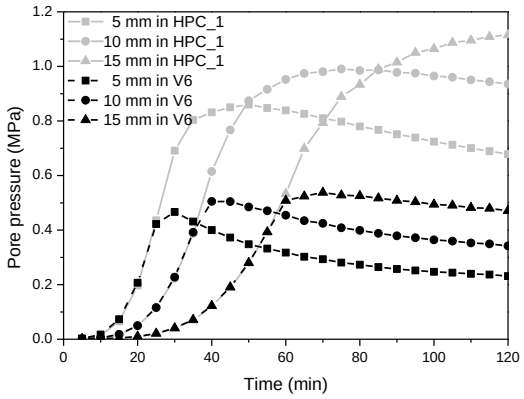

Fig. 3.41 Predicted pore pressure of V6 (with 2 kg/m^3 of PP-fibers) and HPC_1.

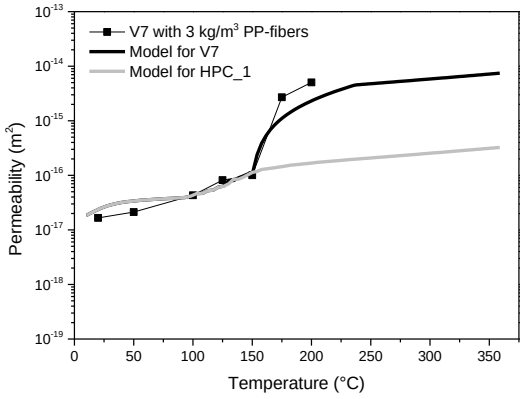

Fig. 3.42 Comparison of predicted permeability of V7 and HPC_1 with the test result.

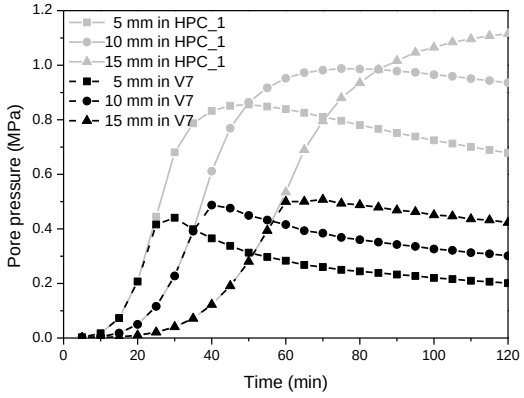

Fig. 3.43 Predicted pore pressure of V7 (with 3 kg/m^3 of PP-fibers) and HPC_1.

The predicted pore pressures in V5, V6 and V7 against temperature are presented in Fig. 3.45. The effect of PP-fibers starts from 165 °C, and the pore pressure deviated the saturating vapor pressure curve. The increasing factors 20 and 30 result in similar reduced pore pressure. It can be concluded that increasing the amount of PP-fibers will not bring much benefit when the increasing factor reaches 20. Specific to the Type 2 PP-fibers, 2 kg/m^3 corresponds to an increasing factor of 20 in the permeability model. In addition, as shown in Fig. 3.13, with this amount of other types of PP-fibers the permeability has increased to the similar level and the effect from a lower amount is dependent on the lengths and diameters of the fibers. Therefore, considering the effects on pore pressure, the added amounts of all the three tested Type of PP-fiber as recommended to be 2 kg/m^3 same as the Eurocode 2 proposed.

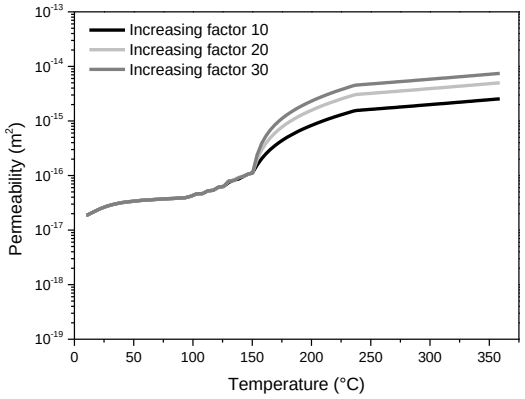

Fig. 3.44 Comparison of predicted permeability of V5, V6 and V7 (1, 2 and 3 kg/m^3 of PP-fibers).

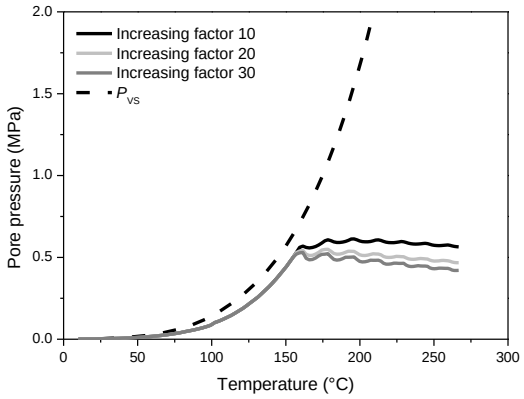

Fig. 3.45 Predicted pore pressure at 15 mm in V5, V6 and V7 (1, 2 and 3 kg/m^3 of PP-fibers).

The modified permeability model can simulate the change of permeability and the pore pressure can be predicted based on the increasing factor. To evaluate the use of PP-fibers, for the known type and amount of PP-fibers, the increasing factor can be applied in the model, e.g. 20 for 2 kg/m^3 of Type 2 PP-fibers. New recipes of PP-fibers should be tested to determine the increasing factor for permeability.

3.6 Conclusions

A Thermo-hydro model (TH-model) has been proposed with a new permeability model that considers the influence of moisture content and PP-fibers. Permeability measurements were carried out by two methods and the Torrent tester was selected to investigate the permeability of concrete after heating. The TH-model and the permeability model were validated by the test results. It is worth examining the key findings within the context described in this chapter:

1. Permeability measurements indicated that the permeability of concrete increases with temperature and pore pressure. In addition, the test results emphasized the influence of moisture content: the more moisture the concrete contained, the lower the permeability. Considering the change of moisture in concrete, the drop of permeability observed in the test can be explained. The permeability should be a function of temperature, pore pressure and moisture content.
2. A permeability model has been proposed and all three factors (temperature, pore pressure and moisture content) are involved. Lower permeability was predicted for high moisture containing specimens. Thanks to the consideration on moisture, the permeability model can also simulate the dent of permeability due to the dehydration of water. For both OPC and HPC, the predictions from the model agreed well with the measured permeability.
3. The proposed TH-model was based on the simplification after Bazant. The new permeability model considers the characteristics of the fluid. The validation of the TH-model was established by comparing the predicted pore pressure with measured values. The model is capable of predicting the pore pressure with respect to the permeability. High pore pressure was predicted in HPC, which is believed to be one important factor for its high susceptibility to explosive spalling.

4. The effect from moisture content on pore pressure was studied using the TH-model. Due to the loss of moisture during heating, higher initial moisture content only results in a slightly higher pore pressure in the shallow region. The effect on explosive spalling will be further discussed in Chapter 4.
5. The PP-fibers prevent explosive spalling by increasing the permeability above the melting point. The effects have been proved by permeability measurement. The modified permeability model considers the permeability increase by introducing the increasing factors, which were determined by test results. The pore pressure was predicted for specimens with various amounts PP-fibers. The results are in favor of the PP-fibers amount of 2 kg/m^3, recommended by Eurocode 2.
6. The test results and simulations have shown that the pore pressure is far lower than the concrete strength at high temperature. The explosive spalling should be predicted by combined mechanism described in Chapter 2. As the pore pressure is an important factor, the TH-model will be used in the spalling prediction to calculate the pore pressure.

4. Criterion for explosive spalling

4.1 Introduction

The mechanisms of explosive spalling have been discussed in Chapter 2, to date, it is widely believed that the spalling is induced by the combined stresses of pore pressure and compressive stresses in the restrained heated region (Bazant 1978, Zhukov 1976, Connolly 1995). One important factor, pore pressure, has been simulated by the TH-model proposed in Chapter 3. The predicted and measured pore pressure agreed well and both have shown that the pore pressure does not reach the magnitude of tensile strength of concrete at high temperatures. To consider other effects i.e. thermal stress and external loads, the combined pore pressure and thermal stress spalling theory after Zhukov (1976) is adopted. This Chapter presents a spalling criterion for explosive spalling of concrete.

All the stresses acting on a heated concrete specimen will be taken into account by a spalling model based on the proposed spalling criterion. The thermal stress in the section will be predicted based on the temperature gradients. The proposed TH-model in Chapter 3 will be used to calculate the pore pressure during heating and the effective stress from pore pressure on the concrete skeleton is studied by introducing the Biot's coefficient *b*. As for the prediction of explosive spalling, the Biot's coefficient will be determined based on test results. The validation of the spalling model will be done against the test results with and without external loads.

Some observations in tests will be discussed in the framework of the proposed spalling criterion. The heating rate of concrete is found to influence the susceptibility to explosive spalling (Klingsch 2013) and the effects will be illustrated by the spalling model prediction. As for the external loads, the test results have shown its contradictive effects on explosive spalling. Apart from the consideration of the spalling criterion, the experimental work was required to investigate the spalling risk of loaded concretes. The permeability measurements of OPC and HPC have shown that the external loads could induce significant change to permeability. The test results of permeability are applied in the spalling model to explain the observations in tests.

The objective of the Chapter is firstly to introduce the framework for considering explosive spalling. Subsequently the influencing factors evaluated with respect to the occurrence of explosive spalling. Full details are presented in this Chapter.

4.2 Governing equations

The test results have shown that the explosive spalling is not purely a result of pore pressure or thermal stress (Jasson 2013). The superposition of stresses proposed by Zhukov (1976) is a useful mechanism to predicted explosive spalling. To involve the effects from pore pressure the Biot's coefficient will be suggested for the criterion based on the test results. The effective stress from pore pressure will be superimposed with other induced stresses such as thermal stress and external loads. The governing equations will be described in this section.

4.2.1 Biot's coefficient

The pore pressure is widely believed to be the trigger of explosive spalling (Bazant 1978, Connolly 1995). The concept of effective stress is very useful to describe the effect of pore pressure on the mechanical response of porous media. As discussed in Chapter 2, Biot's coefficient defines the fraction of pore pressure transferred to the total stress and was first introduced by Biot (1941). The damage behavior of concrete related to pore pressure can be described using the Biot's coefficient. Equations 4.1 and 4.2 give the expression for the effective stress, which was suggested by Geertsma (1957) and Skempton (1960). These are exact and can be considered as fundamental laws for strain in poroelastic systems.

$$\hat{\sigma}_{ij} = \sigma_{ij} - b\sigma_{\mathrm{p}}\delta_{ij} \tag{4.1}$$

$$b = 1-(K_b / K_a) \tag{4.2}$$

Where σ_{ij} denotes the applied stress (measured positive in tension), σ_{p} is the pore fluid pressure, δ_{ij} is the Kronecker delta, b is Biot's parameter, K_{b} is the skeleton bulk modulus and K_{s} is the solid matrix bulk modulus.

To investigate the effective stresses in concrete, series of studies have been carried out to determine the Biot's coefficient. The test by Klimentos (1998) have shown that Biot's coefficient constant is a complex function of porosity, permeability, pore-size distribution, overburden, and confining stress, which means that it is not a constant. Ulm (2004) estimated the poroelastic properties of concrete using a combined experimental-theoretical micro-poromechanics approach, the results showed that the base Biot's coefficient for concrete was between 0.61 and 0.71 at ambient temperature. In addition, Chen (2009) investigated the effect of heat treatment on the poroelastic properties and the results showed that Biot's coefficient approaches 1 when exposed to high temperature.

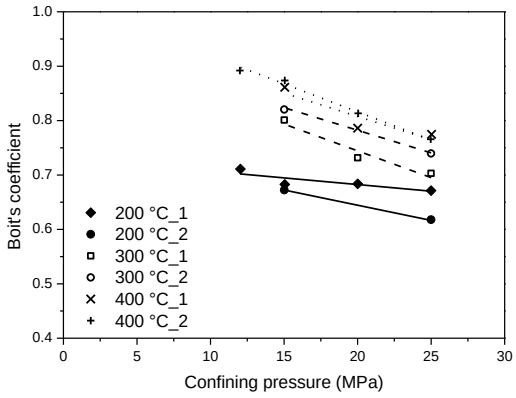

Fig. 4.1 Biot's coefficient b for concrete heated up to 400 °C (Chen et al. 2009).

As for explosive spalling, the measured and predicted pore pressures in Chapter 3 are both in the lower range, i.e. lower than 5 MPa and the spalling temperature is reported in the temperature range from 250 °C to 400 °C (fib Bulletin No. 46 2008). To predict explosive spalling of concrete, the Biot's coefficient for spalling prediction must be determined based on the test results. Fig. 4.1 shows the test results of Biot's coefficient for concrete by Chen (2009). At each temperature point, two specimens were tested. It can be seen that the lower the confining pressure, the higher the Biot's coefficient and the Biot's coefficient increases with temperature. These results show that to predict explosive spalling of concrete, the

commonly used porosity of concrete is far lower than the real fraction of pore pressure that transferred to the matrix. Above 300 °C in the low pressure range, the Biot's coefficient should be higher than 0.85. As for the pore pressure, in the spalling temperature range, the Biot's coefficient *b* is recommended as 0.9, near the upper limit of the measured result.

Furthermore, test results by Felicetti (2013) have suggested that the effective stress coefficient at high temperature is independent from porosity, fiber content and heating rate. Therefore, the proposed Biot's coefficient 0.9 will be applied to both OPC and HPC with or without PP-fibers and the effective stress from pore pressure is given in Equation 4.3:

$$\hat{\sigma}_{\mathrm{P}} = b\sigma_{\mathrm{p}} \tag{4.3}$$

4.2.2 Superposition of stresses

The spalling criterion proposed by Zhukov (1976) has been taken to consider the superposition of stresses in concrete. The spalling criterion is developed based on the scenario shown in Fig. 4.2 a) and all the stresses acting on a heated concrete specimen are involved in a reference system of axes *x*, *y* and *z*. It is assumed by Zhukov that the elastic theory is applicable and the strain in the x-direction may be described by:

$$\varepsilon_x = \frac{1}{E}\left[\sigma_x - v(\sigma_y + \sigma_z)\right] \tag{4.4}$$

Where σ_x is the stress acting in the *x*-direction, σ_y the stress acting in the *y*-direction, σ_z the stress acting in the *z*-direction, *v* the Poisson's ration and *E* the modulus of elasticity. Considering the effective stresses from pore pressure, the stresses acting in each orthogonal direction are summarized in Table 4.1. It is assumed that the specimen is loaded in the *y*-direction and the thermal stress in the *y*-direction and *z*-direction are equal under the uniform heating perpendicular to *x*-direction, as shown in Fig. 4.2 b).

Table 4.1 Stresses acting on a slab heated on one face (1-D model).

Direction	Description	Acting stresses
x-direction	Perpendicular to heated surface	Pore pressure $b\sigma_{\mathrm{p}}$ (tensile)
y-direction	External loads, parallel to surface with loads	Pore pressure $b\sigma_{\mathrm{p}}$ (tensile) Thermal stress σ_{t} (compressive) External loads σ_{L} (compressive)
z-direction	Parallel to heated surface without loads	Pore pressure $b\sigma_{\mathrm{p}}$ (tensile) Thermal stress σ_{t} (compressive)

Applying the acting stresses from Table 4.1 to Equation 4.4, where the effective stress from pore pressure is considered, the total strain observed in a uniaxial loaded specimen is given by

$$\varepsilon_x = \frac{1}{E}\left[b\sigma_{\mathrm{P}} - v(2\sigma_{\mathrm{t}} + \sigma_{\mathrm{L}} + 2b\sigma_{\mathrm{P}})\right] \tag{4.5}$$

The strain energy density in the x-direction w_x may be described by

$$w_{\mathrm{P}} = \frac{1}{2} b\sigma_{\mathrm{P}}\varepsilon_x \tag{4.6}$$

The critical concrete spalling energy $w_{spalling}$, which defines the work needed to cause spalling, can be written as:

$$w_{\text{spalling}} = \frac{1}{2} f_{t,\text{T}} \frac{f_{t,\text{T}}}{E} \qquad 4.7$$

Where $f_{t,T}$ is the tensile strength of concrete at temperature *T*.

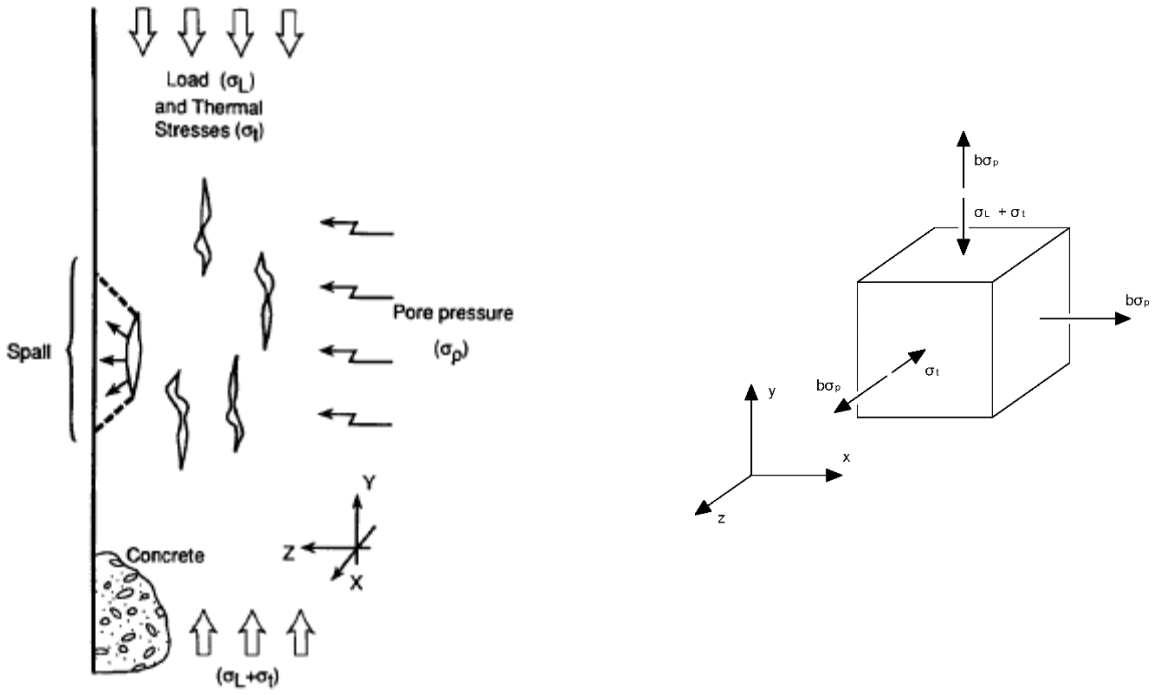

a) Stresses acting in heated concrete (after Zhukov, 1976).

b) Acting effective stresses, considering Biot's coefficient.

Fig. 4.2 Stresses acting in heated concrete.

Spalling is predicted when the strain energy density w_p exceeds the concrete spalling energy, i.e. $w_p \geq w_{spalling}$. Knowing that the spalling occurs in the temperature range from 250 °C to 400 °C, combining Equations 4.5, 4.6 and 4.7, gives a basic criterion $\sigma_{spalling}$ compared to the tensile strength for explosive spalling:

$$\sigma_{\text{spalling}} = \sqrt{(1-2\nu)b^2\sigma_{\text{P}}^2 - \nu(2\sigma_{\text{t}} + \sigma_{\text{L}})b\sigma_{\text{P}}} \geq f_{t,\text{T}} \quad , 250\ ^{\circ}\text{C} \leq \text{T} \leq 400\ ^{\circ}\text{C} \qquad 4.8$$

An explosive spalling of concrete will be predicted when the $\sigma_{spalling}$ reaches the temperature dependent concrete tensile strength $f_{t,T}$ in the explosive spalling temperature range from 250 °C to 400 °C (fib Bulletin No. 46 2008). The restrained thermal stress is in compression near the heated surface and will increase the $\sigma_{spalling}$, so the effects are combined with the pore pressure. The thermal stress σ_t in the *y*-direction and the *z*-direction are in a plane strain condition and can be calculated from the temperature differences:

$$\sigma_{\text{t}} = \frac{E}{1-\nu}\varepsilon_{\text{t}} = \frac{E}{1-\nu} adT \qquad 4.9$$

As for the plate, the thermal stress follows $\sum\sigma_t = 0$ and $\sum M_t = 0$, where ε_t is the thermal strain, α the temperature expansion coefficient and dT the temperature difference. Fig. 4.3 shows an example of a predicted explosive spalling: the tensile strength of concrete decreased during heating and the $\sigma_{spalling}$ increased with the pore pressure. Combining the effects from pore pressure and the thermal stress, the $\sigma_{spalling}$ reached the temperature dependent concrete tensile strength at a depth of 7 mm after 25 minutes. The temperature at the spalling point was between 250 °C and 400 °C, therefore the explosive spalling was predicted at 7 mm after 25 minutes of heating. On the other hand, if the tensile strength reduces to lower than $\sigma_{spalling}$ at a temperature above 400 °C, the degradation of concrete is not considered as explosive spalling. As shown in Fig. 4.4, the tensile strength was low after 120 minutes of heating, but the spalling was not predicted. This result agrees with the observation in the test of HPC with PP-fibers, in which the tensile strength decreased significantly, but the low pore pressure would not trigger explosive spalling. This can be explained by the fact that explosive spalling occurs only when the strain energy density w_x is high enough to induce explosive failure. Details of such protective methods will be discussed in Chapter 5.

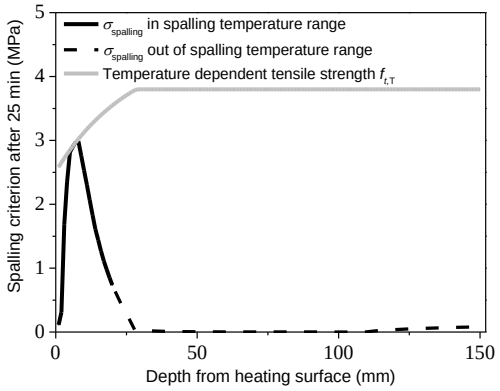

Fig. 4.3 Spalling predicted after 25 minutes.

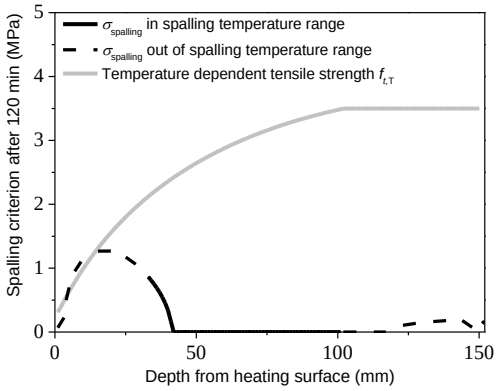

Fig. 4.4 No spalling predicted after 120 minutes.

This proposed spalling criterion takes the framework by Zhukov and considers the effective stress from pore pressure. The TH-model and the modified permeability model are applied to simulate the pore pressure. The spalling temperature range is determined based on the test results and the slow degradation after a long period of heating is not predicted as explosive spalling. The non-spalled concrete will work as isolating, as in the Mont Blanc Tunnel example discussed in Chapter 2, the consequence is different as the spalled sections. In this way, the risk of spalling will not be over-estimated. The consideration of external loads will be validated in Section 4.3 and the effects from external loads will be further discussed in Section 4.5.

4.3 Validation

The validation of the proposed spalling criterion is presented in this section, where the predicted spalling time and depth of an unloaded HPC slab were compared against the observations in the fire test. As for the loaded case, the spalling criterion was calculated for an OPC slab with and without external loads to compare with the test results.

4.3.1 Explosive spalling of HPC

The spalling criterion was applied to the fire tests on HPC slab, which were heated according to the ISO fire curve (ISO-834 2002) at the fire laboratory at EMPA (Swiss Federal Laboratories for Materials Science and Technology). One of the tests was stopped manually when the initial spalling occurred with a loud cracking sound. The depth of the initial spalling was measured and the predicted spalling time from the criterion can be validated against the test duration.

The used HPC mixture had a 28-day compressive strength of 103 MPa, initial moisture content of 3.1 % as measured by concrete moisture encounter (EMPA 2004) and a permeability of 1.05×10^{-18} m^2. The slab with dimensions of $l \times w \times h = 1100 \times 900 \times 150$ mm^3 was tested in a small horizontal gas/oil furnace. The burners start with gas and then switch to oil due to its higher energy content. The temperatures in different depths of the concrete slab were measured by type K thermocouples.

The explosive spalling was observed after 14 minutes of fire exposure as shown in Fig. 4.5 and the depths of spalling were measured after the slab cooling from high temperature. Fig. 4.6 shows the measured depth of the initial spalling, it can be seen that the maximum depth reached 8 mm and the average depth was about 6 mm.

Fig. 4.5 Spalled HPC slab after 14 minutes of fire exposure.

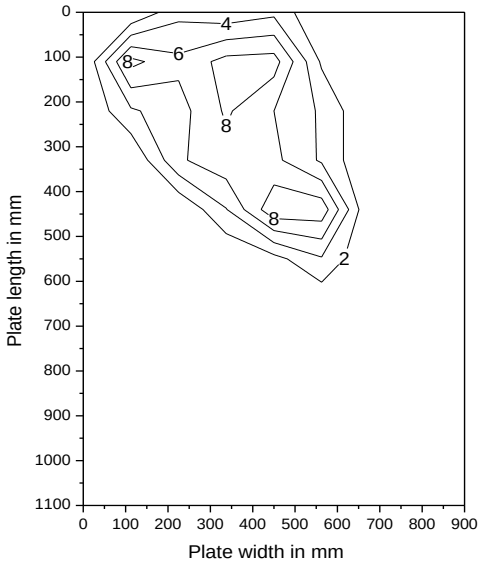

Fig. 4.6 Measured depths of the initial spalling.

The simulation of the fire test was carried out using the proposed TH-model. An agreement of the predicted and measured temperatures was achieved as shown in Fig. 4.7. The furnace temperature followed the ISO fire curve and on the surface and inside of the slab, the predicted temperatures agreed well with the test results. Based on the temperature simulation, the thermal stress was calculated using Equation 4.9 and the effect from the reinforcement was neglected. Fig. 4.8 shows the self-equilibrium thermal stress of the slab section. The compressive thermal stress was induced near the heated surface due to the heat expansion. Inside the slab, the thermal stress was in tension in some parts. Without considering

the reinforcement, the thermal stress is limited to the strength of concrete. For the pore pressure, the proposed TH-model was applied with the measured permeability and moisture content. The results are shown in Fig. 4.9, it can be seen that the pore pressure reached 1 MPa at 5 mm within 20 minutes. For the deeper region, higher pore pressure was predicted in the process of heating.

With the predicted pore pressure and thermal stress, spalling was predicted by the spalling criterion. As shown in Fig. 4.8, the shallow section was in the spalling temperature range from 250 °C to 400 °C and the spalling criterion σ_{spalling} reached the reduced tensile strength of concrete at a depth of 7 mm after a total fire exposure time of t = 19 min. The predicted spalling depth of 7 mm agreed well with the test result, in which the initial spalling occurred at a similar position. The predicted spalling time was 5 minutes later than that in the test. Taking into consideration the uncertainty in high temperature properties, the prediction time of 19 minutes can be taken as acceptable. In general, the presented prediction of spalling time and depth imply that the spalling criterion combining the effects from pore pressure and thermal stress is capable of prediction the spalling with sufficient accuracy.

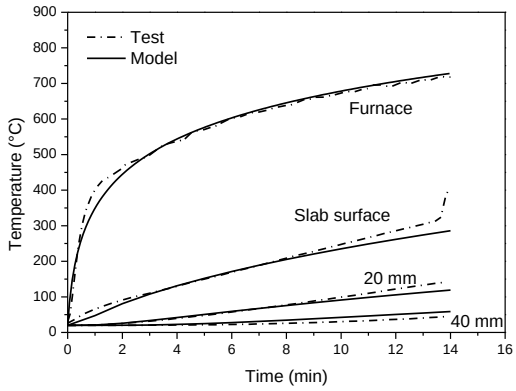

Fig. 4.7 Comparison of measured and predicted temperature for the slab.

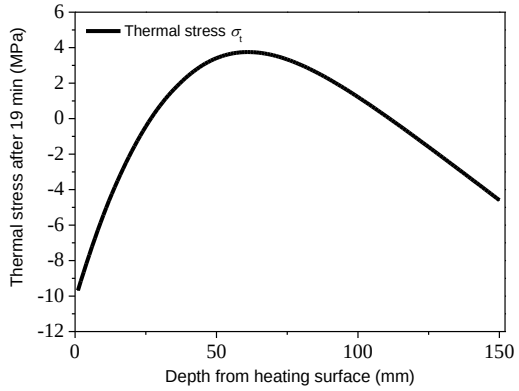

Fig. 4.8 Predicted thermal stress after 19 minutes.

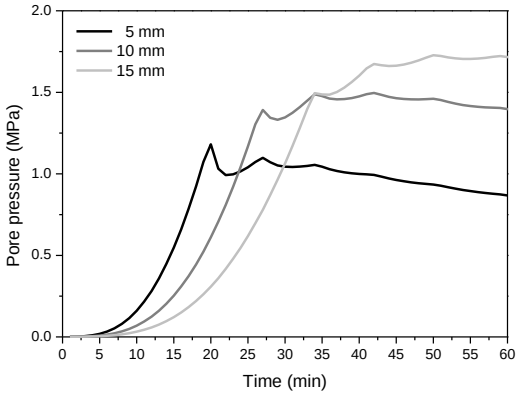

Fig. 4.9 Predicted pore pressure at a depth of 5 mm, 10 mm and 15 mm.

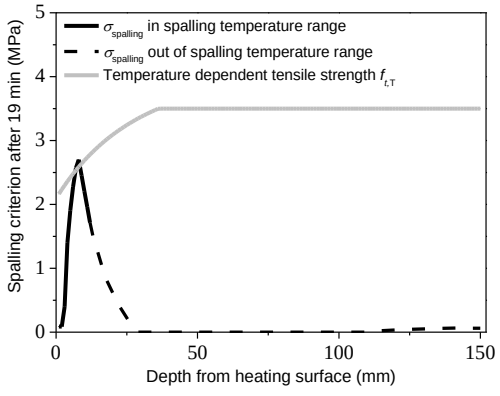

Fig. 4.10 Spalling predicted after 19 minutes (ISO fire curve).

4.3.2 The role of external loads

The proposed spalling criterion involves the external loads, whose effect will combine with thermal stress and pore pressure. As indicated by Equation 4.8, the compressive loads can exacerbate the stress state and make the concrete more susceptible to explosive spalling. The simulations of an OPC slab with and without external loads have been carried out to illustrate the effects.

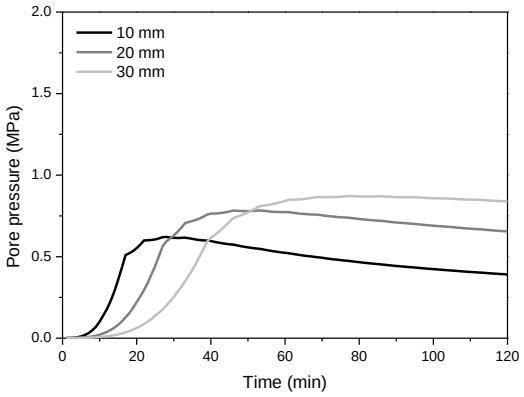

Fig. 4.11 Predicted pore pressure at a depth of 10 mm, 20 mm and 30 mm (ISO fire curve).

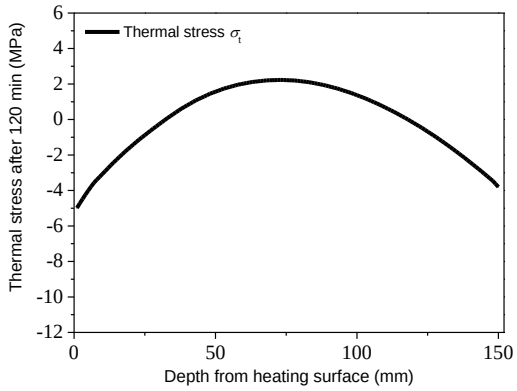

Fig. 4.12 Predicted thermal stress after 120 minutes of ISO fire exposure.

The selected OPC had a tensile strength of 2.45 MPa and was heated according to the ISO fire curve (ISO-834 2002). Fig. 4.11 shows the predicted pore pressure in a slab from TH-model, which was below 1 MPa in the shallow region. Combining with the thermal stress shown in Fig. 4.12, no spalling was predicted after 120 minutes of ISO fire exposure. In Fig. 4.13 it can be seen that the spalling criterion reached the tensile strength but the local temperature was out of the spalling temperature range. The degradation due to long period fire exposure is not predicted as explosive spalling.

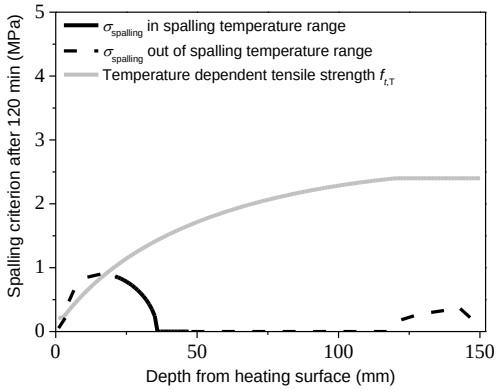

Fig. 4.13 No prediction of spalling after 120 minutes of ISO fire exposure.

When the compressive stress was applied in the *y*-direction, the total stress state is as shown in Fig. 4.14. For simplicity, the redistribution of stress was not considered, Equation 4.8 superimposed the effects linearly. Due to the applied compressive stress, the spalling criterion increased significantly and reached the tensile strength at 44 minutes. Spalling was predicted at a depth of 11 mm, which was in the spalling

temperature range at the predicted spalling time. The effect from external loads has been taken into account: spalling was predicted for a loaded OPC slab, which was not prone to spalling without applying the compressive stress.

The effects from the external loads have been reported in some tests. Carré (2013) tested an ordinary concrete and the measured pore pressure was also around 1 MPa. No spalling was observed after 120 minutes of ISO fire exposure and with 15 MPa of external compressive stress, explosive spalling occurred to the OPC slab. However, in the test, the explosive spalling was not induced by applying 5 MPa compressive loads. In addition, a slight but noticeable decrease in the pore pressure was recorded with the increase of applied loads. This could be explained by an increase of the permeability when compressive stresses increased. Hence, it may be concluded that the effects from external loads can be considered by superimposing the stresses and the evaluating accuracy of the loaded concrete elements depends on the change of permeability due to compressive stress. The permeability under compressive stress will be studied and the pore pressure will be calculated considering the effect from external loads.

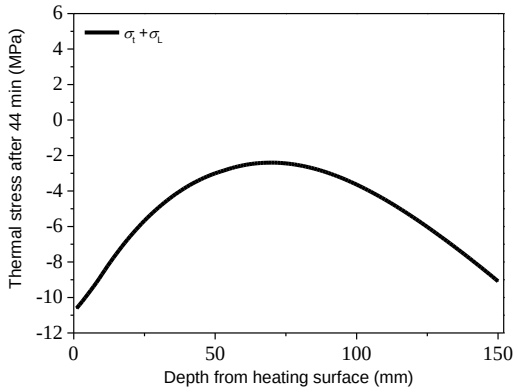

Fig. 4.14 The thermal stress and external loads.

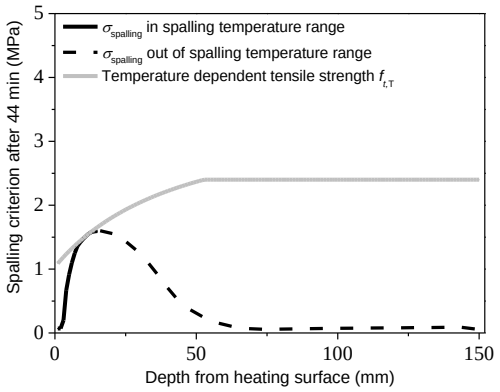

Fig. 4.15 Spalling predicted in the loaded OPC after 44 minutes of ISO fire exposure.

The proposed spalling criterion has been validated against the experimental behavior of concrete. The predicted spalling time and depth of the HPC slab agreed well with the test results. As for the external loads, the spalling criterion has involved the compressive stress and higher susceptibility to spalling can be explained by the superposition of the stresses. Therefore, the proposed spalling criterion can be taken as a useful framework to predict explosive spalling. In addition, with the help of a modified permeability model, the protective methods, i.e. PP-fibers and protective lining, can also be evaluated by the spalling criterion and the details will be shown in Chapter 5.

The permeability of concrete, moisture content of concrete and the heating rate are influential to the explosive spalling (Jasson 2013). Using the proposed spalling criterion, the effects from these factors on explosive spalling will be discussed in the following sections. The role of external loads in determining the susceptibility of concrete to spalling will be examined by the experimental tests and the proposed spalling criterion later in this Chapter.

4.4 The effects from permeability and moisture content on explosive spalling

It is widely believed that concretes become more susceptible to explosive spalling with lower permeability and less susceptible to explosive spalling with lower moisture content (Meyer-Ottens 1972, Connolly 1995, Jasson 2013). The effect from low permeability has been involved in the TH-model to predict the pore pressure. As has been discussed in Chapter 3, the moisture content influences the permeability of concrete and the change of pore pressure due to various moisture contents has been predicted by the TH-model. However, only a minor effect on pore pressure has been noticed in the shallow region of concrete and the difference of pore pressure may not explain the effect from moisture content. The effect from moisture content has been further discussed by the spalling criterion.

The proposed spalling criterion considers the moisture content with respect to both pore pressure and thermal stress. The latent heat due to the vaporization of water has been involved in the change of specific heat of concrete in Chapter 3. The specific heat increases in the concrete with high moisture content in the temperature range from 100 °C to 200 °C, corresponding to the latent heat. The heat transfer slows down in the temperature range from 100 °C to 200 °C and the thermal gradient increases in the vaporization zone. As a result, the thermal stress is higher near the heated surface. To illustrate the effect, a concrete slab with high and low moisture content exposed to ISO fire curve has been simulated. As shown in Fig. 4.16, the thermal stress in the concrete slab with 3 % moisture content reached higher than that with 0.4 % moisture content due to the vaporization of water. As for the pore pressure, a discussion in Chapter 3 shows that higher pore pressure will be predicted in the shallow region of concrete with high moisture content. As shown in Fig. 4.17, the high moisture content resulted in higher pore pressure in the shallow region and the development of pore pressure was postponed compared to that in concrete with low moisture content by the vaporization of higher moisture content. Considering the combined stress from pore pressure and thermal stress, the spalling criterion takes the effects from moisture content into account and the higher risk due to moisture content can be explained.

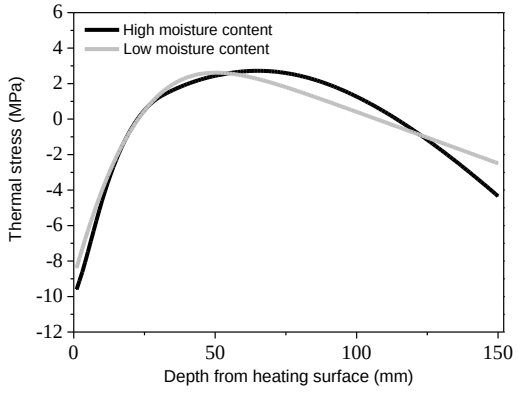

Fig. 4.16 Predicted thermal stress in concrete with high and low moisture content when heated according to ISO fire curve.

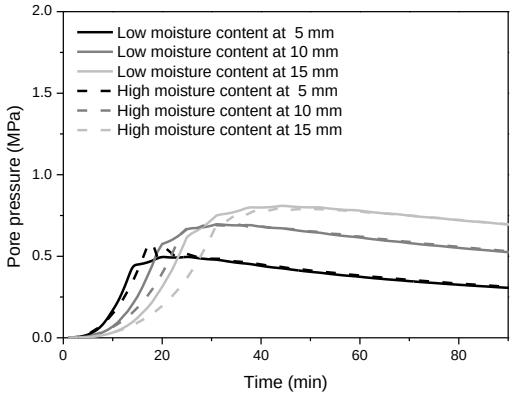

Fig. 4.17 Comparison of predicted pore pressures of concrete with high and low moisture content.

To study the effects from permeability and moisture content, the boundary permeability for liability to spalling has been proposed by a series of simulations. Equation 4.8 indicates that spalling is predicted when the spalling criterion reaches the tensile strength. The higher tensile strength is, the higher the spalling

criterion the concrete can withstand. Knowing the spalling criterion is related to the permeability, the permeability boundary of susceptibility to explosive spalling is influenced by the tensile strength as well. To study the effect from permeability, a relatively low tensile strength of 2.5 MPa is assumed to get a conservative permeability boundary. Some calculations from the spalling criterion are shown in Fig. 4.18. For the unloaded concrete slab with a tensile strength of 2.5 MPa, when heated according to ISO fire curve, the permeability boundary of susceptibility to spalling is proposed as 2×10^{-17} m^2. Explosive spalling is prone to occur in the unloaded concrete with a permeability lower than 2×10^{-17} m^2 and the risk of spalling reduced with the decrease of moisture content, because of the slightly higher pore pressure and thermal stress. However, the effect from moisture content is not as significant as Harmathy (1965) proposed. As shown in Fig. 4.18, the predicted spalling risk from the spalling criterion increased marginally with moisture content. Similar trend has been proposed by Sermehmetoglu (1977) and observed by Zheng (2010), which can be explained by the fact that the difference of moisture content will offset during heating. It can be seen that the permeability boundary is dependent on the tensile strength as well: the boundary of permeability moves to the left in Fig. 4.18 with the increase of tensile strength and vice versa. The effect from tensile strength has not been further validated because of the lack of test results, which should be addressed in the future. The proposed permeability boundary of 2×10^{-17} m^2 for concrete slab heated according to ISO fire curve corresponds to a relatively low tensile strength, which can be taken as a conservative value.

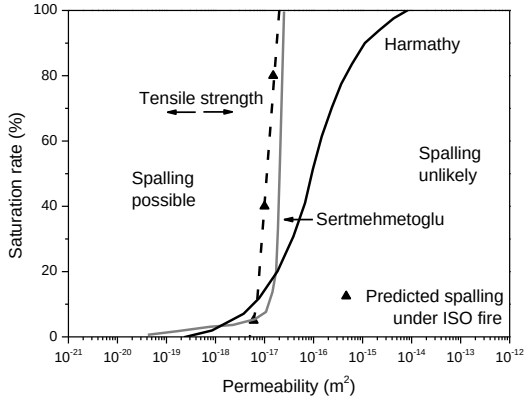

Fig. 4.18 Liability to spalling.

To study the risk of spalling, moisture content will be measured with permeability as the input for the TH-model, as the permeability changes with moisture content. In addition, the moisture content will be considered in the spalling criterion, which influences the thermal stress as well. The strategy of spalling risk evaluation will be presented in Chapter 5.

4.5 The role of heating rate

Test results have indicated that increasing the rate of heating promotes the likelihood of explosive spalling (Connolly 1995). The effect of heating rate on explosive spalling has been investigated by the spalling criterion under the exposure of three fire scenarios, namely hydrocarbon standard fire (Eurocode 1 2012), ISO fire curve (ISO-834 2002) and 10 K/min. The three fire scenarios are selected to represent high, medium and low heating rates, as shown in Fig. 4.19.

The high heating rate according to the hydrocarbon fire curve is given as:

$$T = 20 + 1280 \times (1 - 0.325e^{-0.167t} - 0.675e^{-2.5t}) \quad 4.10$$

The medium heating rate according to the ISO fire curve is given as:

$$T = 20 + 345 \times \log(8t + 1) \quad 4.11$$

The low heating rate of 10 K/min is given as:

$$T = 20 + 10 \times t \quad 4.12$$

Where *T* is the temperature at the time of *t* in minutes.

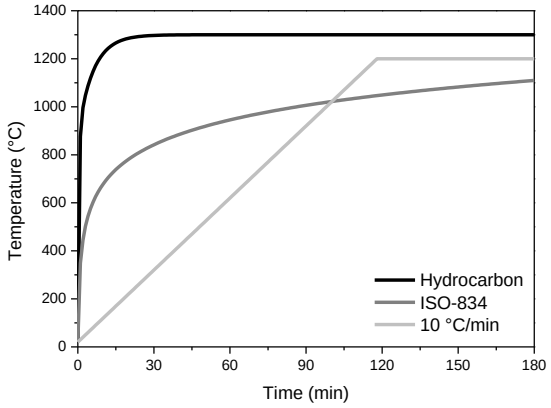

Fig. 4.19 Time-temperature curves for the fire scenarios used in the analysis.

4.5.1 The effects of heating rate on thermal stress

The temperatures in a concrete slab were simulated according to the three fire scenarios and the predicted thermal stress is shown in Fig. 4.20. As expected, the higher the heating rate is the higher the induced thermal stress. Fig. 4.20 a) shows the thermal stress in the heated slab after 10 minutes of exposure, under hydrocarbon fire the temperature was highest and the intensive heating induced a high temperature gradient and thermal stress. The heating scenario of 10 K/min induced a limited temperature rise on the surface, accordingly the thermal stress was modest in the slab. After 20 minutes of exposure, as shown in Fig. 4.20 a), the thermal stress under hydrocarbon fire and ISO fire was close, which was limited by the tensile strength due to self-equilibrium. The predicted thermal stress in the slab under the hydrocarbon fire was lower than that at 10 minutes, which indicated that the effect from high heating rate reduced with heating. As for the exposure for 60 minutes, the induced thermal stress by low heating rate was close to that under high heating rate as well, as shown in Fig. 4.20 a).

It can be seen from the predictions that a high heating rate will induce high thermal stress and in the early stage of heating, this effect is more significant.

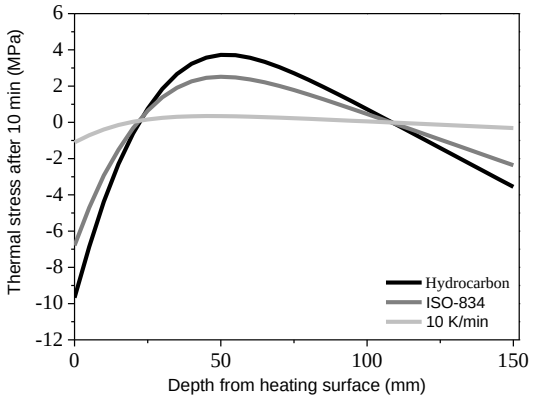

a) Thermal stress after 10 minutes.

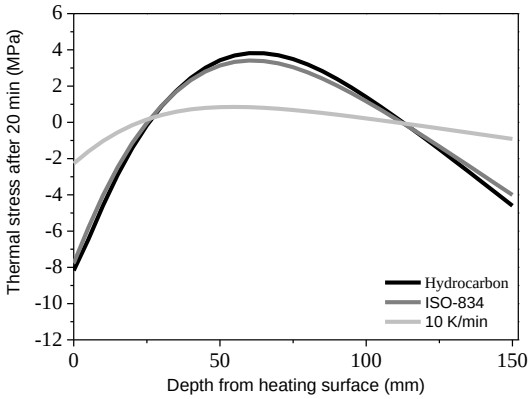

b) Thermal stress after 20 minutes.

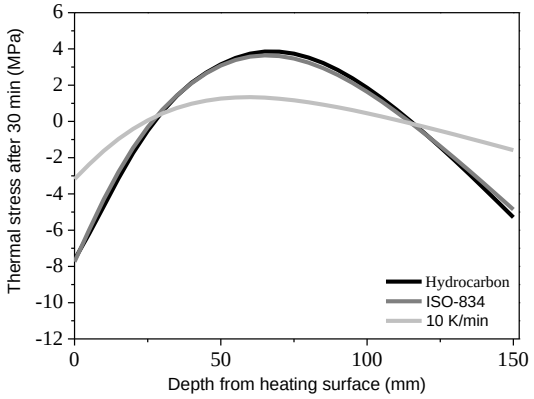

c) Thermal stress after 30 minutes.

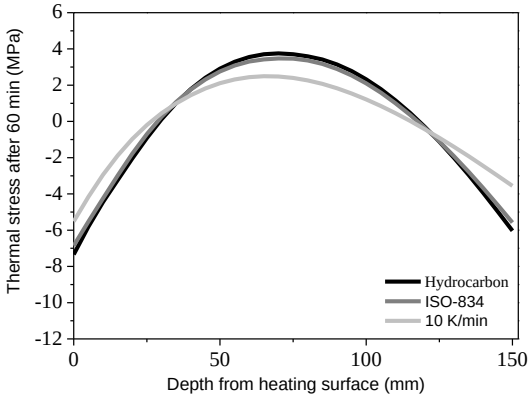

d) Thermal stress after 60 minutes.

Fig. 4.20 Predicted thermal stress in a concrete slab exposed to the three fire scenarios.

4.5.2 The effects of heating rate on pore pressure

As for pore pressure, effects on both OPC and HPC were investigated by the TH-model. The pore pressure of mixtures with permeability of 3×10^{-16} m^2 and 3×10^{-18} m^2 respectively, have been simulated. The predicted pore pressures at 10 mm in OPC are shown in Fig. 4.21. Under high heating rate, i.e. hydrocarbon fire curve, highest pore pressure has been predicted. Low heating rate of 10 K/min induced lowest pore pressure.

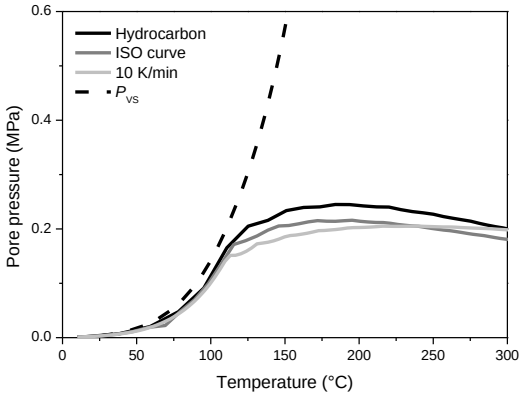

Fig. 4.21 Predicted pore pressure at 10 mm in OPC (3×10^{-16} m^2) when exposed to the three fire scenarios.

The simulation of pore pressure for HPC indicated higher pore pressure under high heating rate as well. Fig. 4.22 shows the predicted results, it can be seen that the time of high pore pressure corresponds to the rise of temperature and the peak value of pore pressure was lower after longer fire exposure. Similar to OPC, pore pressure has been predicted to increase with the severity of heating, which agrees with the test results (Bangi & Horiguchi 2010). Therefore, by inducing higher pore pressure and thermal stress, intensive heating should increase the spalling risk. The effect on explosive spalling will be discussed in the next section.

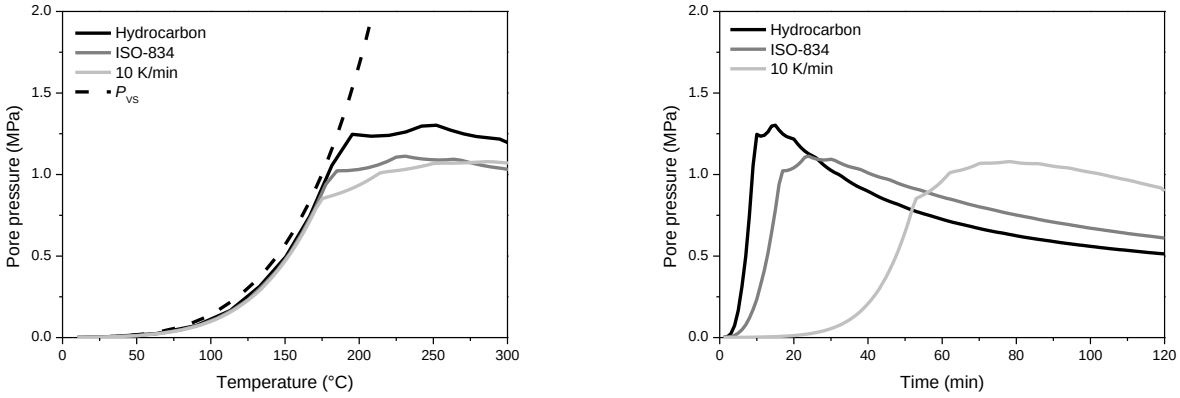

a) Pore pressure against temperature. b) Pore pressure against time.

Fig. 4.22 Predicted pore pressure at 10 mm in HPC (3×10^{-18} m^2) when exposed to the three fire scenarios.

4.5.3 The effects of heating rate on explosive spalling

To illustrate the effect of heating rate on spalling risk, a concrete slab heated according to hydrocarbon and ISO fire curves has been simulated by the spalling criterion. The assumed permeability was 2×10^{-17} m^2, on the right side of the permeability boundary for liability to spalling as proposed in Section 4.2, which did not induce explosive spalling under ISO fire. As shown in Fig. 4.23, the spalling criterion reached the tensile strength outside of the spalling temperature range and no explosive spalling was predicted. On the other

hand, under a hydrocarbon fire, the temperature reached 900 °C in 8 minutes and an explosive spalling was predicted by the high pore pressure and thermal stress in the same concrete slab. As shown in Fig. 4.24, in the spalling temperature range, the spalling criterion reached the reduced tensile strength after 54 minutes of hydrocarbon fire exposure. The high heating rate reduced the permeability boundary for liability to spalling proposed for ISO fire curve. It can be concluded the risk of explosive spalling increases with increasing heating rate, because of the induced higher pore pressure and thermal stress. The proposed permeability boundary in Fig. 4.18 will move left under modest heating and move right under intensive heating.

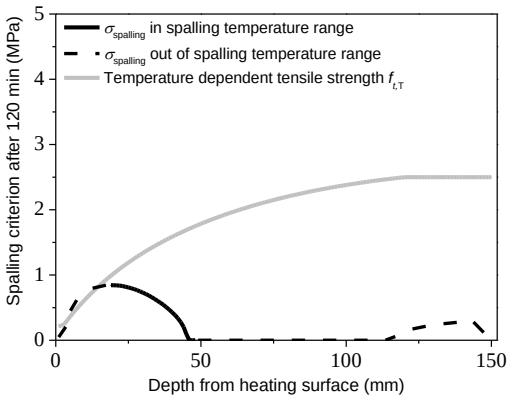

Fig. 4.23 No spalling predicted after 120 minutes of ISO fire exposure (2×10^{-17} m^2).

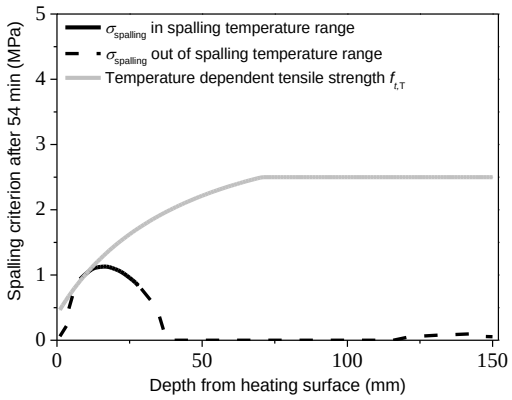

Fig. 4.24 Spalling predicted after 54 minutes of hydrocarbon fire exposure (2×10^{-17} m^2).

Apart from influencing the spalling risk, the severity of the fire plays a role in the pattern of explosive spalling as well. Klingsch (2013) reported from the test that under high heating rates the spalling depth was shallow and the spalling occurred layer by layer with cracking sounds; low heating rates resulted in a deeper spalling, occurring with one single loud bang. The proposed spalling criterion based on the combined mechanism is capable of considering the pattern of explosive spalling as well. The spalling of slab made of HPC with permeability of 2×10^{-18} m^2 has been simulated according to the three fire scenarios. The predictions are made with an assumed tensile strength of 3.5 MPa, as shown below.

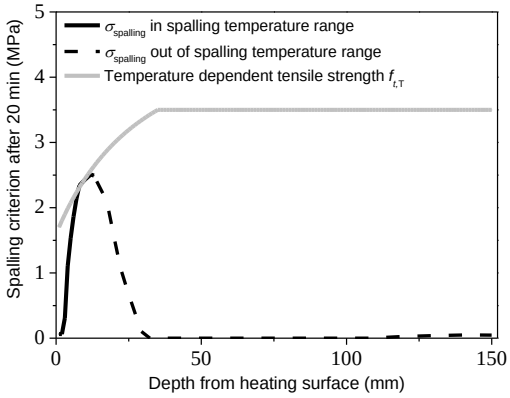

Fig. 4.25 Spalling predicted at 8 mm after 20 minutes of hydrocarbon fire exposure.

Under hydrocarbon fire as shown in Fig. 4.25, the spalling criterion predicted that the heating according to the high heating rate led to an explosive spalling after 20 minutes and the spalling depth was 8 mm. Under lower heating rate, the spalling was predicted deeper in the section. As shown in Fig. 4.26, the spalling of a slab exposed to the ISO fire curve was predicted to occur after 48 minutes and the spalling depth was 10 mm. Similarly, the prediction of spalling induced by the heating rate of 10 K/min shown in Fig. 4.27 indicates a greater spalling depth of 14 mm. It can be seen that the different depths of predicted spalling corresponded to the observation in test: the depth of spalling increases with the decrease of heating rate. The pattern of spalling can be simulated by the proposed spalling criterion with respect to heating rate. This trend can be attributed to the higher pore pressure and the higher thermal stress near the heated surface induced by the high heating rate.

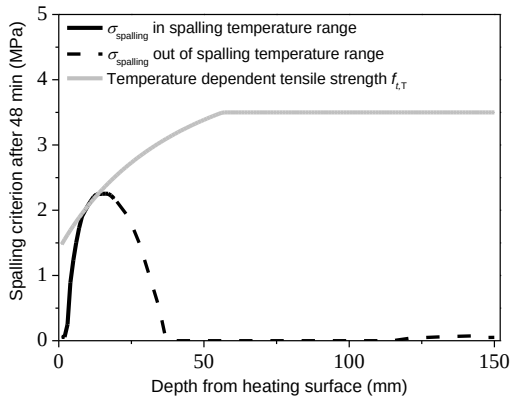

Fig. 4.26 Spalling predicted at 10 mm after 48 minutes of ISO fire exposure.

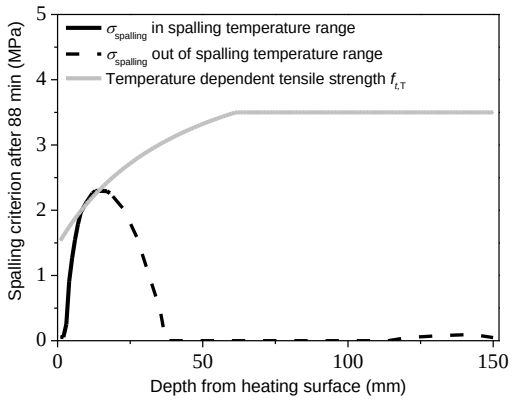

Fig. 4.27 Spalling predicted at 14 mm after 88 minutes under the heating rate of 10 K/min.

This section has investigated the heating rate, whose influence on explosive spalling can be explained in several ways. According to the spalling criterion, under high heating rate, the pore pressure and the thermal stress are higher. As a result, the concrete is more susceptible to explosive spalling and the permeability boundary for liability to spalling decreases with increasing heating rate. Referring to the pattern of spalling, the prediction agreed with the observations in test that low heating rate resulted in deeper spalling, which is usually more violent (Klingsch 2013). This effect will be considered in the protective methods, as presented in Chapter 5.

4.6 The role of external loads

The proposed spalling criterion involves the effect from external loads and the combined stresses indicates higher risk of explosive spalling, as discussed in Section 4.3. Some observations in tests can be explained by the spalling criterion, i.e. external loads induced explosive spalling in OPC with low permeability. However, the accuracy of the perdition was influenced by the change of permeability due to compressive stresses. Because the measured pore pressure varied with load levels (Carré 2013), the effect from external loads should not be linearly superimposed with the pore pressure and thermal stress, without considering the change of permeability of concrete under external loads.

To investigate the effect from external loads on permeability, the permeability of concrete are measured under axial compressive stresses. The measured permeability under various load level will be used as input

for the spalling criterion. The explosive spalling will be evaluated accordingly and the role of the external loads will be discussed in this section.

4.6.1 Permeability under external loads

The permeability of concrete is influenced by the external loads (Lu & Fontana 2015). The compressive stress may induce a lower permeability, when the concrete matrix is compressed denser. However, the permeability has been observed higher under certain levels of external load, because the development of micro-cracks may increase the permeability of concrete. To evaluate the spalling risk of concrete under external loads, the effects from external loads on permeability must be considered. The permeability was measured by the Torrent permeability tester, when various load levels applied on the specimens. Both OPC and HPC have been investigated, the details of the tests are listed in Appendix C.

It is noticeable that the permeability of HPC_1 increased sharply under 20 MPa of compression, because of the micro-cracks. The significant increase of permeability can prevent high pore pressure in concrete, the test results will be used in the spalling model to evaluate the spalling risk under external loads in the next section.

4.6.2 Effects from external loads on explosive spalling

There are only limited studies dealing with the effects of external loads on spalling, nevertheless, the results are contradictive: some claim the loading level did not increase the spalling risk (Ali et al 2004), however in some tests spalling increased significantly with increased compressive stress (Boström 2007). The proposed spalling criterion involves the effects from external loads with respects to both superposition of stresses and the change of permeability. The simulations of a concrete slab under different levels of external loads have been carried out to illustrate the consideration of external loads. The contradictive observations in tests will be discussed in the framework of spalling criterion.

The measurement of the permeability of HPC_1 under compressive stresses has shown that 20 MPa of external stress induced an increase of permeability to 1×10^{-14} m^2. In the simulation, a slab with an initial permeability of 3×10^{-18} m^2 and a tensile strength of 3.8 MPa was studied and the heating rate was according to the ISO fire curve. The permeability was assumed as 1×10^{-14} m^2, when the slab was under an external stress of 20 MPa. The spalling criteria for unloaded and loaded slabs are shown in Fig. 4.29 to Fig. 4.30.

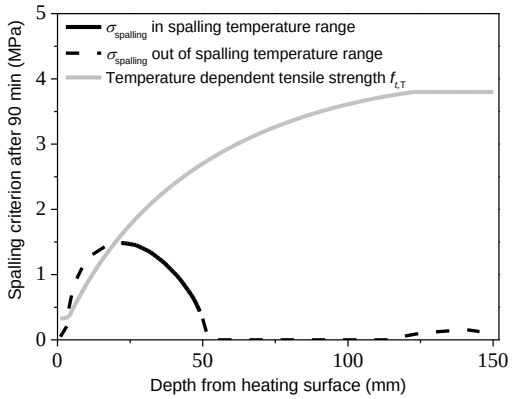

Fig. 4.28 No spalling predicted after 90 minutes for the unloaded slab.

The unloaded slab has been simulated and no spalling was predicted after 90 minutes of ISO fire exposure. Because of the assumption of a high tensile strength of 3.8 MPa, the boundary for liability to spalling is lower than 3×10^{-18} m^2, the spalling criterion did not reach the tensile strength in the spalling temperature range. These parameters were assumed to illustrate the contradictive effects from external loads, further tests should be carried out to validate the simulation of loaded slabs.

For the slab under 10 MPa compressive stress, the permeability was still 3×10^{-18} m^2 as measured in the permeability test under compressive load. The predicted pore pressure and thermal stress were combined with the 10 MPa of compressive stress by Equation 4.8, the prediction is shown in Fig. 4.29. The explosive spalling was induced by the external load after 32 minute of ISO fire exposure. It can be seen that with the compressive stress of 10 MPa, the spalling criterion was higher than that of the unloaded case. This result can explain how the external loads induced higher severity of explosive spalling, as observed in the tests by Boström (2007).

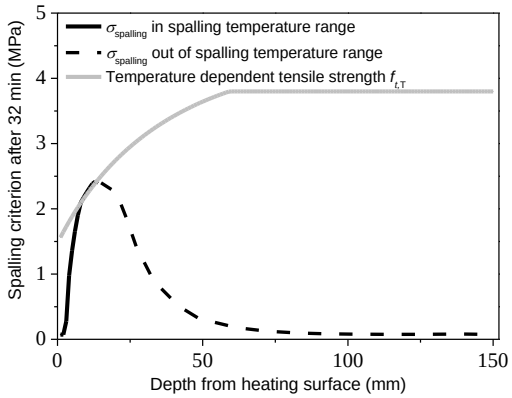

Fig. 4.29 Spalling predicted after 32 minutes for the slab under 10 MPa compressive load.

As for the slab under 20 MPa of compressive load, the permeability was taken as 1×10^{-14} m^2 according to the test results shown in Fig. 4.30. With the high permeability due to the development of micro-cracks, the pore pressure in the slab was predicted to be low. Combining the pore pressure with the thermal stress and

external compressive stress, the spalling criterion did not reach the tensile strength in the spalling temperature range. As shown in Fig. 4.30, the spalling criterion was modest and no spalling was predicted for the slab under 20 MPa of compressive load. This case simulates that the spalling risk can be reduced by applying external stress and the observation by Ali (2004) can be explained in the framework of the proposed spalling criterion. The absence of spalling can be attributed to the increased permeability and the decrease of pore pressure offsets the effect from the compressive stress.

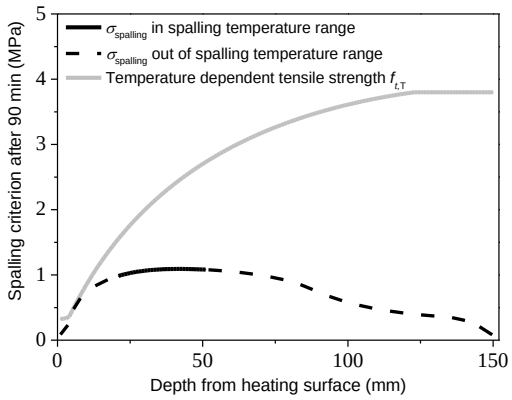

Fig. 4.30 No spalling predicted after 90 minutes for the slab under 20 MPa compressive load.

The simulations based on the assumed parameters were carried out and the three case studies have illustrated the various effects from external loads on explosive spalling. The contradictive observations in tests can be explained by considering the change of concrete permeability and the superposition of compressive stresses. It can be concluded that the external load increases the risk of explosive spalling by intensifying the stress state and explosive spalling can be prevented by the induced micro-cracks, especially in the brittle HPC.

It should be noticed that the cracks in concrete may distribute randomly and the permeability may not increase uniformly. Further tests should be carried out to study the influence of external load. The proposed criterion can be used as a framework to evaluate the effects, which should be validated against test results.

4.7 Conclusions

A spalling model has been proposed based on a spalling criterion similar to the considerations by Zhukov (1976). The validation of the prediction has been achieved by comparing against test results. The permeability measurement under compressive load has been carried out. The results provided input for the criterion to consider the effects from external loads. Some parameter studies have been performed in the framework of the proposed criterion. Here are some key conclusions summarized in the context:

1. The proposed spalling criterion involving pore pressure, thermal stress and external loads can consider explosive spalling induced by different fire scenarios. The predicted spalling time and depth by the spalling model agreed well with the test results. The spalling model can be used as a

framework to evaluate the effects from permeability, moisture content, heating rate and external loads.

2. The risk of explosive spalling increases with the decrease of permeability. A boundary permeability has been proposed as 2×10^{-17} m^2, with lower permeability the explosive spalling is more likely to occur. The boundary value is influenced by moisture content, tensile strength and heating rate.
3. Intensive heating increase the risk of spalling, because of the high pore pressure and thermal stress. The heating rate plays a role in the pattern of spalling as well: high heating rate induces shallow spalling and under low heating rate, the spalling is deeper and more violent. This trend agreed with the observations in tests.
4. External loads have been reported to induce contradictive effects on explosive spalling. The various effects can be explained by the spalling criterion. In general, the compressive load exacerbates the risk of spalling. The prevented spalling case by external loads can be attributed to the development of micro-cracks.
5. The modified permeability model will be used to consider the increased permeability by PP-fibers. The isolating effect from coating or plate will be simulated by the model as well. There are some recommended protective methods to prevent explosive spalling, the spalling model will be used to evaluate the effects. The practical application of the proposed spalling model will be presented in Chapter 5.
6. The spalling model provides a method to consider the above mentioned factors, some observations can be explained. However, to predict spalling more accurately, further tests should be carried out to validate and refine the model. The load effects should be further studied by permeability measurements and fire tests. The spalling model does not involve the reinforcement, whose effect on thermal stress and permeability should be tested for practical use as well.

5. Protective methods and spalling risk evaluation

5.1 Introduction

The use of high performance concrete (HPC) is appreciated due to advantages over ordinary concrete (OPC), e.g. higher strength and improved durability. However, the high susceptibility to explosive spalling during a fire has become a concern for the use of HPC. The discussion in previous chapters has shown that the low permeability of HPC is widely believed as the reason for its higher spalling sensitivity than OPC. To limit the risk of explosive spalling, several protective methods have been recommended. These methods can be grouped into two categories: polypropylene fibers (PP-fibers) and insulating materials. Several tests have been performed to study these methods and the positive effects will be shown in this chapter. The Type 2 PP-fibers used in Chapter 3 have been investigated, with the amount 2 kg/m^3 (recommended by Eurocode 2) and 3 kg/m^3, the effects to prevent explosive spalling in a HPC slab were tested. Similarly, protective mortar and plate were used as insulating materials in the fire test to HPC slabs, the thicknesses of the materials for various protection levels have been determined.

To investigate the protective mechanism, simulations of these methods have been carried out using the spalling model based on the spalling criterion. PP-fibers are believed to prevent spalling by increasing the permeability and the effect from insulating materials is mainly attributed to preventing the high thermal stress and fast degradation of concrete. The modified permeability model proposed in Chapter 3 considers the increase of permeability by PP-fibers and the effect on explosive spalling will be validated against the test results. The use of PP-fibers will be discussed and some suggestions will be offered. As for the insulating materials, the use of both protective mortar and plate will be simulated by the spalling model and the thickness of the insulating material will be studied. The use of these methods will be discussed in the framework of the proposed spalling criterion.

In fire safety design, the proposed spalling model can be used to predict the explosive spalling and to evaluate the protective methods. As shown in Chapter 4, the simulation from the spalling model is based on some parameters, e.g. permeability of concrete, moisture content. To evaluate to risk or protective methods accurately, the input for the models should be well determined. The measurements of parameters will be discussed. However, the measurements of some parameters are not always possible or very costly, especially the permeability of concrete at high temperatures. Therefore, based on the previous test results, the proposed permeability model can be used to assume the change of the permeability of concrete. A strategy using the spalling model will be introduced according to the experimental conditions.

5.2 Polypropylene fibers

The addition of PP-fibers has been proved valid for spalling protection of concrete in fire by test results (Ali et al 1996, Klingsch 2013). The effect is mainly attributed to the increase of permeability by the melting of PP-fibers, as a results, high pore pressure can be prevented. The effect from PP-fibers on permeability has been discussed in Chapter 3 and the reduced pore pressure can be predicted accordingly. The use of PP-fiber contents are normally expressed by ration of weight per volume, e.g. 2 kg/m^3 as recommended by Eurocode 2.

However, as shown in the permeability measurements of concrete with PP-fibers, the amount by weight was not the only factor that could influenced the spalling protection. The fiber geometry also affects the

increase of permeability. It has been concluded that the number of fibers per unit volume is a decisive factor. This conclusion agrees with test results by Heo (2012). As shown in Fig. 5.1, the severity of spalling was correlated to the number of fibers per unit volume and the liability to spalling was expressed by the fiber numbers as well. The greater the number of fibers added, the lower the susceptibility to explosive spalling. It can be seen that with the same amount by weight, the use of thin fibers is favorable for the spalling protection of concrete. On the other hand, the permeability measurements in Chapter 3 have shown that above the amount of 2 kg/m^3, the tested three types of fibers have shown similar effectiveness, the influence from types on the increase of permeability were limited.

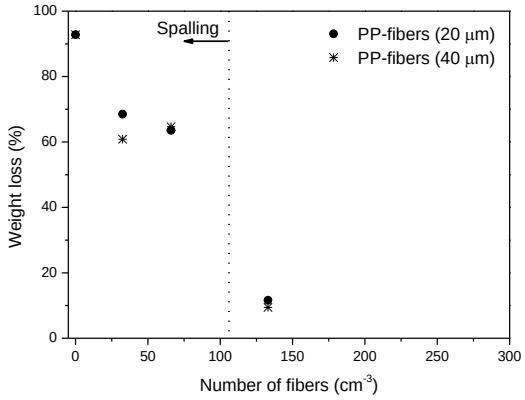

Fig. 5.1 Weight loss induced by spalling as a function of fiber number/cm^3 (Heo et al 2012).

Therefore, to prevent explosive spalling effectively, the thin PP-fibers (Type 2 with a diameter of 18 μm, as described in Chapter 3) were taken as standard. The amount of 2 kg/m^3, as recommended by Eurocode 2, will be validated by the test on a HPC slab. This process will be simulated by the spalling model, which considers the effects from PP-fibers. Based on this validation, other usage of PP-fibers, with various amount or type, can be evaluated against this standard recipe. The permeability increase will be compared against the standard recipe by Torrent measurements and the protective effect will be evaluated by the spalling model. The strategy of evaluation will be discussed in Section 5.5.

5.2.1 Experimental investigation

The use of PP-fibers has been tested on a HPC slab with dimensions of $l \times w \times h$ = 1100 × 900 × 150 mm^3. To validate the effects from PP-fibers, a dense HPC was chosen, with a high compressive strength over 120 MPa (Klingsch 2013). The amounts of 2 kg/m^3 and 3 kg/m^3 of Type 2 PP-fibers were tested according to ISO fire curve simultaneously on the slab, which consists of two segments, each measuring $l \times w \times h$ = 1100 × 450 × 150 mm^3. As shown in Fig. 5.2, the left part was made of HPC with 2 kg/m^3 of Type 2 PP-fibers, the right one of HPC with 3 kg/m^3 of Type 2 PP-fibers. Before the test, the specimen was cured in a humid environment for 28 days, where the temperature was kept at 20 °C and the relative humidity was 95 %.

The HPC slab containing the two segments with different amounts of PP-fibers was tested for 120 minutes at the fire laboratory at EMPA. According to the ISO fire curve, the temperature in the furnace was over 1000 °C after 120 minutes of heating. The temperatures at different positions over the slab were measured by type K thermocouples and the results will be used to validate the simulation in the next section. During

the test, moisture was noticed coming out of the specimen. No spalling was observed during the 120 minutes test and both parts of the concrete slab remained intact. No significant difference was noticed between the two parts.

It can be seen that 2 kg/m^3 of Type 2 PP-fibers can prevent explosive spalling in HPC. The recommended amount by Eurocode 2 is feasible for the thin PP-fibers. Higher amounts did not bring benefits in the tested slab. The validated 2 kg/m^3 of Type 2 will be recommended for practical use, other types or amounts of PP-fibers will be compared to this valid recipe. The evaluation by the spalling model will be shown in next section.

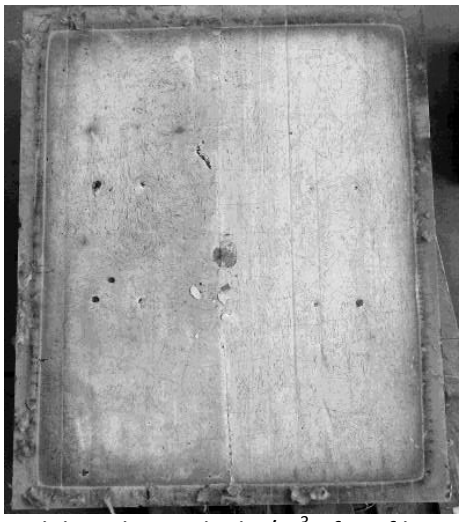

Fig. 5.2 HPC slab with 2 and 3 kg/m^3 of PP-fibers (l = 6 mm, $\emptyset$ = 18 μm) after 120 min of ISO-fire exposure.

5.2.2 Simulation by spalling model

The modified permeability model for PP-fibers has been proposed in Chapter 3 and an increasing factor has been introduced to the model. The use of PP-fibers has been taken into account in pore pressure simulation.

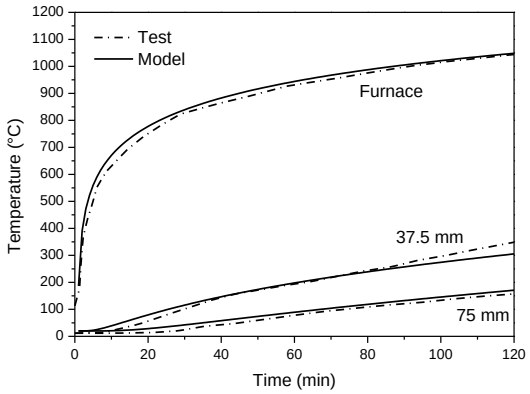

Fig. 5.3 Comparison of measured and predicted temperature for the slab.

To investigate the effects on the susceptibility to explosive spalling, the modified permeability model will be applied in the spalling model. The prediction will be validated against the test as described above.

The simulation of temperatures in the slab has been carried out and the predicted and measured temperatures are shown in Fig. 5.3. The furnace was heated according to the ISO fire curve and it can be seen that the predicted temperatures agreed generally well with the test results at different locations. The predicted temperatures were further used for the simulation of thermal stress. As shown in Fig. 5.4, after 120 minutes of ISO fire exposure, the thermal stress was about 7 MPa in compression near the heated surface. The predicted stresses will be combined with pore pressure by the spalling criterion.

To simulate the pore pressure, the permeability at ambient temperature of the tested HPC was measured by the Torrent permeability tester and the result was 1.25×10^{-18} m^2 (Klingsch 2013). As proposed in Chapter 3, the increasing factor for 2 kg/m^3 of Type 2 has been taken as 20. Using the modified permeability model, the pore pressure predicted by the TH-model has been presented in Fig. 5.5. The pore pressure was predicted to be higher in the deeper part; at the depth of 15 mm, the predicted pore pressure was below 0.8 MPa. Compared to the HPC without PP-fibers, the effect was significant.

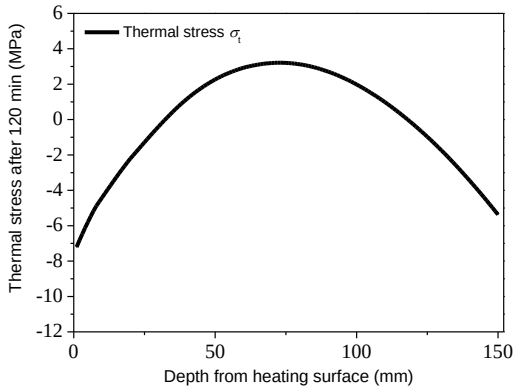

Fig. 5.4 Predicted thermal stress after 120 minutes.

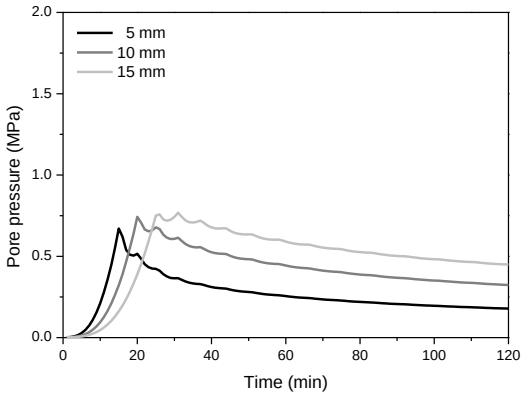

Fig. 5.5 Predicted pore pressure at depths of 5 mm, 10 mm and 15 mm.

Applying the spalling criterion, the risk of spalling has been evaluated by combining the stresses induced by the ISO fire. As shown in Fig. 5.6, the tensile strength of concrete reduced with time, the spalling criterion increased near the heated surface, no explosive spalling was predicted in two hours. During the heating, the spalling criterion did not reach the reduced tensile strength in the spalling temperature range. Out of the spalling temperature range, the heated surface may have degraded significantly, but not predicted to spall off from the specimen.

The simulation agreed with the test results, the effect from the standard recipe of PP-fibers has been taken into account by the increasing factor of 20. The proposed spalling model has been proved capable of evaluating the use of PP-fibers. With a higher amount of PP-fibers, e.g. 3 kg/m^3, the pore pressure would be predicted lower and the effect should be better according to the permeability measurements. No spalling occurred either, as the test result has shown.

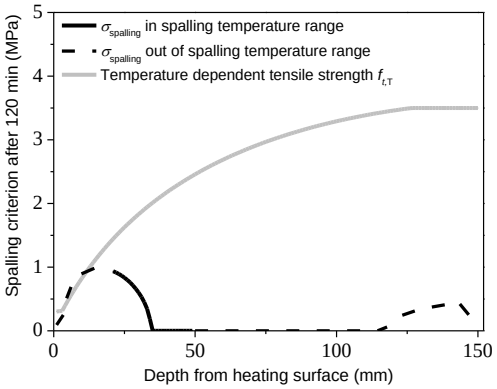

Fig. 5.6 No spalling predicted for the HPC slab with 2 kg/m^3 of PP-fibers after 120 minutes.

As for the case of 1 kg/m^3 of PP-fibers, the increasing factor was proposed as 10 in Chapter 3, the simulation was carried out as well. As shown in Fig. 5.7, the pore pressure was predicted slightly higher than that with 1 kg/m^2 corresponding to the less significant increase of permeability. The spalling criterion was higher, but still not sufficient to reach tensile strength in the spalling temperature range, as shown in Fig. 5.8. According to the prediction, 1 kg/m^3 of the Type 2 PP-fibers are also effective in preventing explosive spalling under ISO fire. Some test results have confirmed that lower amounts of PP-fibers, e.g., 1.0 kg/m^3 and 1.5 kg/m^3 could also prevent explosive spalling (Klingsch 2013), the usage should be validated by fire tests or simulations.

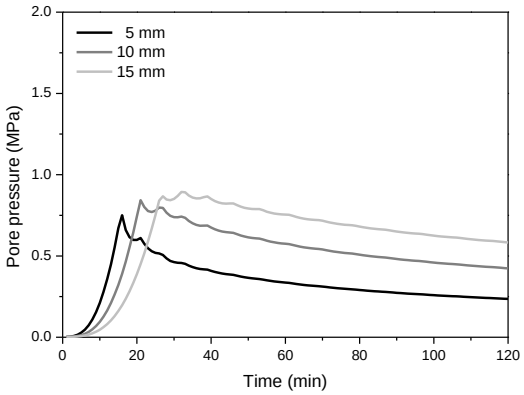

Fig. 5.7 Predicted pore pressure at depths of 5 mm, 10 mm and 15 mm.

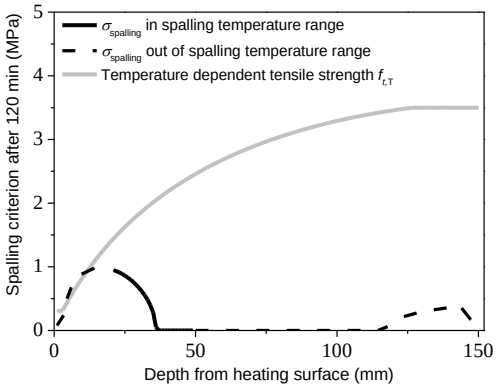

Fig. 5.8 No spalling predicted for the HPC slab with 1 kg/m^3 of PP-fibers after 120 minutes.

5.2.3 Practical considerations

The tests and simulations have shown that the addition of PP-fibers is capable of preventing explosive spalling and the increase of permeability is the major factor in the effect. In this section, the considerations for the practical usage of PP-fibers with respects to amount, type and workability will be discussed.

The recipe, 2 kg/m^3 of Type 2 PP-fibers, has proved capable of preventing explosive spalling in HPC by test. With a lower amount 1 kg/m^3, the effectiveness of the Type 2 has been validated by the spalling model based on the spalling criterion, using the results from the permeability measurement. As for other types of PP-fibers, the amount of 2 kg/m^3 is recommended, when no experimental data is available. Because with 2 kg/m^3, complying with Eurocode 2, the measured permeability increased equally in the concrete with different types of PP-fibers, as shown in Chapter 3. However, with lower amount, the effects on preventing spalling may be dependent on the diameter or length of the used PP-fibers. In this situation, fire test on the PP-fibers containing concrete element or permeability measurement at high temperature should be carried out. The effect can be validated by the test result or the spalling criterion.

The diameter of fibers has no significant effect on the spalling of concrete in fire, based on the test results. Since the water vapor size is significantly smaller than pores, the flow of vapor transport is more influenced by the connectivity of the pores (number of fibers) rather than the diameter of the pores (Heo 2012). Hence, with the same amount by weight, thin PP-fibers are recommended to prevent spalling. However, when using very fine fibers, there is a risk that they may stick together in bundles and not distribute evenly in the concrete (Smith 2010). In the laboratory, for the used PP-fibers with the 18 μm and 36 μm diameters, the mixing was not an issue, no clumps of fibers have been observed in the specimens (Fig. 5.9). In addition, the ESEM observation on PP-fibers in Chapter 3 has shown well distributed channels left by the melting of PP-fibers. For practical use, the mixing difficulties should be considered and the diameter can be a factor influencing the protective effect.

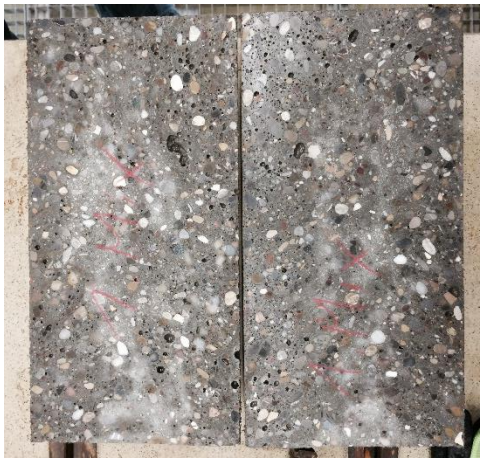

Fig. 5.9 Specimen of HPC with PP-fibers.

The addition of PP-fibers may result in a negative effect on workability. The fine fibers with greater surface area may demand extra cement paste or addition of admixtures, which may increase the cost. The selection of PP-fibers should take the practical aspect into account as well.

In this section, the benefits of using PP-fibers in HPC have been proved by test and simulation. A standard recipe of 2 kg/m^3 of Type 2 PP-fibers is proposed, other usage of PP-fibers can be evaluated by fire test or compared against the standard recipe by the spalling criterion. As for practical use, apart from the ability to counteract explosive spalling, the difficulties and negative effects from the addition of PP-fibers should be considered as well.

5.3 Protective mortar

The application of protective mortar is an option to improve the fire resistance of concrete. The insulating material can postpone the degradation of HPC. With insulating material, the rate of heat transfer in concrete slows down and explosive spalling in HPC can be postponed or prevented, due to the low thermal stress and pore pressure. To validate the effects, tests on protected concrete slabs were carried out. HPC slabs with protective mortar of different thicknesses were tested. The thicknesses of the mortars have been determined for different protection levels.

To analyze the thickness of protective mortar, the thermal and mechanical properties of the protective mortar were measured. The parameters of mortar, including thermal conductivity, density and specific heat have been applied in the spalling criterion to evaluate the effects. The postponed explosive spalling has been predicted according to the applied mortar with various thicknesses. The evaluation of the protective methods using the spalling criterion has been validated by comparing with the test results. Further simulations of the HPC with protective mortar have been carried out and the usage of the protective method has been discussed.

5.3.1 Experimental investigation

The HPC specimens were cast using the M2 mixture after Klingsch (2013), with a 28-day compressive strength of over 110 MPa. The dense mixture was prone to explosive spalling due to its low permeability. Similar to the test on PP-fibers, the slabs with dimensions of $l \times w \times h = 1100 \times 900 \times 150$ mm^3 were tested at the fire laboratory at EMPA. The heating rate was according to the ISO fire curve. After 15 minutes of exposure, small concrete segments released from the concrete surface and spalled into the furnace. As shown in Fig. 5.10, without protective methods, the HPC slab made of M2 spalled significantly. The mixture will be used further to test the effect from the protective mortar.

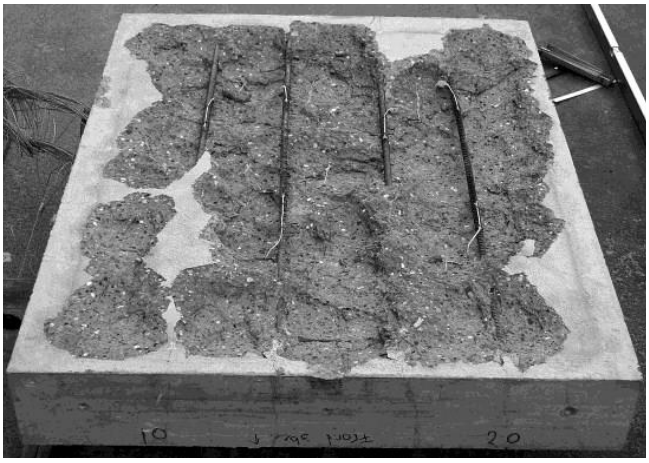

Fig. 5.10 Spalled HPC slab without protective mortar.

After the curing of the HPC, the protective mortar was sprayed onto the slab surface, as shown in Fig. 5.11. To achieve a sufficient bond between the mortar and the concrete, the surface of the slab was sand blasted and cleaned with water, then, the mortar was sprayed. After spraying, the density of the mortar was 1132 kg/m^3 and the air content was about 15 %. To prevent explosive spalling for two hours, mortar with three different thicknesses, 10 mm, 20 mm and 30 mm was used. Type K thermocouples were mounted on the surface of mortar and in the HPC slab to measure the temperature distribution during the tests. The

measured temperatures will be used to validate the simulations. The test lasted for two hours or was stopped manually when explosive spalling occurred.

With 10 mm of protective mortar, the explosive spalling was not prevented for two hours. An explosive spalling occurred with a single loud bang after a fire exposure of 119 minutes. The measured temperature on the interface was 407 °C, when the spalling occurred. Fig. 5.12 shows the specimen after the explosive spalling, the maximum spalling depth was about 63 mm. Different from the small segments in the unprotected slab, a bulky layer of concrete spalled from the slab with 10 mm of protective mortar and the spalling occurred at a deeper position than the unprotected slab.

Fig. 5.11 Test specimen with protective mortar.

With insufficient protection, the explosive spalling may be more violent and induce serious consequences. The reinforcement was left uncovered and exposed to the fire, the bearing capacity was lost immediately after the occurrence of spalling. Therefore, the protective design for explosive spalling must be well validated, the thickness of the coating must be sufficient to prevent spalling.

Fig. 5.12 Spalled HPC slab with 10 mm of protective mortar.

As for the slabs with protective mortar of thickness 20 mm and 30 mm, no explosive spalling was observed after two hours. The slab with 20 mm of mortar remained intact as shown in Fig. 5.13Fig. 5.13. The interface temperature was limited to 242 °C, which was still outside of the spalling temperature range. It was noticed that the mortar was damaged on the corner of the specimen, which can be attributed to the

degradation of the mortar at high temperatures. In addition, such damage was also observed in the 30 mm case. Hence, in practical usage, the robustness of the mortar should be considered to ensure the protective effect.

From the test results, it can be concluded that the protective mortar was effective to limit the risk of explosive spalling. With 20 mm thickness, the explosive spalling was prevented for two hours and the interface temperature was still slightly below the spalling range. The mortar with a thickness of 30 mm, limited the interface temperature below 180 °C, was too conservative for two hours of ISO fire exposure. However, when the protection was inefficient, the explosive spalling was only postponed and the occurrence can be even more violent. Therefore, the thickness of the protective mortar is a critical factor in practical usage. To further investigate the effects from the protective mortar, the tests were simulated. Some observations will be explained by the spalling criterion and the thickness of protective mortar will be studied.

Fig. 5.13 HPC slab with 20 mm of protective mortar after 120 minutes of ISO fire exposure.

5.3.2 Simulation by spalling model

The prediction of explosive spalling is based on the temperature distribution in the HPC slab. When the protective coating is applied to the slab, the material parameters of the mortar are necessary for the simulation. Therefore, tests on the mortar have been performed and the thermal conductivity, temperature dependent density and specific heat have been measured at the Institute for Polymers (D-MATL), ETH Zurich (Klingsch 2013).

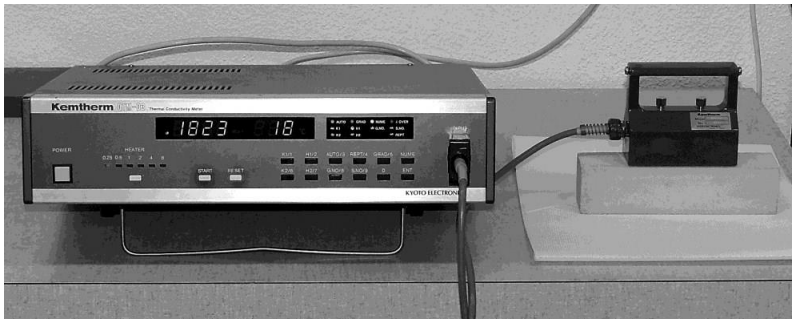

Fig. 5.14 Measurement of initial thermal conductivity.

The experimentally determined material properties will be used to predict the temperature in the HPC slabs. The simulation will be validated by comparing against the temperature measured by the type K thermocouples. Furthermore, the spalling criterion will be calculated for the HPC slabs that were protected by different thicknesses of protective mortar. Details will be presented in this section.

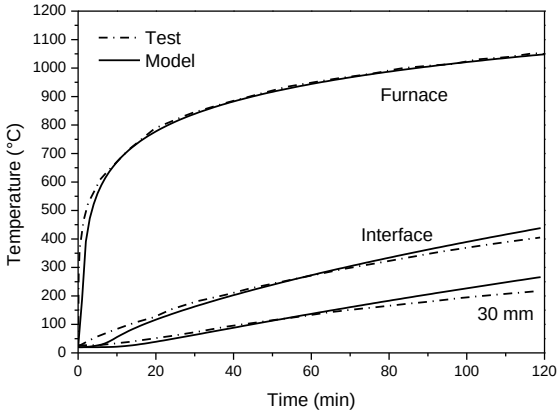

Fig. 5.15 Comparison of measured and predicted temperature for the slab protected by 10 mm of mortar.

Using the material properties from the experimental measurements, the temperatures in the slab with 10 mm of protective mortar have been simulated. The predicted temperatures at different positions have been presented in Fig. 5.15, together with the measured results from above mentioned test. It can be seen that the predicted temperatures generally agreed well with the test results. At the interface, the model overestimated the temperature slightly. This bias can be attributed to the use of small specimens in the material properties measurement. The small specimen with greater surface area to volume ratio contains less moisture than the large slab used in the test. Since the difference is limited, the measured material properties will be taken as valid for the temperature simulation.

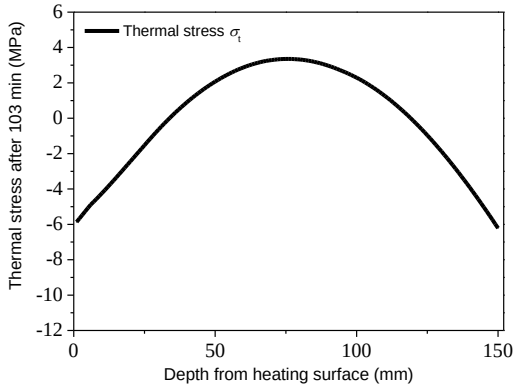

Fig. 5.16 Predicted thermal stress in the slab after 103 minutes (10 mm of mortar).

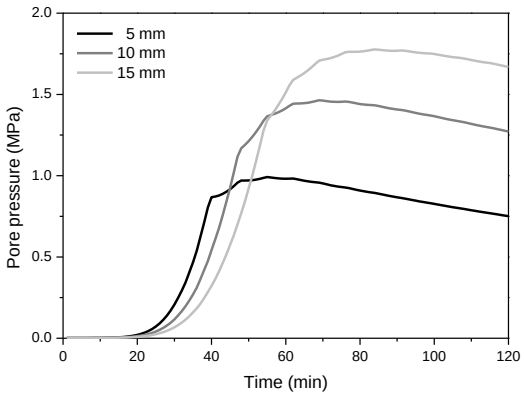

Fig. 5.17 Predicted pore pressure in the slab at depths of 5 mm, 10 mm and 15 mm (10 mm of mortar).

Based on the predicted temperatures in the slab, the thermal stress in the HPC slab with 10 mm of protection has been calculated. With the protective mortar, the heating rate on the surface was reduced and the thermal stress was lower during heating compared to the raw slab without protection. The simulated thermal stress at 103 minute is shown in Fig. 5.16 and the compressive stress on the heated surface was about 6 MPa. The temperature distribution was also used to predict the pore pressure in the HPC slab, as shown in Fig. 5.17. The result shows that the pore pressure did not rise significantly until 30 minutes of fire exposure, because of the insulating effect from the mortar. The predicted pore pressure increases with the depth from the heated surface. With 10 mm of protective mortar on the M2 slab, the pore pressure at the depth of 10 mm reached about 1.5 MPa. As the next step, the predicted thermal stress and pore pressure have been combined in the framework of spalling criterion.

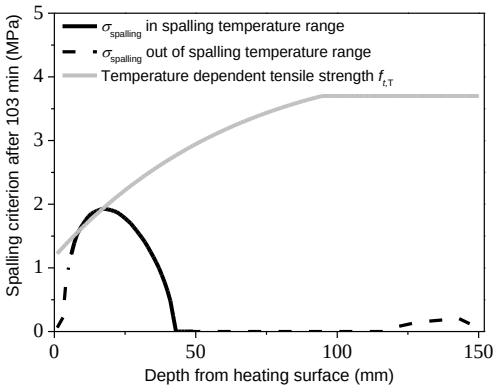

Fig. 5.18 Spalling predicted for the HPC slab with 10 mm of protective mortar after 103 minutes.

As shown in Fig. 5.18, the spalling criterion reached the temperature dependent tensile strength after 103 minutes. The predicted spalling time is close to 119 minutes observed in the tests. It can be seen that the effect from the applied protective coating can be considered by the proposed spalling model. As for the spalling depth, the predicted spalling occurred at a depth of 12 mm. Although after long period of exposure, the segment deeper than 5 mm was still in the spalling temperature range, the depth of 12 mm was still prone to spalling. The predicted 12 mm was greater than the raw slab simulated in Chapter 4 and the greater depth agreed with the observations in test that with protection the spalling occurred deeper and more violent. However, the predicted spalling depth was still far shallower than the test result (63 mm). One possible reason can be the reinforcement used in the specimen, which influenced the stress state in the test. In the case of 10 mm of protective mortar, the difference between the predicted and measured depths of spalling cannot be fully explained by the spalling criterion.

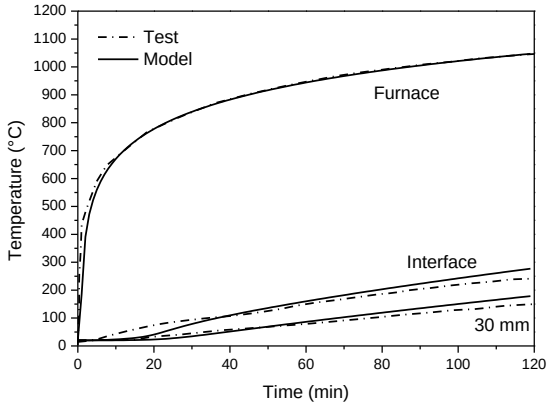

Fig. 5.19 Comparison of measured and predicted temperature for the slab with 20 mm of mortar.

Further simulations have been performed on the test with 20 mm of protective mortar. The same material properties as in the case of 10 mm were used. The predicted temperatures have been compared with the measured results in Fig. 5.19. Similar to the simulation for 10 mm of protective mortar, the interface temperature was also slightly overestimated, but the difference was limited. With this general agreement with test results, the thermal stress and pore pressure have been predicted.

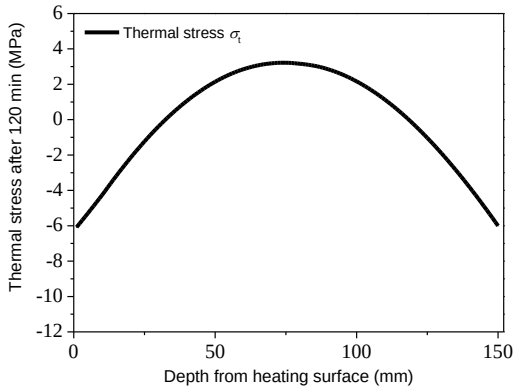

Fig. 5.20 Predicted thermal stress after 120 minutes of ISO fire exposure (20 mm of mortar).

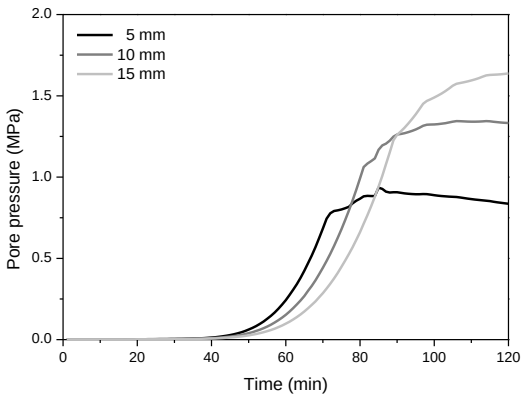

Fig. 5.21 Predicted pore pressure at depths of 5 mm, 10 mm and 15 mm (20 mm of mortar).

The predicted thermal stress after two hours of ISO fire exposure has been presented in Fig. 5.20. The maximum stress induced by the thermal gradient decreased with increasing thickness of protective mortar. At the end of test, the difference was not significant. As for the pore pressure, the increase was further postponed by the thicker protection. The studies in Chapter 3 have shown that a lower heating rate will induce lower pore pressure. As shown in Fig. 5.21, due to the slower heat transfer, the predicted pore pressure was also lower than that of the slab with 10 mm protection. At 10 mm, the peak pore pressure was about 1.3 MPa. The simulation has illustrated the effects from the thicker mortar.

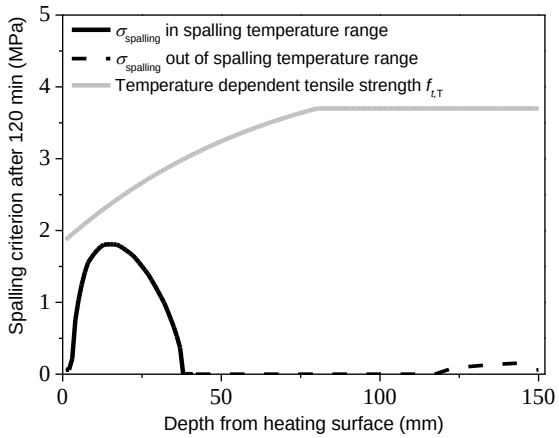

Fig. 5.22 No spalling predicted for the HPC slab with 20 mm of protective mortar after 120 minutes.

Considering all the effects, the spalling model did not predict explosive spalling in two hours, which agreed with the test result. As shown in Fig. 5.22, the spalling criterion did not reach the tensile strength, although the shallow part of the protected slab was in the spalling temperature range. Since no spalling occurred in the test and the predicted safety margin was still large, the use of 20 mm protective mortar can be validated to protect the HPC slab for two hours, when it is exposed to ISO fire.

5.3.3 Considerations on practical use

It has been shown that the thickness of protective mortar can be proposed by the spalling model. The prediction agreed well with the test under ISO fire. In fire safety design, the effects from fire scenarios should also be considered. In addition, the protection level varied with situations and budgets. With respect to these factors, the use of protective mortar will be discussed by the spalling model.

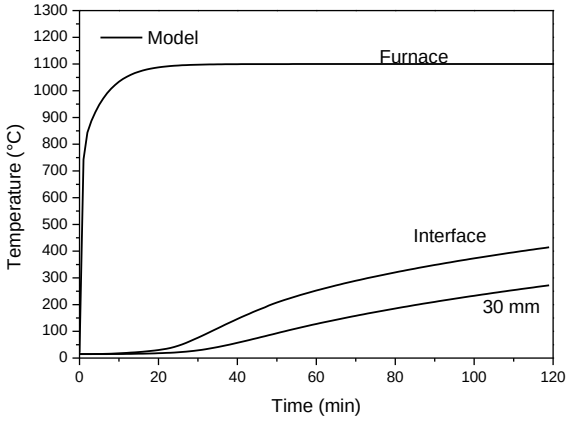

Fig. 5.23 Predicted temperature for the slab exposed to hydrocarbon fire (20 mm of mortar).

In Chapter 4, the influence from fire scenarios has been investigated that the risk of explosive spalling increases with the severity of fire. As for the fire safety design, the fire scenarios have been compared using the spalling model. The hydrocarbon fire has been applied in the model to compare with the ISO fire that was used in test and simulations. As shown in Fig. 5.23, under the high heating rate described in Chapter 4, the temperatures were predicted to increase faster. After 120 minutes of exposure, the temperature at the interface reached 400 °C.

Similar to the previous cases, thermal stress and pore pressure has been predicted using the same material properties. Heated at a high rate, the peak thermal stress was predicted to be higher, but after two hours of exposure, as presented in Fig. 5.24, the predicted thermal stress was modest, because the modulus of elasticity decreased on the heated surface. As for the pore pressure, Fig. 5.25 shows the results at different depths. Comparing to the case under ISO fire, the predicted pore pressure was higher according to the high heating rate. It can be seen that by increasing the thermal stress and pore pressure, high heating rate offsets the effects from the protective method. Using the proposed spalling model, the risk for the protected slab under hydrocarbon fire has been analyzed. As shown in Fig. 5.26, in 120 minutes, although no explosive spalling was predicted, the safety margin was quite small. The induced spalling criterion was close to the tensile strength. The used protective mortar with a thickness of 20 mm is not considered capable of preventing explosive spalling for two hours, when the slab is exposed to hydrocarbon fire. For the required protection time of two hours, thicker mortar is recommended, e.g. 25 mm, to prevent explosive spalling when heated by hydrocarbon fire.

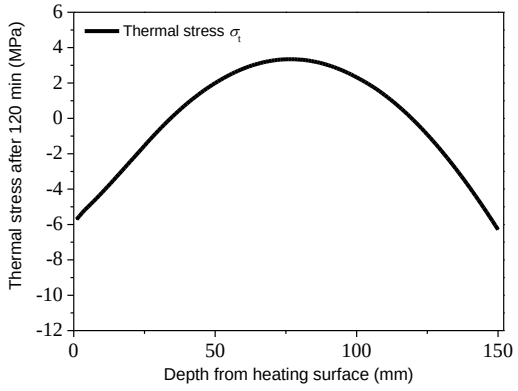

Fig. 5.24 Predicted thermal stress after 120 minutes of hydrocarbon fire exposure (20 mm of mortar).

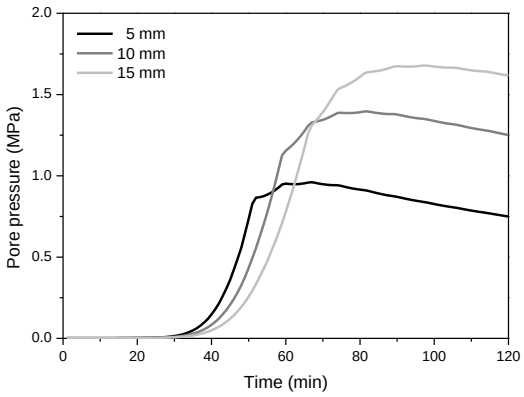

Fig. 5.25 Predicted pore pressure under hydrocarbon fire (20 mm of mortar).

As the simulation has shown, the fire scenarios influence the protective effect. The spalling model evaluates the protective mortar with respect to heating rate, some guidelines for the thickness of protective coating can be provided in fire safety design.

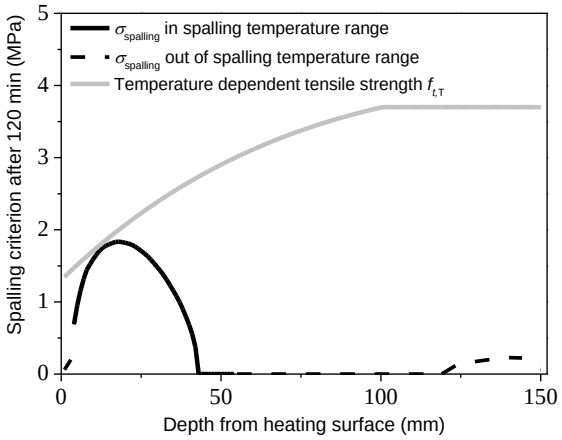

Fig. 5.26 No spalling predicted for the HPC slab with 20 mm of protective mortar after 120 minutes of hydrocarbon exposure.

The thickness of protective mortar depends on the required protection level, thicker protection provides better safety margin. Yet the used thickness is limited by structural situations and budget, a thin layer of coating is more applicable and less expensive. The application of the protective mortar will be studied for the high protection level, i.e. under high heating rate for a long period of exposure, the maximum required thickness will be predicted.

The hydrocarbon fire curve has been applied to represent the high heating rate, and the required protection time is assumed to be ten hours. Using the experimental properties for the mortar, as described above, the temperature distribution in the slab has been simulated. The temperature distribution after ten hours of exposure has been presented in Fig. 5.27. It can be seen that the protective mortar prevented the fast temperature rise, however, the temperature at the interface between the mortar and the HPC slab was over 700 °C due to the long period of exposure. The induced stresses have been simulated based on the prediction of temperature.

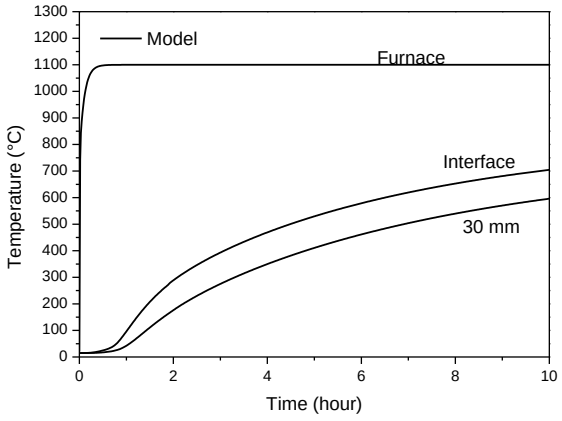

Fig. 5.27 Predicted temperature for the slab with 30 mm of mortar when exposed to hydrocarbon fire.

The thermal stress was low because of the thick protective mortar, even under high heating rate. After ten hours, the temperature gradient was low and the modulus of elasticity decreased with the degradation of concrete. Hence, as shown in Fig. 5.28, the thermal stress was modest in the segment. As for the pore pressure, as shown in Fig. 5.29, the increase of pore pressure followed the increase of temperature, the peak value was about 1.3 MPa at a depth of 10 mm. With protective mortar of 30 mm thickness, the pore pressure was modest, even when heated according to the hydrocarbon fire curve.

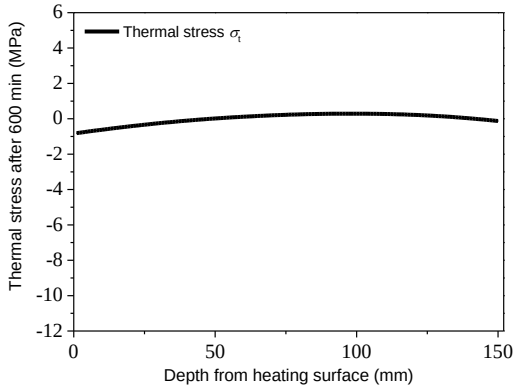

Fig. 5.28 Predicted thermal stress after 10 hours of hydrocarbon fire exposure (30 mm of mortar).

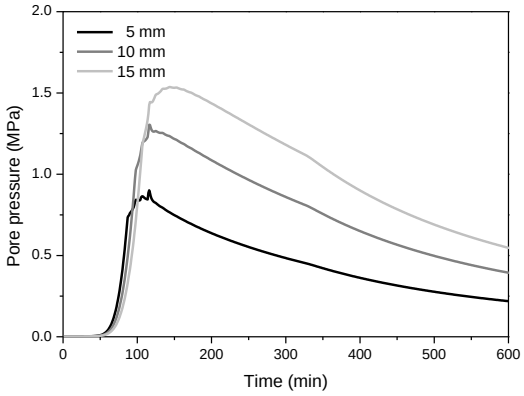

Fig. 5.29 Predicted pore pressure under hydrocarbon fire (30 mm of mortar).

The risk of explosive spalling has been predicted based on the predicted stress state during the two hours of hydrocarbon fire exposure. The spalling criterion is shown together with the temperature dependent tensile strength of concrete in Fig. 5.30, which indicates no occurrence of explosive spalling. The reduced thermal stress prevented the spalling criterion in reaching the tensile strength in the spalling temperature range. After ten hours, the temperature for most of the segment was above the upper boundary for explosive spalling (400 °C). Even a longer time of high temperature exposure, will not induce explosive spalling, because the spalling criterion will be reduced further with the drying of moisture. The high temperature must have induced degradation of concrete, however the risk of spalling was limited. Therefore, to prevent explosive spalling, 30 mm of protective mortar can prevent explosive spalling from intensive heating for unlimited time. The spalling criterion suggests that thicker mortar would not be necessary. These results should be validated by test in the future.

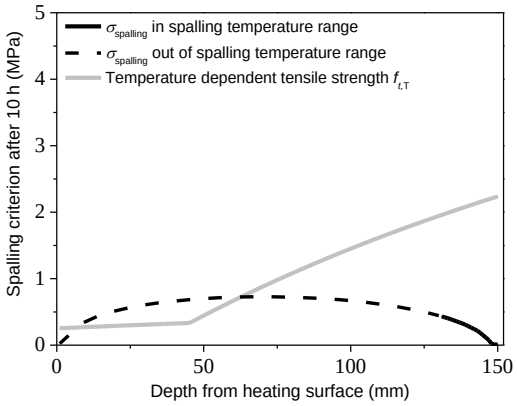

Fig. 5.30 No spalling predicted for the HPC slab after 10 hours.

In existing structures, the protective mortar has proved capable of preventing explosive spalling. The thickness depends on the fire scenario and the protection time, test results have indicated thicknesses for various protection levels. Against the test results, the spalling model based on the spalling criterion has been validated. The simulations have shown that the effects from protective mortar of various thicknesses can be evaluated by the spalling model. On the other hand, the spalling model can provide guideline for the used thickness. The validated model will be used to evaluate the use of protective plate, the next section will provide an example of practical use for fire safety.

5.4 Protective plate

Another insulating material, protective plate, provides similar effects as protective mortar. In addition, the plates are easy and fast to install, which is an advantage in practical use. A widely used protective plate has been analyzed to prevent explosive spalling on HPC slab. The validated spalling model has been applied to guide the experimental study. The protective level was set to prevent explosive spalling to the HPC slab, when it exposed to ISO fire for 90 minutes. Based on the technical properties of the protective plate, the depths of plates were proposed by the simulation. The tests were carried out to study the effects of the plate and to valid the spalling model.

This study on protective plate illustrated the use of spalling model for practical use. Details of the simulation and test will be presented in this section and the use of protective plate will be discussed as well.

5.4.1 Prediction from spalling model

The insulating plates can provide protection against high temperatures, since the heat transfer is slowed down by the material with low thermal conductivity. To illustrate the effects on explosive spalling, a widely used protective plate has been studied, whose technical properties of the plate are listed in Table 5.1. It is obvious that the effect on protection is related to the thickness of the plate. To protect the HPC sufficiently and economically, the thickness is important factor in practical use. According to the protection level, preventing explosive spalling for 90 minutes under ISO fire, the thickness of the plate has been predicted by the spalling model.

Table 5.1 Technical data for the used protective plate (Promat AG 2014).

	Units	Properties	
Bulk density	kg/m^3	870	
Thermal conductivity	W/m K	20 °C	0.17
		100 °C	0.19
		200 °C	0.21
Specific heat capacity	kJ/kg K	0.92	

Similar to the protective mortar, the heat transfer in slab protected by plate is considered in two layers, as shown in Fig. 5.31. In the layer of protective plate, the temperature will be predicted based on the brief properties provided by the manufactory, some of them are assumed constant. The simulation in concrete is based on the HPC used in Section 4.3.1 using the properties as given in Eurocode 2.

Fig. 5.31 HPC slab protected by insulation plate.

As for the protection level, the plate with a thickness of 10 mm has been recommended. With the protective plate with the proposed thickness, the predicted temperatures are presented in Fig. 5.32. It can be seen that the temperature at interface is predicted to be 350 °C after 90 minutes of ISO fire exposure. A segment of the HPC slab will be in the spalling temperature range. The risk will be further analyzed using the spalling model.

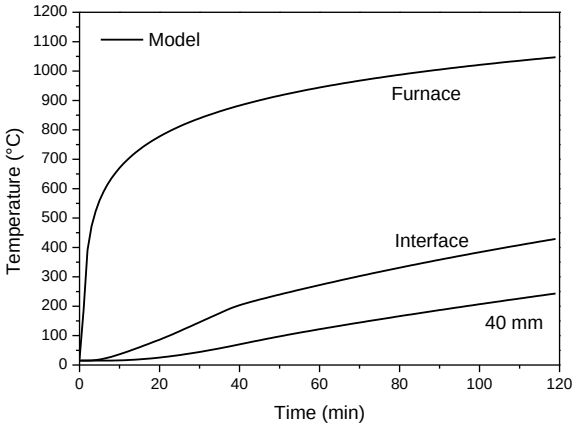

Fig. 5.32 Predicted temperature for the slab with 10 mm of insulation plate.

Based on the temperature calculation, the thermal stress is simulated, as shown in Fig. 5.33. At 103 minute, the compressive stresses on the heated surface were about 6 MPa. The predicted pore pressures are presented in Fig. 5.34, the results are slightly lower than that without protection. This difference can be attributed to the reduced heating rate, when the HPC slab was protected by the insulating plate.

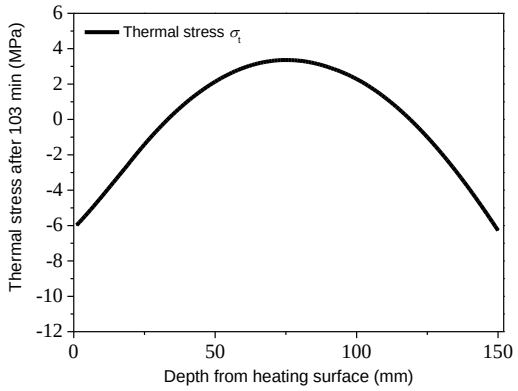

Fig. 5.33 Predicted thermal stress after 103 minutes of ISO fire exposure (10 mm of insulation plate).

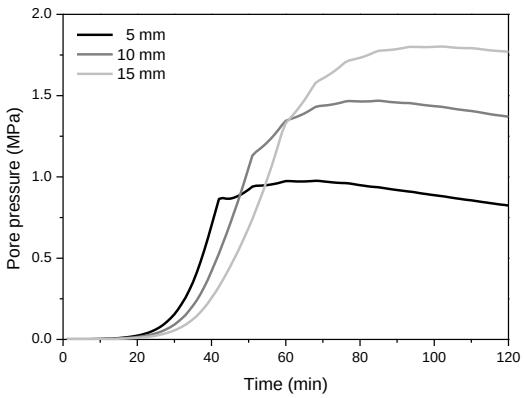

Fig. 5.34 Predicted pore pressure under ISO fire (10 mm of insulation plate).

The explosive spalling was predicted to occur after 103 minutes of heating. Fig. 5.35 shows the spalling criterion with tensile strength of concrete. The prediction indicated that the spalling criterion reached the temperature dependent tensile strength at a depth of 14 mm. The proposed 10 mm of protective plate is predicted to prevent the HPC from explosive spalling for 103 minutes. The simulation will be validated by test results in next section.

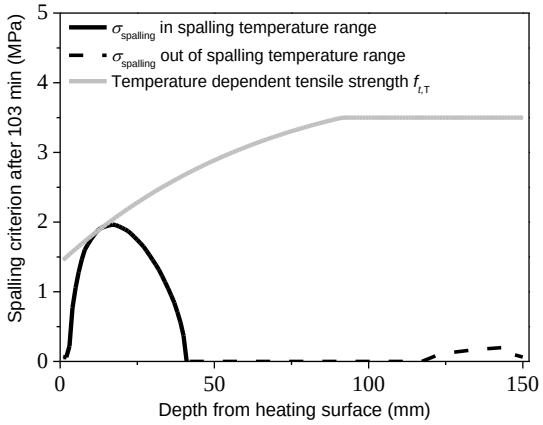

Fig. 5.35 Spalling predicted for the HPC slab with 10 mm of protective plate after 103 minutes.

One solution that is more conservative has been simulated. The temperature of the HPC surface would be limited below the lower boundary of spalling temperature range (250 °C) by the plate with a thickness of 18

mm. After 90 minutes of ISO fire exposure, the temperature at the interface was predicted to be lower than 250 °C. This simulation of this conservative scenario has been carried out.

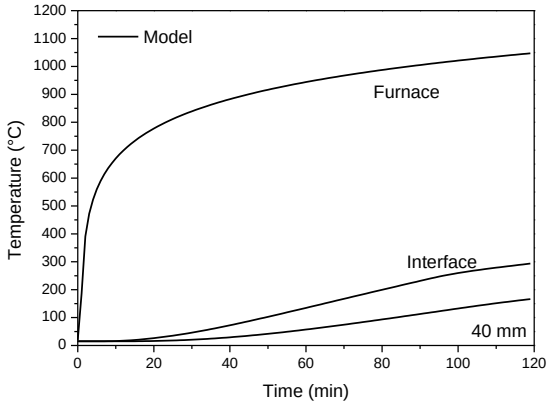

Fig. 5.36 Predicted temperature for the slab 18 mm of insulation plate under hydrocarbon fire.

The thermal stress after 90 minutes of heating has been shown in Fig. 5.37 and the pore pressures are in Fig. 5.38. It can be seen that the thicker plate postponed the development of pore pressure. In 90 minutes, the peak value of pore pressures was predicted below 1.2 MPa in the whole section.

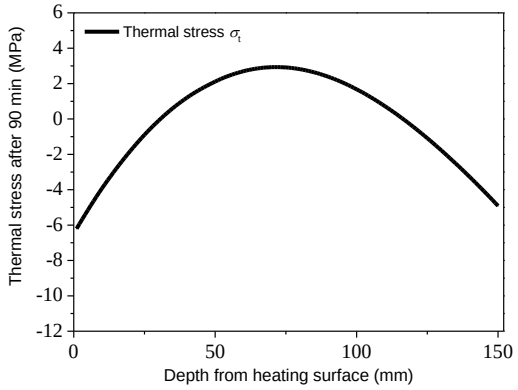

Fig. 5.37 Predicted thermal stress after 90 minutes of hydrocarbon fire exposure (18 mm of insulation plate).

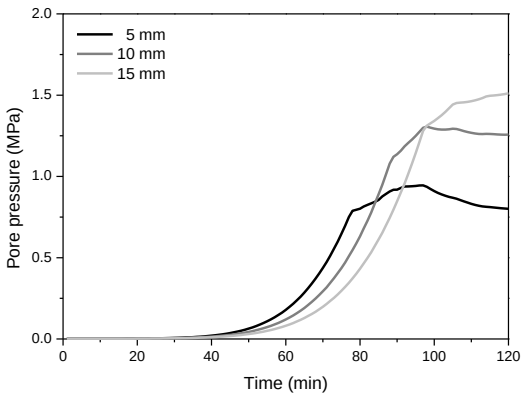

Fig. 5.38 Predicted pore pressure under hydrocarbon fire (18 mm of insulation plate).

As expected, with the conservative application of the protective plate, no explosive spalling will be predicted by the spalling model. The whole section was out of the spalling temperature range within 90 minutes. There was a huge safety margin in the heated segment, the spalling criterion was still much lower than the tensile strength. It seems that the fire safety design will be conservative, when the scenario is proposed based on the limit of temperature.

To validate the use of protective plate, these two simulated scenarios have been studied by tests. The tests were carried out according to the conditions assumed in the simulations. The thickness of the protective

plate for this protection level has been determined, details will be presented in next section and the use of the spalling model for fire safety design will be discussed.

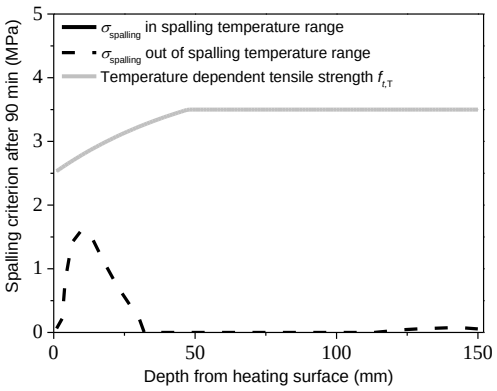

Fig. 5.39 No spalling predicted for the HPC slab with 20 mm of protective mortar after 120 minutes.

5.4.2 Experimental investigation

The tests were carried out at the fire laboratory at EMPA, the protective plates were applied to the HPC describe in Chapter 4, which was susceptible to explosive spalling without protective method. As shown in Fig. 5.40, the HPC slab spalled after 14 minutes with an averaged spalling depth of 6 mm. If the test was not stopped manually after the initial spalling, the spalling would continue and depth would increase to 60 mm in 30 minutes (Lu & Fontana 2015). The proposed two scenarios, the protective plates with thicknesses of 10 mm and 18 mm were investigated. As in the simulation, the tests were performed according to the ISO fire curve.

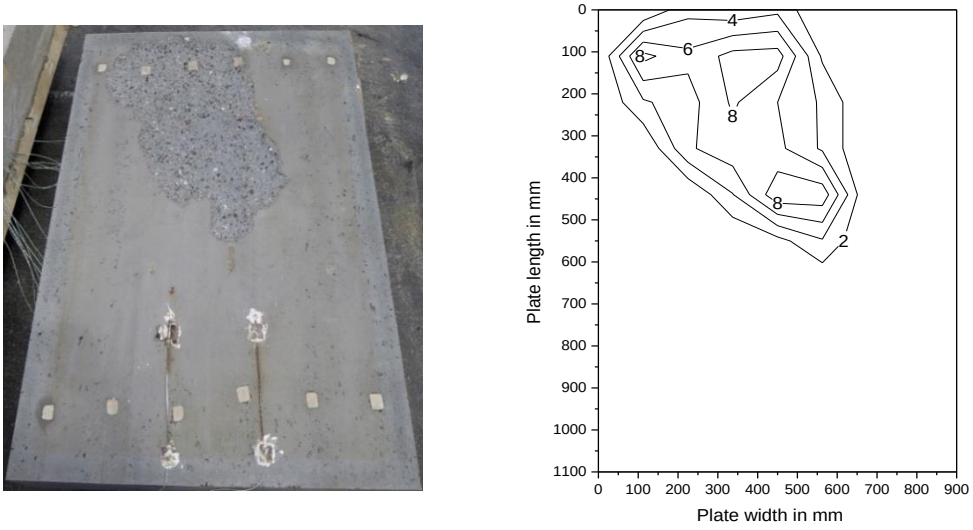

Fig. 5.40 Spalled HPC slab after 14 minutes of ISO fire exposure.

The protective plates were installed on the surface of HPC by nails as shown in Fig. 5.41 and some thermocouples were placed on the surface to measure the temperatures during the test.

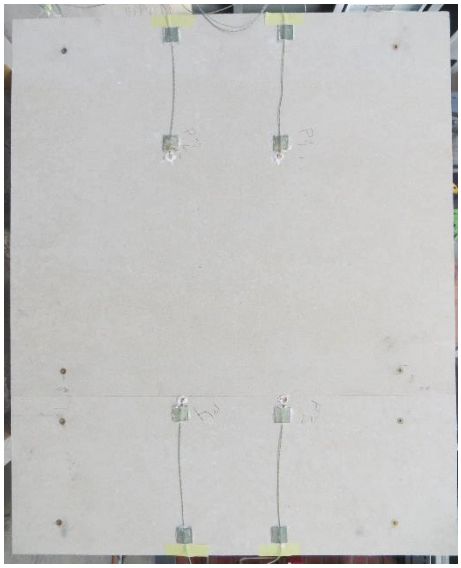

Fig. 5.41 HPC slab with 10 mm of protective plates and thermocouples.

With protective plate of 10 mm, the explosive spalling occurred to the protected slab after 106 minutes of ISO fire exposure. The protection for 90 minutes has been achieved. The prediction of 103 minute can be taken as acceptable comparing to test result. The proposed thickness of 10 mm has been proved effective for the protection level. The measured temperatures at different positions have been shown in Fig. 5.42. It can be seen that the measured temperatures were lower than the prediction, which can be attributed to the conservative technical data given by the manufactory. In the test, the protective plate provided better effect than expected.

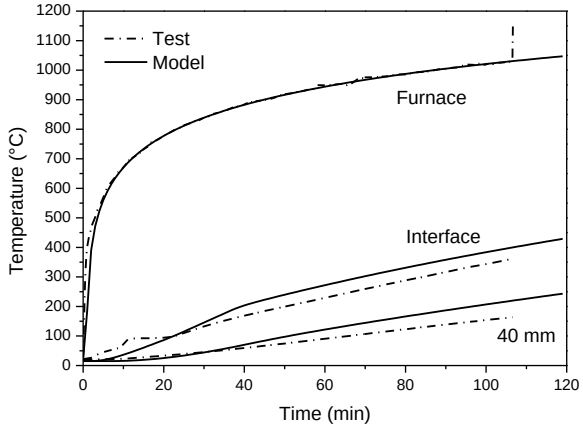

Fig. 5.42 Comparison of measured and predicted temperature for the slab with 10 of protective plate.

As for the spalling depth, the averaged spalling depth in the test was 20 mm. The spalled slab is shown in Fig. 5.43, the protective plates fell off when spalling occurred and the maximum spalling depth reached 25 mm. The spalling position coincided with the depth of reinforcement. It has been discussed that lower

heating rate or protection will induce a deeper spalling. As expected, the spalling occurred in the protected slab was deeper than that in the raw slab (6 mm). The predicted result underestimated the spalling depth to be 14 mm. As discussed in the case of protective mortar, one reason can be attributed to the reinforcement, which influences the stress state.

In general, the spalling criterion has taken the effects from the protective plate into account, a guideline for the test has been provided, which has been validated by the test result. The protection time agreed well with the observation in test, but the prediction of spalling depth should be further investigated.

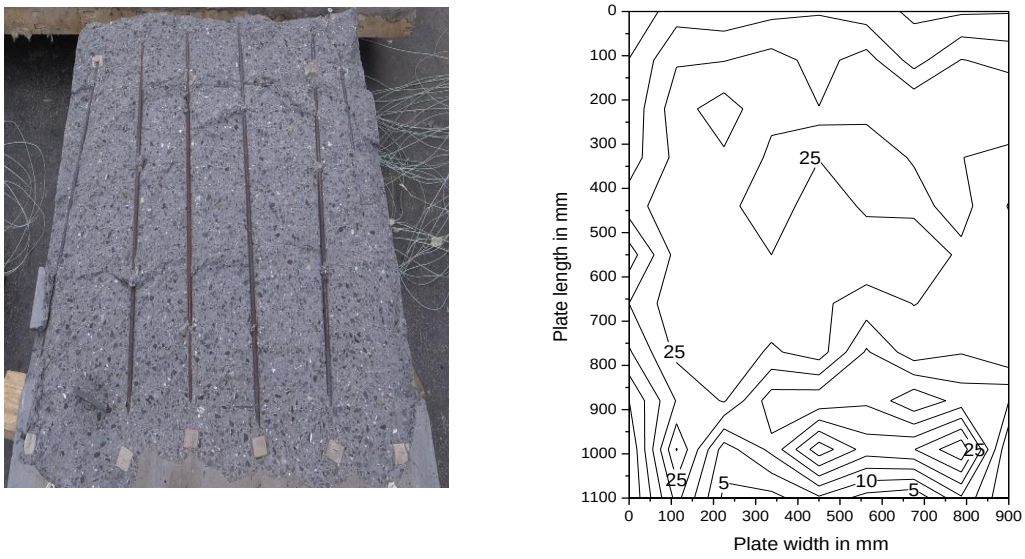

Fig. 5.43 Spalled HPC slab with 10 mm of protective plate after 106 minutes of ISO-fire exposure.

The test on the thick protective plate has shown better effect, but conservative. With 18 mm of protective plate, the interface temperature was limited below 250 °C, the measured temperatures were even lower than predicted, due to the conservative thermal properties given by the manufactory.

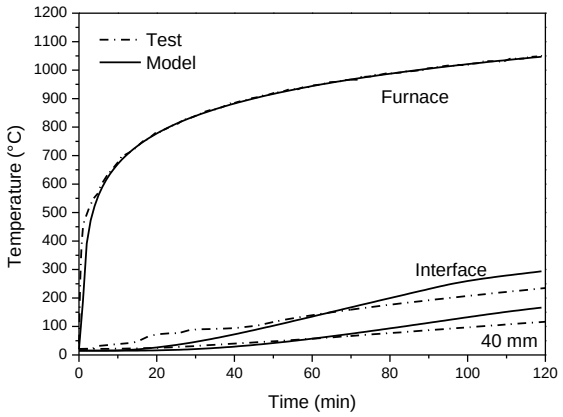

Fig. 5.44 Comparison of measured and predicted temperature for the slab.

In the test, no explosive spalling was observed for 120 minutes, longer than the protection target, the protected slab remained intact as shown in Fig. 5.45. The simulation has shown that the whole section was still out of the spalling temperature range. The test has also indicated that for the protection level of 90 minutes, 18 mm of protective plate provided overprotection against explosive spalling. Hence, it can be concluded that if the fire safety design were based on the limit of temperature, the solution would be very conservative and costly.

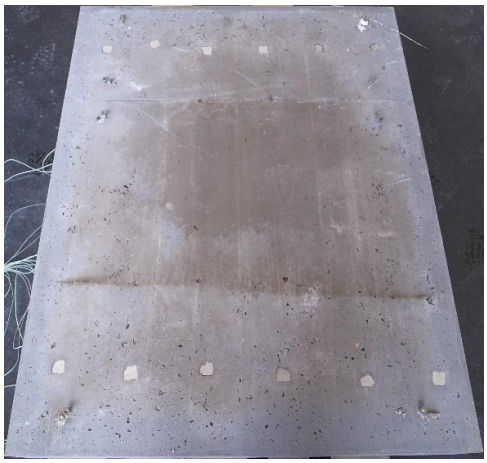

Fig. 5.45 HPC with 18 mm of protective plate after 120 minutes of ISO-fire exposure.

5.4.3 Consideration on practical use

The protective plate has been proved capable of preventing explosive spalling and the use can be guided by the spalling model, i.e. the thickness can be determined according to the protection levels. In addition, the easy installation is an advantage in application. Hence, the protective plate is a good option for protection against explosive spalling. In this section, some factors related to the practical use will be discussed.

Fig. 5.46 The joint of plates on the protected HPC slab.

The protective plates are usually supplied with certain dimensions and the plates can be connected to the concrete element by the nails. With the limited dimensions, the element will be covered by pieces of plates and there must be some joints between the plates, as shown in Fig. 5.46. The test results have shown that

the heat transfer was not influenced by the joint, no significant difference was noticed between the areas under joint and the plate (Lu & Fontana 2015). The fast installation using nails is proposed and extra process for the joint is not necessary. Due to these advantages, the application of protective plate is much faster than the above mentioned mortar and no hardening or conditioning time is necessary. The commonly used protective plates are flat, which are suitable to great area of flat concrete. For the curvy surface or areas with many corners, the protective mortar is recommended.

During the test, the protective plate has been heated to almost 1000 °C and the plate turned brittle. Although they were still connected to the concrete by the nails during the test, some pieces dropped from the slab when the specimen was removed from the furnace. Therefore, the distance of the nails should be considered to provide robust connection.

The use of protective plate has been evaluated by the spalling model. With the proposed thicknesses, the tests have proved that protective plates are feasible for protection against explosive spalling. Meanwhile, the spalling model is validated to guide the fire safety design. The predicted thickness of protective plate is more reasonable than the evaluation exclusively base on the temperature restriction. For the existing flat HPC element, the protective plate is a good option against explosive spalling.

5.5 Evaluation strategy

Since the fire test is usually very expensive and time consuming, the evaluation of protective methods is a big concern in practice. Without valid evaluation, the protective methods can be insufficient to reduce the spalling risk or be too costly providing overprotection. To facilitate the fire safety design, the validated spalling model can be used to provide guideline for practical protective methods. The evaluation strategy will be introduced according to the experimental conditions.

5.5.1 Only test at ambient temperature is possible

Some parameters of concrete used in the model can be known from the mixture. Yet some parameters change with temperature. If the test at high temperature is not possible, the properties of concrete will be assumed according to Eurocode 2 or proposed model. The concrete permeability at high temperature can be predicted by the proposed model. As described in Chapter 3, the calculation is based on the initial permeability and moisture content at ambient temperature. The permeability will be measure at ambient temperature using the Torrent permeability tester, at the same time, the moisture content will be measure by the concrete moisture encounter. The pattern of permeability will be predicted with respect to temperature and moisture content.

In the case of concrete with PP-fibers, when the recipe is known, the increasing factor can be determined based on the test results. For the amount of more than 2 kg/m^3, the permeability at high temperature can be predicted applying the increasing factor of 20. However, less than this amount, the type of PP-fibers, i.e. diameter and length, has effect on the permeability as well. The increasing factor should be assumed lower than 10 to get a cautious result.

Without the experimental conditions for high temperature measurements, the evaluation relies mainly on the data base collected in previous test. The effects can be simulated, but with limited reliability.

5.5.2 Test at high temperature is possible

When the properties of concrete can be measured at high temperature, the prediction will be based on the particular parameters for the studied element. The permeability will be measured as describe in Chapter 3, both methods of hot and residual permeability measurements are useful for the permeability model. The simulation of pore pressure will be more accurate. Apart from the moisture encounter, the moisture content can be also determined by the mass loss after heating. The tensile strength decreases with temperature. If the pattern can be measured against temperature, the prediction of spalling time can be more reliably.

As for the use of PP-fibers, the increasing factor will be determined by the permeability test. The permeability at the temperature point of 175 °C will indicate the proper increasing factor for the concrete with PP-fibers. In this case, all types and recipes of PP-fibers can be considered by the modified permeability model and the risk will be evaluated by the spalling model accordingly.

Tests at high temperature can provide key parameters for the model. The tests can be carried out on a specimen of the studied element. With these tests, the cost will be lower than fire test and the reliability of the evaluation will be improved.

5.5.3 Fire test is possible

If the fire test will be performed, the test results provide more convincing proof for the effectiveness of the used protective method. Meanwhile, the results will be compared with the spalling model. As for the model, the evaluation strategy will be similar as the process done in Section 5.4, the measurements of permeability will be carried out together with test on moisture content. The spalling risk will be predicted and the thickness of protective methods will be proposed before the test. Using the date, the simulation promotes the fire test and reduces the test cost. When unexpected results are observed, the simulation can be used to analyze the process.

The protective methods will be proposed by the spalling model based on the measurements. The effectiveness of protective methods will be proved by the test. The test results will be used to validate the spalling model as well.

5.6 Conclusions

The protective methods and their effects on spalling risk have been discussed in this chapter. The validations of the three methods have been achieved by the fire tests. The spalling model based on the spalling criterion has been used to simulate the effects from the protective methods and the results agreed well with the test results. This provides a validation to the protective methods. In practice, the spalling model can facilitate the fire safety design. Some key findings are summarized here.

1. The two methods, namely PP-fibers and insulation of concrete element are all capable of preventing explosive spalling of HPC. They are applicable in different situations. The use of protective methods needs valid guidelines in practical fire safety design. Apart from the costly fire test, a spalling model for evaluation is practical and useful.

2. The recipe of 2 kg/m^3 of Type 2 PP-fibers has been proved effective in preventing explosive spalling in fire tests. The spalling model considers the influences from the recipe of PP-fiber with a simplified increasing factor. Taking as the recipe as standard, the application of other types and amounts of PP-fibers can be analyzed by the increasing factor, which is determined based on permeability measurements. The effects from other recipes can be evaluated comparing to the standard recipe.
3. The protective mortar slows down the heat transfer in concrete, therefore, the explosive spalling can be postponed or prevented. The positive effect has been validated by the fire test. However, insufficient protection may induce deeper and more violent spalling, which has been observed in tests and simulated by the model. The spalling model has been validated by the test results, the effects can be simulated and shown to be in good agreement with the test results. In addition, the thickness of protective mortar has been proposed for a high protection level, which is due to be validated by test.
4. Using the validated spalling model, the guideline for the test on protective plates has been provided. The observations in fire tests agreed well with the predictions, that the protective plate can also prevent explosive spalling. Thereby, an example for practical fire safety design has been presented.
5. To evaluate the risk of explosive spalling, a strategy has been introduced for the use of the spalling model. When the experimental condition is limited, the effects of protective methods can be predicted using the proposed models for concrete properties. With equipment for test at high temperatures, the accuracy of prediction can be improved by the test results. As for the fire test, the spalling model works as a guideline, similar to the use in the test on protective plates.

6. Conclusions and prospects

6.1 General

Explosive spalling is a main concern in the use of high performance concrete (HPC). The higher susceptibility of HPC to explosive spalling is mainly attributed to the lower permeability than ordinary Portland concrete (OPC). On the other hand, test results have shown that the thermal stress and external loads are further important factors. A combined stresses mechanism is proposed and many observations in test can be qualitatively explained. However, the explosive spalling of concrete cannot yet be quantitatively predicted due to the lack of a framework considering all the relevant factors found in research. The prediction of spalling risk has been rarely improved by the research, meanwhile, the protective methods against explosive spalling must be validated by fire tests, which makes the fire safety design very costly. Therefore, the first goal of this dissertation is to develop a method for predicting explosive spalling, which connects test results to practical design. Secondly, the risk of explosive spalling can be comprehensively analyzed according to various fire scenarios. Finally, guidelines for protective methods should be provided to facilitate the fire safety design in practice.

To achieve these objects, experimental and numerical studies have been carried out. The permeability of OPC and HPC has been tested. The influences from high temperatures and moisture content have been studied on the basis of both hot and residual permeability measurements. A permeability model has been proposed and applied in the Thermo-Hydro model (Dwaikat & Kodur 2009) to simulate the pore pressure. Considering pore pressure and thermal stress, a spalling model based on a spalling criterion has been proposed to predict explosive spalling. Many parameters have been analyzed in the study. As for the protective methods, the effects from e.g. polypropylene fibers (PP-fibers) and insulating coatings have been studied. The main conclusions from the work and the prospects for further research will be shown in the following sections.

6.2 Conclusions

From the study presented in the dissertation, the main conclusions are drawn:

1. **Explosive spalling** of concrete can seriously change the behavior of the structure. Spalling must be evaluated and in many cases limited by protective methods. The combined stress mechanism, considering both pore pressure and thermal stress, can explain a lot of observations related to explosive spalling. Using the mechanism, the influences from permeability, heating rate, moisture content, tensile strength, external loads etc. can be taken into account.
2. **Permeability** of concrete increases generally with temperature and pore pressure. In addition, the permeability decreases with the moisture content. The drop of permeability observed in the temperature range of 150 °C to 250 °C can be attributed to a moisture clog and the dehydrated water. Based on these observations and test results of concrete with different moisture contents, a permeability model has been proposed and the predicted results are in close agreement with the tested permeability.
3. The use of **PP-fibers** has been investigated, the increase of permeability has been explained by melting of added PP-fibers. The test results have indicated that types and amount of PP-fibers influence markedly the permeability. The proposed permeability model has been modified to

consider the protective effects from PP-fibers. Increasing factors of permeability have been proposed for different recipes of PP-fibers.

4. The proposed permeability model is used in the **Thermo-Hydro model** to predict the pore pressure. The calculated results for both OPC and HPC have been validated against measured pore pressure in test (Mindeguia 2010). The influences from permeability and moisture content have been considered. High pore pressure has been predicted in HPC with low permeability, which can explain its higher susceptibility to explosive spalling than OPC. High moisture content results in low permeability, the effect can be offset during the heating process by evaporation of liquid water, hence, the predicted pore pressure increases modestly. Regarding the use of PP-fibers, lower pore pressure has been predicted due to the increase of permeability.
5. **A spalling model** has been proposed based on **the spalling criterion** of combined stresses from both pore pressure and thermal stress. The criterion is taken as a basis to evaluate the spalling risk. The verification of the spalling model has been performed by predicting spalling time and depth of test results from literature and own tests. The spalling model can consider effects from PP-fibers and insulating material and be used as a basis for guidelines for fire safety design.
6. According to the spalling criterion, many observations in tests can be explained. The high susceptibility of HPC to explosive spalling can be attributed to the low permeability, which increases the pore pressure. Therefore, the combined stress induced by high temperature is higher in HPC. Although the influence on pore pressure is limited, **moisture content** is taken as an important factor to the explosive spalling. Its influence on heat transfer increases the thermal gradient and thermal stress in concrete, it increases the vapor production and it reduces the permeability. High spalling risk is predicted with high moisture content, which agrees also with test results. The spalling risk with **external loads** has been simulated by the spalling model. The effects of under compressive stresses are investigated by the permeability test. When the permeability is not increased by the external loads, the spalling risk will increase; when micro-cracks develop due to the compressive stresses, the permeability of concrete will increase significantly, the risk of spalling can decrease. The contradictive results in test can be explained by the spalling model.
7. As a simplified limit for the liability to explosive spalling, a **boundary permeability** has been proposed as 2×10^{-17} m^2 for the unloaded concrete slab heated according to ISO fire curve. Concrete slab with lower permeability can be susceptible to explosive spalling, when heated according to ISO fire curve. The limit permeability increases with the increase of moisture content and **heating rate**, i.e. the spalling risk increases in the specimen with high moisture content or under high heating rate.
8. Using PP-fibers to **prevent the explosive spalling** has been validated by test results. The change of permeability due to the melting of PP-fibers is considered by introducing the increasing factor for permeability in the permeability model. Thereby, the proposed permeability model is capable of evaluating the influence of PP-fibers. Permeability measurements have shown that, although the diameter of PP-fibers influences the protective effect, the number of fibers per unit volume is the decisive factor and the thin fibers are recommended. However, the influence reduces, when an amount of over 2 kg/m^3 of PP-fibers is added to the concrete. Therefore, the recommended amount by Eurocode 2 of 2 kg/m^3 is taken as feasible for thin PP-fibers. Other fibers combination will be compared against the validated use of PP-fibers. The increasing factors for permeability will be used in the developed spalling model for different fiber combinations.

9. **Insulating materials** protects the concrete from high thermal stress. Two kinds of insulating materials, namely insulating plates and insulating mortars, have been tested up to now. It has been shown that both of them are capable of preventing explosive spalling, when sufficient protection thicknesses are applied. However, the severity of spalling may increase if the insulating materials are not thick enough to prevent spalling. Hence, the thickness of insulating material must be determined carefully in practice. Apart from the costly fire tests, the insulating materials can be also evaluated by the proposed spalling model. An example for a practical fire safety design is presented in Chapter 5, the proposed thickness of protection has been validated by the test results. The insulating plates of the proposed thickness prevented explosive spalling according to the protection level.
10. The proposed **evaluation method** based on the spalling criterion is able to facilitate the spalling analysis and fire safety design. The accuracy of the prediction can be further improved by calibration to test results and by measuring the properties of concrete. An evaluating strategy has been introduced for the evaluation of spalling risk, the measurements of concrete properties are listed according to the actual experimental conditions.

6.3 Prospects

While this research project leads to progresses reducing the knowledge gap described in Chapter 2, based on the scientific knowledge, this dissertation also highlighted the need for further research in many areas. The following are some of the key prospects for the further studies:

1. **Permeability of concrete** needs to be studied at residual and hot conditions with a generally accepted method, a testing standard should be proposed based on the comparison of various methods.
2. **Permeability of concrete with various fibers** combinations should be investigated (with different levels of preload). Based on the comprehensive test results, the increasing factors for the permeability model should be proposed not only for PP-Fibers but also for other fiber combinations. The geometry and the amount of PP-fibers should be optimized to prevent spalling effectively.
3. The effects from **external loads** have been involved in the spalling criterion, some observations can be explained. However the prediction of explosive spalling considering external loads is not yet validated. Concrete under stress needs to be tested. To evaluate the spalling risk under loads, load effects on permeability and spalling behavior should be taken into account in the spalling model.
4. The proposed one dimensional spalling model can predict spalling in slabs or walls. Some **local effects** e.g. in corners or in round sections of beams or columns must be studied by two dimensional model. The spalling model should be developed further to consider these elements.
5. The permeability is related to the concrete strength. In general, the higher the strength, the lower the permeability and the higher the spalling risk. However, some test results (Lim et al. 2013) have shown that the size and type of aggregates can influence decrease of permeability with strength. The **mixtures of concrete** should be investigated, a mixture with high strength and high permeability will be beneficial in terms of explosive spalling.

The knowledge from the above mentioned investigation, allows the assessment of explosive spalling of concrete and of protective methods for the fire situations. Especially for the application of HPC, the reliable assessment of spalling without testing is important as simplified fire resistance models and tables are only valid if no spalling occurs.

Appendix A (refer to Chapter 3.3.3)

Effects of moisture content on the permeability of concrete

To study the effect of moisture content, the permeability of OPC (OPC_1), HPC (HPC_1) and HPC with PP-fibers (HPC_1_P2) were measured, the mixtures are listed in Table A.1. The difference between OPC and HPC is investigated as well as the effect of PP-fibers.

Table A.1 Mixtures of concrete to study the effect of moisture content.

Components	Units	HPC_1	HPC_1_P2	OPC_1
Cement CEM I 52.5R	kg/m^3	580		-
Cement CEM I 42.5	kg/m^3			300
Silica fume	kg/m^3	63.8		-
Aggregate 0-8 mm	kg/m^3	1538		2010
PP-Fibers (Type 2)	kg/m^3	-	2	-
Superplasticizer	kg/m^3	8.7		4.5
Water	kg/m^3	195.8		182.4
W/C ratio	-	0.34		0.61
28 day compressive strength	MPa	105	102	40

The moisture content decreases quickly at the beginning phase of pre-drying, afterwards the moisture content changes slower, until the moisture content is constant by drying at 105 °C. For this reason, the following pre-drying intervals are chose to study the concrete with different moisture content; the specimens without drying were measured as well.

- without pre-drying
- 1 day pre-drying
- 2 day pre-drying
- 3 day pre-drying
- 7 day pre-drying
- 14 day pre-drying

The mass loss of the specimen was measured after the individual pre-drying time, as shown in Fig. A.1. The evaporable water loss starts at a temperature of 105 °C, the drying process is faster at the beginning for all the mixtures. The mass of OPC is almost constant after 7 days of drying. The result of 14 day pre-drying OPC indicates less mass loss than that of 7 day pre-drying, these unexpected results may come from the variability of specimens. The HPC's mass decreases more slowly, due to the low permeability. During the pre-drying at 105 °C, adding PP-fibers (HPC_1_P2) has shown little influence on the mass loss.

Apart from the initial moisture content due to pre-drying, the mass of the specimens throughout the permeability test was measured as well. The mass decreased further during heating, which is attributed to the loss of non-evaporable water at higher temperature. Some results of pre-dried specimens will be shown together with the results of specimens without drying, to illustrate the influence of moisture content on permeability.

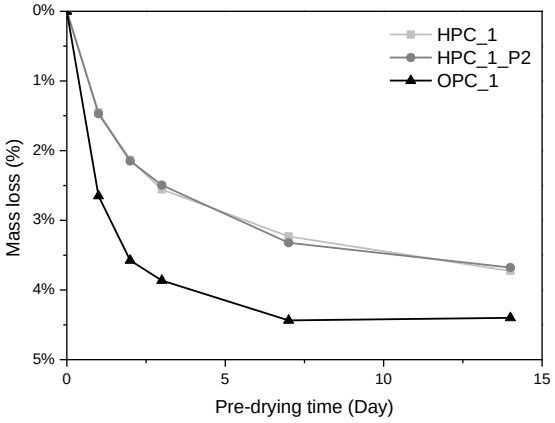

Fig. A.1 Mass loss of concrete after pre-drying at 105°C.

A.1 Measurement without pre-drying

The specimens were kept in humid conditions. To avoid additional mass loss, they were kept for only 10 minutes in the furnace when the desired furnace temperatures were achieved. Fig. A.2 shows the mass loss of specimens without pre-drying. It can be seen that all of the mixtures showed similar mass loss rates, the mass decreased faster in the higher temperature range above 100 °C. The OPC lost mass a little faster than the HPC. The influence of PP-fibers was only noticeable above the melting point of PP-fibers (160-170 °C). The permeability increase by PP-fibers could have accelerated the drying of water vapor. The final mass loss of the OPC was 4.7 %, including the non-evaporable water. Therefore, as shown in Fig. A.1, the OPC was almost dry after 7 days of drying. As for the HPC, the final mass loss was 4.9 %, with PP-fibers the value was 5.9 %. This higher amount of lost water is corresponding to the higher water content as listed in Table A.1. It can be seen that after pre-drying for 14 days, there is still some evaporable water in the HPC.

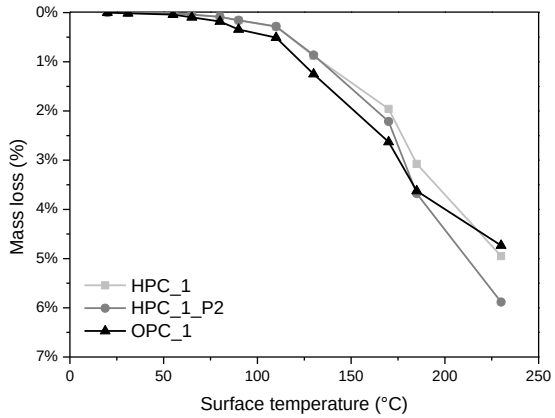

Fig. A.2 Mass loss during heating.

The residual permeability is presented against the surface temperature of specimens in Fig. A.3. In general, the permeability increases with temperature. Similar to the previous test results (Schneider 1989), a drop in

permeability was observed for temperatures higher than120 °C. The permeability of OPC is higher than HPC without PP-fibers, which is the reason why HPC is more susceptible to spalling than OPC. PP-fibers increased the permeability by melting at about 160-170 °C. With high initial moisture content, the permeability increased significantly in all three mixtures. This will be discussed with the help of a permeability model in the Section 3.4.

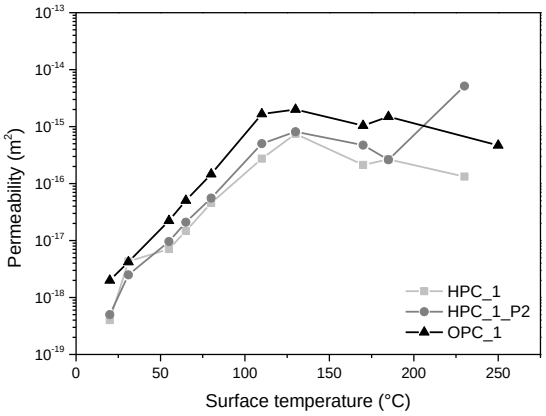

Fig. A.3 Permeability of specimens without pre-drying.

A.2 Measurement of one day dried specimens

After one day of drying, the mass loss during tests is less, yet the total loss after the heating is almost the same as the case without drying, as shown in Fig. A.4 a) and b). The mass decrease of OPC was modest during the heating, due to the pre-drying. However, mass loss in HPC was still significant due to the lower permeability and the slower drying process. The effect of PP-fibers is noticeable above the melting point as observed in the non-pre-dried case.

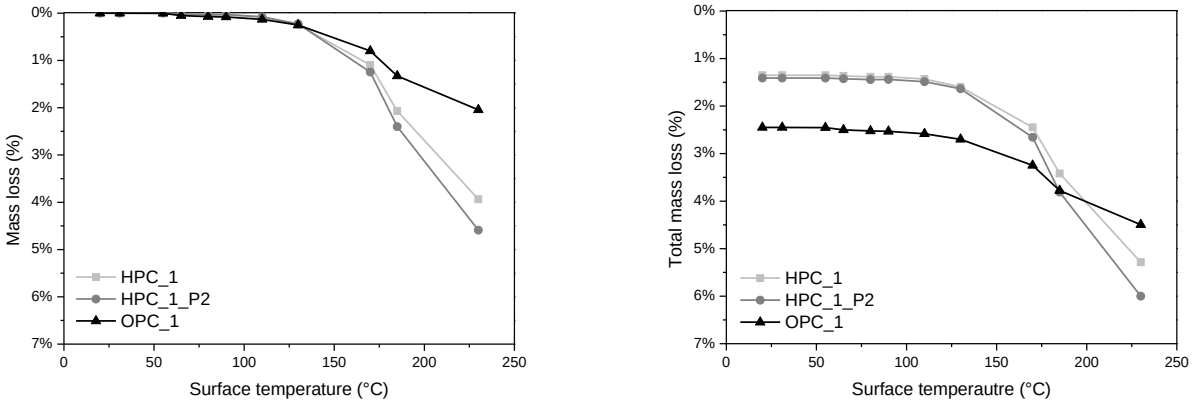

a) Mass loss during heating. b) Total mass loss after heating.

Fig. A.4 Mass loss of specimens dried for one day

As mentioned, the permeability changes with moisture content, the lower initial moisture contents of the three mixtures resulted in higher permeability. Fig. A.5 shows the measured permeability of specimens after one day of drying. Because of the low moisture content, the permeability of OPC was higher, but the increase during heating was modest, because of the lack of high pore pressure in the dry specimen. The initial permeability of HPC is also higher after pre-drying, after heated at high temperature, the permeability of HPC still increased significantly, even slightly higher than that of OPC at some temperatures. Like the non-pre-dried case, the permeability of HPC_1_P2 increased more above the melting point of PP-fibers. It can be seen that the moisture content changed the initial permeability and influenced the trend at high temperature.

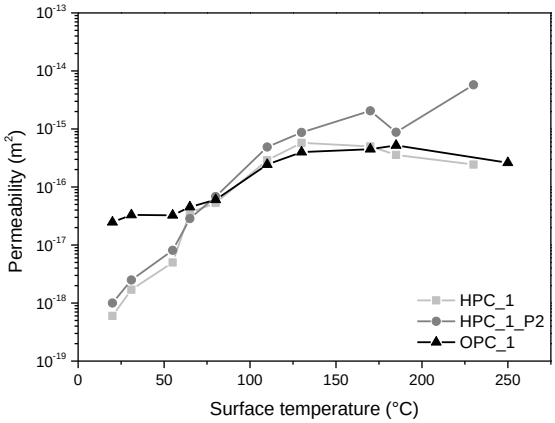

Fig. A.5 Permeability of specimens dried for one day.

A.3 Measurement of specimens dried for three days

After three days of pre-drying, the mass loss is similar to the observation in the one day dried case, only the change of mass is less significant, especially in OPC. The mass loss is presented in Fig. A.6: the final loss of mass in OPC was 5.0 %, in HPC was 6.0 % and with PP-fibers the value was 6.5 %.

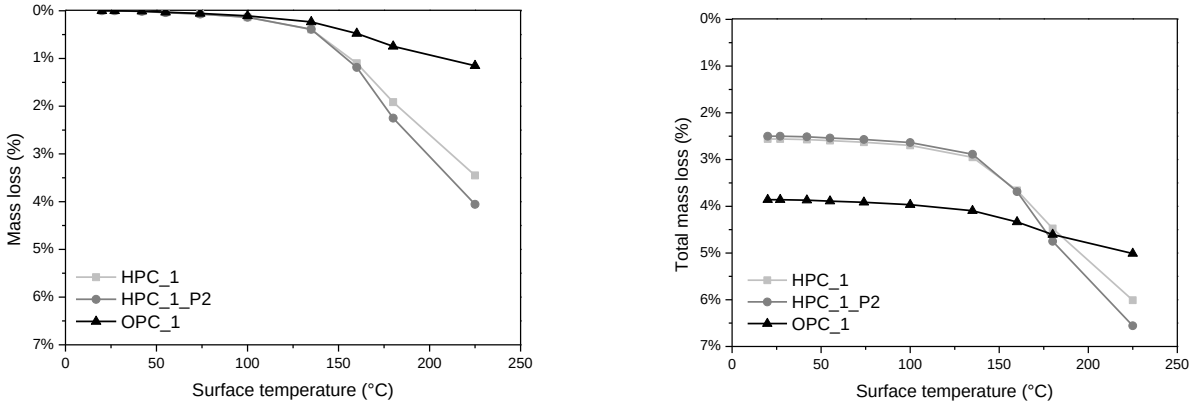

a) Mass loss of during heating. b) Total mass loss after heating.

Fig. A.6 Mass loss of specimens dried for three days.

The initial permeability of the three day dried specimens was higher than the one day dried ones. Fig. A.7 shows the measured permeability. In OPC, the permeability increased slightly with temperature, but no significant increase or drop was noticed. Also in the drier case of fourteen day dried specimen (will be shown in next section), the permeability of OPC was almost stable at high temperature. As for the HPC after three days of drying, there was still some evaporable water in the specimen. The permeability increased with temperature, but the increase was not so vigorous, above 100 °C, the permeability is similar to that with higher moisture content. From 150 °C, a drop was observed, which should be related to the moisture content as well, especially the dehydrated water in this temperature range. PP-fibers increased the permeability above its melting point, below the melting point, the permeability changed similarly as that of the HPC without PP-fibers.

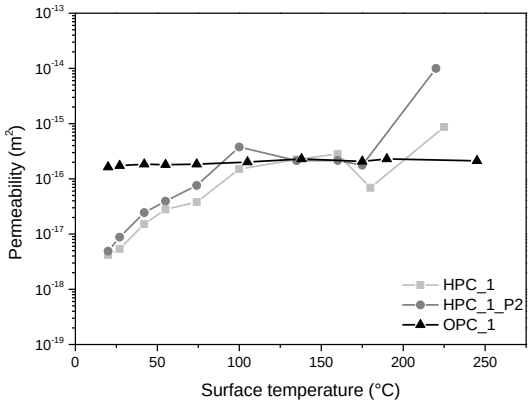

Fig. A.7 Permeability of specimens dried for three days.

A.4 Measurement of specimens dried for fourteen days

The mass loss of the fourteen day dried specimens is shown in Fig. A.8. The mass of all three specimens was almost constant until 140 °C. It can be assumed that the evaporable water was almost dried after fourteen days of drying. At higher temperatures, the HPC lost more mass than the OPC. This difference of mass loss is due to the higher amount of dehydrated water in HPC than in OPC because of the higher amount of cement in HPC. As given in Equation 3.52, a higher amount of cement will result in more dehydrated water at high temperature. Accordingly, the mass decrease in three day dried HPC can be related to the high amount of dehydrated water. As for the total mass loss, longer pre-drying results in more total loss in HPC, but for OPC, the total mass loss is independent of the pre-drying. This is attributed to the lower permeability of HPC and the HPC needs more time to dry.

With lower moisture content, the permeability increased linearly with temperature, as shown in Fig. A.9. The permeability of OPC after fourteen days of pre-drying is similar to that of three day dried specimen. The initial permeability was similar to that of three day dried samples, and the permeability increased slightly with temperature, no dent was observed either. The permeability of this drier HPC increased linearly with temperature, the permeability was not higher than OPC through the measurement. The initial permeability was identical to the three day dried HPC, but the increase during heating was smoother, and no significant dent was noticed. HPC with PP-fibers showed no difference to the HPC without PP-fibers below the melting point. With low moisture content, the permeability increased more above 165 °C.

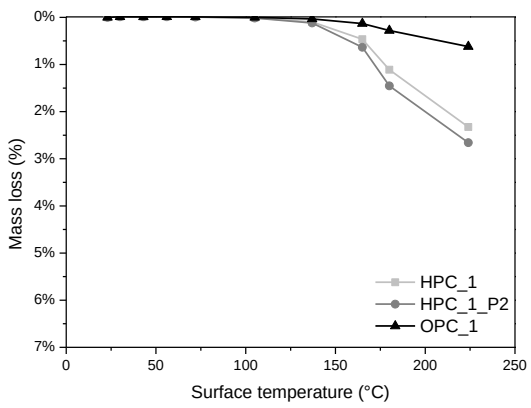

a) Mass loss of during heating.

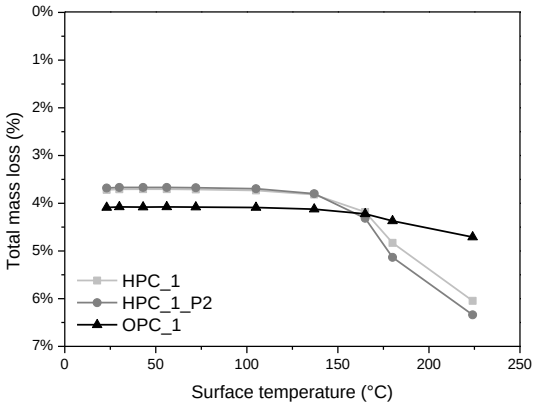

b) Total mass loss after heating.

Fig. A.8 Mass loss of specimens dried for fourteen days.

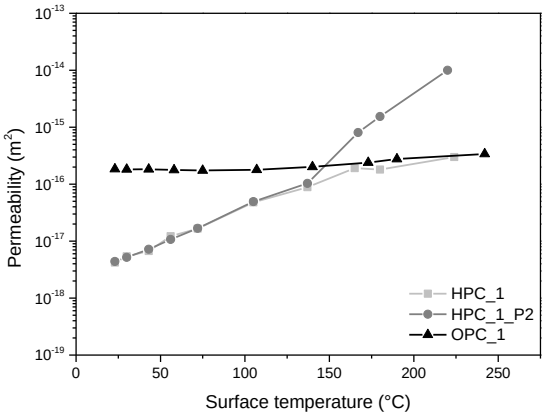

Fig. A.9 Permeability of specimens dried for fourteen days.

Appendix B (refer to Chapter 3.3.4)

Effects of fibers on the permeability of concrete

To study the effects of fibers on the permeability of concrete, three types of PP-fibers with various amounts were added to the concrete HPC_1. The details of PP-fibers are listed in Table B.1. Mixture V6 (same as the HPC_1_P2 in previous section) with 2 kg/m^3 of Type 2 PP-fibers (Klingsch 2014) is capable of preventing spalling and is chosen as the standard mixture. The others mixtures are chosen to illustrate the effects of the amount, length and diameter of PP-fibers. In addition, the mixture HPC_1 without fibers was measured as a comparison to mixtures with PP-fibers.

Table B.1 Mixtures with PP-fibers used in the permeability test.

Mixture	Type of PP-fibers	Amount of PP-fibers
HPC_1	Without PP-fibers	-
V2	Type 1: ø = 32 µm, L = 6 mm	1 kg/m^3
V3		2 kg/m^3
V4		3 kg/m^3
V5	Type 2: ø = 18 µm, L = 6 mm	1 kg/m^3
V6		2 kg/m^3
V7		3 kg/m^3
V8	Type 3: ø = 32 µm, L = 20 mm	2 kg/m^3

As observed in the previous section, the measurement by the Torrent method is dependent on the thickness of the specimen, the specimens with a thickness of 40 mm were measurable until 250 °C. To get results of permeability at higher temperatures, the thicknesses of specimens were compared, as shown in Fig. B.1. Based on the permeability test results, the concrete disc thickness was chosen to be 80 mm. The HPC_1 specimens with this thickness provided measurement until 350 °C, higher than that with 40 mm or 60 mm thicknesses, yet the same as the 100 mm thick specimens.

Fig. B.1 Specimens with thicknesses of 60 mm, 80 mm and 100 mm.

Before the experiments, the cylinder disks with the thickness of 80 mm were dried at a temperature of 105 °C for 25 days. The mass loss of the specimens is presented in Fig. B.2. The drying rates of the specimens were similar, mass of specimens decreased with pre-drying closely.

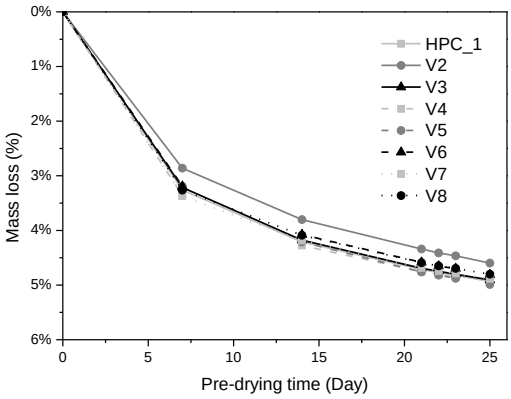

Fig. B.2 Mass loss of the specimens.

In the experiments, the specimens were kept for 60 minutes after the desired temperatures were achieved. To analyze the influences of PP-fibers in terms of type and amount, the results will be presented as permeability. The relative permeability $k_{T,\text{rel}}$ is defined by the following equation:

$$k_{T,\text{rel.}} = \frac{k_T}{k_{T,\text{initial}}} \qquad \text{B.1}$$

Where k_T is the permeability of the specimen at temperature T and $k_{T,\text{initial}}$ is the initial permeability of the specimen at room temperature. The specimens were kept for 1 hour to get uniform heating, and the relative permeability will be presented against the furnace temperature. In addition, the mass loss was measured during the experiments, the relation between the permeability and moisture will be further discussed.

B.1 High performance concrete (HPC)

The relative permeability of HPC_1 at high temperature is shown in Fig. B.3. After long time pre-drying, in the temperature range to 125 °C, the permeability raised smoothly with temperature. From 150 °C, a dent of permeability was observed, the increase with temperature was slowed down, the permeability even decreased in some temperature range. The drop disappeared when the specimen was heated to higher temperature. Together with the mass loss measurement, as shown in Fig. B.4, the drop of permeability is resulted in by the evaporable water due to dehydration from about 150 °C. The low permeability range was accompanied with a faster change of mass of the specimen. The mass change came mainly from the evaporation of the dehydrated water. Before the dehydrated water escaped from the specimen, the induced high pore pressure accelerated the evaporating. It can be assumed that, at high temperature, permeability is not the only factor to influence the drying rate, but also the pore pressure, as the drying rate was higher during the drop of permeability.

It can be seen that the permeability generally increased with temperature, the drop could be related to the change of moisture content. The temperature range of 150 °C to 250 °C is critical for explosive spalling as well, the drop of permeability must be considered to evaluate the risk.

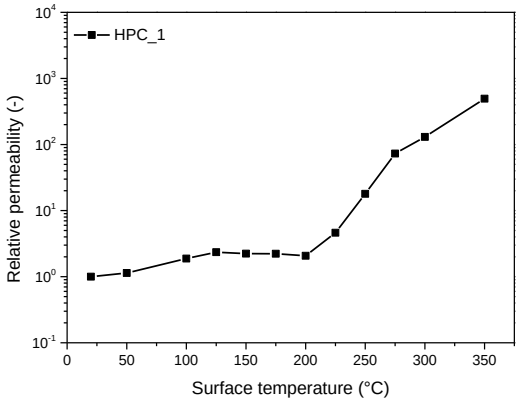

Fig. B.3 Relative permeability of HPC_1 without PP-fiber.

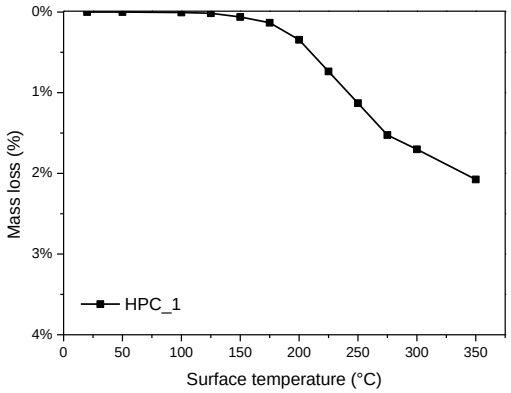

Fig. B.4 Mass loss of HPC_1 without PP-fiber.

B.2 Type 1 PP-fibers

The Type 1 PP-fibers are relatively thick and the diameter is twice that of Type 2. As shown in Fig. B.5, below the melting point of PP-fibers, there was a drop of permeability noticeable at the temperature of 150 °C; from 175 °C, the permeability was increased significantly, corresponding to the melting point of the PP-fibers. As the measurement range of the Torrent permeability tester is limited to 1×10^{-14} m^2, the measurement is not possible when the permeability rises to the limit. With more Type 1 PP-fibers, the permeability reached at lower temperature to the measurement limit of 1×10^{-14} m^2. In the measurement range, the permeability increased more significantly in the specimen with a higher amount of PP-fibers as well. For the specimen with 1 kg/m^3 of PP-fibers, the measurement was possible until 300 °C, the increase of permeability was modest compared to that of the specimens containing higher amount of PP-fibers.

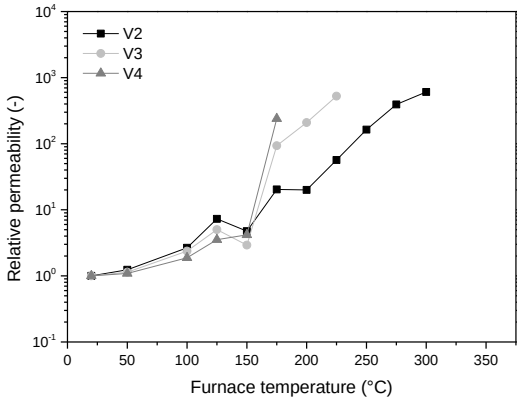

Fig. B.5 Relative permeability of HPC with Type 1 PP-fibers.

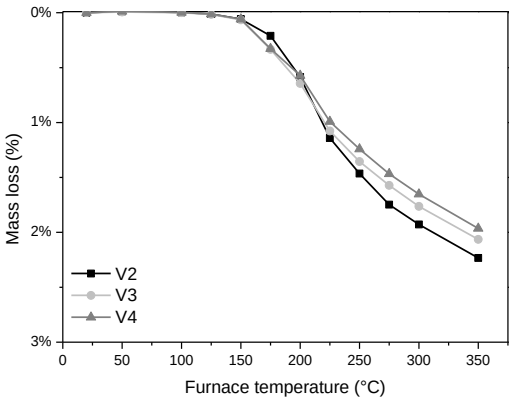

Fig. B.6 Mass loss of HPC with Type 1 PP-fibers.

As for the change of mass, Fig. B.6 presents the mass loss of the three mixtures during heating. With low amount of PP-fibers, V2 lost the least water below 200 °C, yet lost the most in the high temperature range. Owing to the same amount of cement, the dehydrated water should be similar in the three mixtures, the slower mass loss in V2 is attributed to the low permeability; at higher temperature, the higher change rate of mass in V2 is related to the high pore pressure. More moisture in V2 induced another drop in permeability as shown in Fig. B.5 at 200 °C. Accordingly, the higher pore pressure accelerated the drying at higher temperature. So the above-mentioned assumption that the pore pressure influences the drying still holds.

B.3 Type 2 PP-fibers

The permeability of HPC with Type 2 PP-fibers is shown in Fig. B.7. The permeability of all three mixtures increased significantly by this type of PP-fibers and higher amount of PP-fibers resulted in a greater permeability rise above the melting point (about 160-170 °C). There was drop in permeability around 150 °C as well, and the drop was avoided by the PP-fibers. Even in the specimen with 1 kg/m^3 of Type 2 PP-fibers, no drop in permeability was noticed above the melting point of PP-fibers.

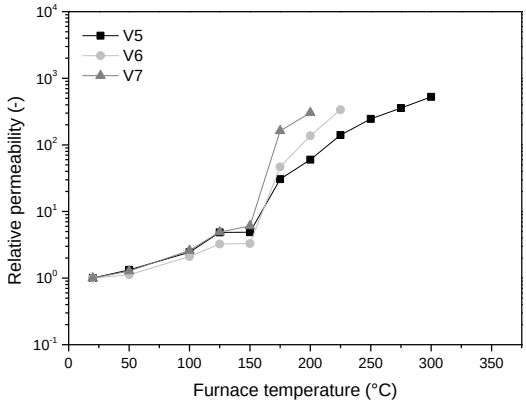

Fig. B.7 Relative permeability with Type 2 PP-fibers.

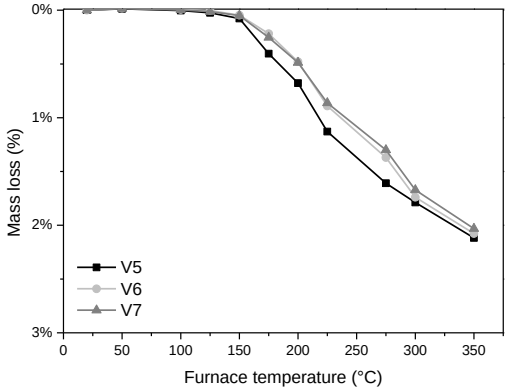

Fig. B.8 Mass loss of HPC with Type 2 PP-fibers.

Different from the case with Type 1 PP-fibers, V5 with 1 kg/m^3 of Type 2 PP-fibers lost mass faster than the other two mixtures. The relative lower permeability of V2 led to higher pore pressure and accordingly faster drying of moisture. Compared to V2, it can be concluded that 1 kg/m^3 of Type 2 increased the permeability enough to avoid the high moisture content due to dehydration, so no drop in permeability or slow drying was observed. In V6 and V7, the mass loss was relatively slower, because of the higher permeability and lower pore pressure, as discussed previously.

B.4 Type 3 PP-fibers

Type 3 PP-fibers have the same diameter as Type 1, the test result in Fig. B.9 shows the effect of the length of the PP-fibers. With the same amount of 2 kg/m^3 Type 1 and Type 2 PP-fibers, the permeability increased similarly. Only at the temperature point of 150 °C, there was a drop in permeability observed in the

specimen of V3. From 150 °C to 170 °C, both permeability of the specimens raised significantly, which corresponds to the melting point of PP-fibers. It can be seen that with 2 kg/m^3 fibers, the effect of the length of PP-fibers is negligible, no noticeable difference was observed.

The mass loss of V3 and V8 is compared in Fig. B.10. The mass of V3 decreased a little faster than V8, which is in accordance with the slightly lower permeability of V3 at high temperature. However, the difference was also very modest, and so the influence of the length of PP-fibers on permeability is limited.

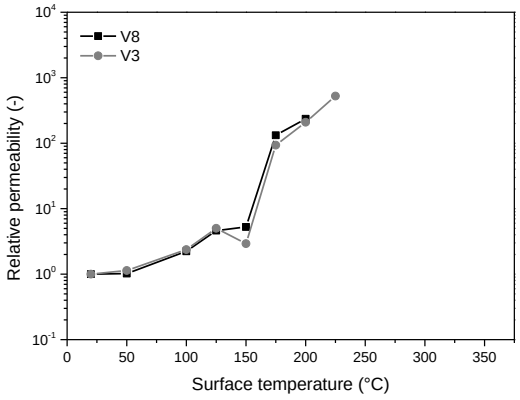

Fig. B.9 Relative permeability of HPC with Type 3 PP-fibers.

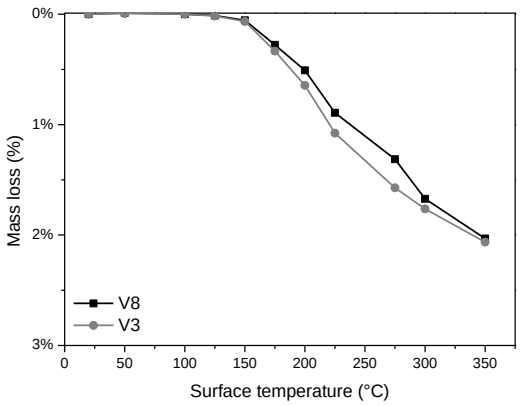

Fig. B.10 Mass loss of HPC with Type 3 PP-fibers.

Appendix C (refer to Chapter 4.6.1)

Effects of external loads on the permeability of concrete

To consider the effects from external loads, the concrete permeability was measured by the Torrent permeability tester, when various load levels applied on the specimens. The test setup for the measurement of permeability under axial compressive stress is shown in Fig. C.1. The test was carried out until the permeability was out of the measurement range of the Torrent permeability tester, then the value of permeability was assumed as 1×10^{-14} m^2.

Fig. C.1 Test setup for the permeability measurements under axial compressive stress.

The permeability of OPC, HPC with and without PP-fibers was investigated. The same mixtures as in Chapter 3 were used, namely OPC_1, HPC_1 and HPC_1_P2. The test specimens were cast into cubes with dimensions of 150 mm × 150 mm × 150 mm. The load level was determined against the compressive strength, which was the averaged value of four measurements of 28 day old concrete specimens. The compressive strength of OPC_1, HPC_1 and HPC_1_P2 were 40.4 MPa, 100.9 MPa and 98.2 MPa.

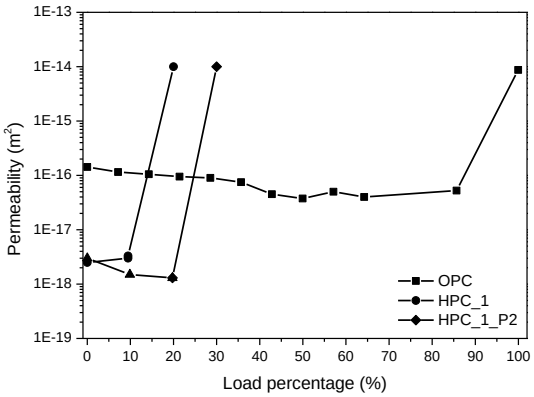

Fig. C.2 Measured permeability of OPC, HPC with and without PP-fibers under axial compressive stress.

The compressive loads on concrete led to a significant change of permeability for all three tested mixtures. As shown in Fig. C.2, the permeability of OPC decreased slightly under the low load levels and a sharp

increase of permeability was observed when a compressive stress around the compressive strength was applied. This increase can be attributed to the destruction of the specimen. As for HPC_1, a jump of permeability occurred under a load level far lower than the compressive strength and the measurement range of the permeability tester was reached. Therefore, the permeability of HPC_1 under about 20 MPa was assumed to be 1×10^{-14} m^2, the same as the measurement range. Similarly, the permeability of HPC_1_P2 was not measurable above the load levels of 30 %. The observed jump of permeability of HPC with and without PP-fibers can be attributed to the micro-cracks developed under compression.

Fig. C.3 Specimen of HPC_1 after measurement.

HPC is more brittle than normal strength concrete and the brittleness of HPC could result in micro-cracks that develop under low load levels (Gettu 1990). Fig. C.3 shows specimen HPC_1 after the measurement, cracks are noticeable after compression of 30 MPa. The bearing capacity of the specimen was not much influenced by such cracks, because the compressive strength would be far higher. However, the permeability of HPC was found to be more sensitive to the applied loads. Therefore, the effect from external loads on permeability can induce the change of pore pressure. This explains the observation in tests that the pore pressure decreased when the compressive stresses were applied (Carré 2013). To predict the explosive spalling under external loads, apart from the superposition of the applied stresses with other acting stresses, the change of permeability should be taken into account by the spalling criterion as well.

Literature

1. DIN 4102-4 Brandverhalten von Baustoffen und Bauteilen; Zusammenstellung und Anwendung klassifizierter Baustoffe, Bauteile und Sonderbauteile, DIN Deutsches Institut für Normung e. V., 1994.
2. DIN EN 1992-1-2 Eurocode 2: Bemessung und Konstruktion von Stahlbeton- und Spannbetontragwerken, DIN Deutsches Institut für Normung e. V., 2004
3. DIN EN 1992-1-2 Eurocode 2: Nationaler Anhang - National festgelegte Parameter - Eurocode 2: Bemessung und Konstruktion von Stahlbeton- und Spannbetontragwerken - Teil 1-2: Allgemeine Regeln - Tragwerksbemessung für den Brandfall, DIN Deutsches Institut für Normung e. V., 2006
4. EN 1991-1-2, Eurocode 1: Actions on structures - Part 1-2: General actions - Actions on structures exposed to fire, DIN German Institute for Standardization, 2012.
5. fib Bulletin No. 46 (2008), Fire design of concrete structures - structural behavior and assessment. State of the art report, fib, Lausanne, Switzerland.
6. ISO 834-1 (2002), Fire-resistance test - elements of building construction. 2002: International Organization for Standardization.
7. Proceq co. (2007), Permeability tester technic guide, Zürich, Switzerland.
8. Promat Ltd. (2014), Technical Data Sheet for Promatect-H plates.
9. Tramex moisture encounter, EMPA (2004): technical measurement report, EMPA, Dübendorf, Switzerland.
10. Abraham O. and Dérobert X. (2003), Non-destructive testing of fired tunnel walls: the Mont-Blanc tunnel case study, NDT&E International 36 (2003) 411–418.
11. Akhtaruzzaman A. A. and Sullivan P. J. E. (1970), Explosive spalling of concrete exposed to high temperature, Concrete Structures Research Report, Imperial College, Great Britain.
12. Ali, F., Nadjai, A., Silcock, G. and Abu-Tair (2004), A., Outcomes of a major research on fire resistance of concrete columns, Fire Safety Journal 39. 433–445.
13. Ali, F. and A. Nadjai (2008), Fire Resistance of Concrete Columns Containing Polypropylene and Steel Fibers. ACI Special Publication 255, 255.
14. Ali F. A., Connolly R. and Sullivan P. J. E. (1996), Spalling of High Strength Concrete at Elevated Temperatures, J. Applied Fire Science, Vol 6(1) 3-14, 1996-7.
15. Bangi M.R. and Horiguchi T. (2010), Pore pressure measurement inside hybrid fiber-reinforced high strength concrete under high temperature condition. Structure in Fire 2010.
16. Barret (1854), On the French and other methods of constructing iron floors, Civil Engineering and Architect's Journal, Vol XVII, pp 94.
17. Bažant Z. P. (2005), Concrete Creep at High Temperature and its Interaction with Fracture: Recent Progress, Concreep-7 Conference: Creep, Shrinkage and Durability of Concrete and Concrete Structures, Nantes, France, pp 449–460.
18. Bažant Z. P. and Kaplan M. F. (1996), Concrete at high temperatures: material properties and mathematical models, Longman Group Limited.
19. Bažant Z. P. and Prat P. C. (1988), Effect of temperature and humidity on fracture energy of concrete, ACI Materials Jour. Vol 84, pp. 262–271.
20. Bažant, Z. P. and Thonguthai, W. (1978), Pore pressure and drying of concrete at high temperature, Proc. ASCE, J. of the Engrg. Mech. Div., 104, 1058–1080.
21. Bažant, Z. P. and Thonguthai, W. (1979), Pore pressure in heated concrete walls—theoretical prediction, Mag. of Concrete Research, 31, 67–76.
22. Biot M. A. (1941), General theory of three - dimensional consolidation, Journal of applied physics 12 (2), 155-164.

23. Bošnjak J., Ožbolz J., Sharma A. and Periškiæ G. (2013), Permeability of concrete at high temperatures and modelling of explosive spalling. 8th International Conference on Fracture Mechanics of Concrete and Concrete Structure, Toledo, Spain, March 10-14.
24. Boström L., Wickström U. and Adl-Zarrabi B. (2007), Effect of specimen size and loading conditions on spalling of concrete, Fire and materials, Fire Mater. 2007; 31:173–186.
25. Carré H., Pimienta P., La Borderie C., Pereira F. and Mindeguia J.-C. (2013), Effect of compressive loading on the risk of spalling, Concrete Spalling due to Fire Exposure – Proceedings of the 3rd International Workshop, Paris.
26. Castillo C. and Durrani A. J. (1990), Effect of transient high temperature on high-strength concrete, ACI Materials Journal, vol. 87, no. 1, pp. 47–53.
27. Chen X. T., Davy C.A., Skoczylas F. and Shao J.F. (2009), Effect of heat-treatment and hydrostatic loading upon the poro-elastic properties of a mortar, Cement and Concrete Research 39, 2009, 195–205.
28. Collet Y. and Tavernier E. (1976), Etude des Propiétés du Béton Soumis a des Témperatures Élevés, Group de Travail, Comportement du Matériau Béton en Fonction de la Température, Brussels, Belgium, November 1976.
29. Connolly R. J. (1995), The spalling of concrete in fires, PhD thesis, Ashton University, Birmingham, United Kingdom.
30. Dougill J. W. (1971), The effect of high temperature on concrete with reference to thermal spalling, PhD thesis, Imperial College, London.
31. Dwaikat M.B. and Kodur V.K., (2009), Hydrothermal Model for Predicting Fire Induced Spalling in Concrete Structural Systems, Fire Safety Journal, 44(3), pp. 425-434.
32. England G. (1971), Migration of moisture and pore pressures in heated concrete. Proceedings of first International Conference on Structural Mechanics in Reactor Technology, 3 (H), B erlin, 22-26.
33. Faure, R. M. and Karray M. (2007), Investigation of the Concrete Lining after the Mont Blanc Tunnel Fire, Structural Engineering International, Volume 17, Number 2, May 2007, pp. 123-132(10).
34. Felicetti R. and Lo Monte F. (2013), Concrete spalling: Interaction between tensile behaviour and pore pressure during heating, Concrete Spalling due to Fire Exposure – Proceedings of the 3rd International Workshop, Paris.
35. Felicetti R., Gambarova P. G., Rosati G. P., Corsi F. and G. Giannuzzi (1996), Residual mechanical properties of high-strength concretes subjected to high-temperature cycles, in Proceedings of the International Symposium of Utilization of High-Strength/High-Performance Concrete, pp. 579–588, Paris, France.
36. Gary, M. (1916), Brandproben an Eisenbetongbasuten, Deutcher Ausschlutss für Eisenbetong, Heft 33, Berlin, Germany, (in German).
37. Gawin D., Majorana C. E. and Schreßer B. A. (1999), Numerical analysis of hygro-thermal behaviour and damage of concrete at high temperature, Mech. Cohes.-Frict. Mater. 4, 37-74.
38. Geertsma, J. (1957), The effect of fluid pressure decline on volumetric changes of porous rocks: Petroleum Transactions, AIME, 210, 331–340.
39. Gettu R., Bažant Z. P. and Karr M. E. (1990), Fracture Properties and Brittleness of High-Strength Concrete, Materials Journal, V.87, Issue 6, pp 608-618.
40. Harmathy, T. Z. (1965), Effect of moisture on the fire endurance of building materials, Moisture in Materials in Relation to Fire Tests, ASTM Special Technical Publication No. 385, pp 74-95, 1965.
41. Harmathy T. Z. (1969), Simultaneous Moisture and Heat Transfer in Porous Systems with Particular Reference to Drying, Ind. Eng. Chern., pp. 92-103.

42. Harmathy T. Z. (1971), Moisture and heat transport with particular reference to concrete, NRCC 12143, National Council of Canada, 1971
43. Harmathy T. Z. and Allen L. W. (1973), Thermal properties of selected masonry unit concrete, Journ. Amer. Concr. Inst, 70(2), pp.132-142, 1973.
44. Hasenjäger (1935), Über das Verhalten des Betons und Eisenbetons im Feuer und die Ausbildung von Dehnungsfugen im Eisenbetonbau, Dissertation, Techniche Hochschole Braunschweig.
45. Heo Y.S., Sanjayan J. G., Han C. G. and Han M. C. (2012), Limited effect of diameter of fibres on spalling protection of concrete in fire, Materials and Structures (2012) 45:325–335.
46. Hertz K. (1992), Danish Investigations on Silica Fume Concretes at Elevated Temperatures, ACI Materials Journal, July-August, 1992.
47. Hertz K. (2003), Limits of Spalling of Fire-Exposed Concrete" Fire Safety Journal 38 (2003), pp.103-116.
48. Hildenbrand G. and Peehs M. (1978), Untersuchung der Wechselwirkung von Kernschmelze und Reaktorbeton, Kraftwerk Union Erlangen / Reaktortechnik.
49. Incropera F. P. and DeWitt D. P. (2002), Fundamentals of heat and mass transfer, John Wiley & Sons Australia, Limited, 2002.
50. Ingberg et al. (1925), Fire tests of building columns, Technologic paper No. 184, U. S. Bureau of Standards, USA.
51. Jacobs F. P. (1994), Permeabilität und Porengefüge zemntgebundener Werkstoffe, PhD thesis, ETH Zürich, Zürich, Switzerland.
52. Jasson R. (2013), Fire spalling of concrete – Theoretical and experimental studies, PhD thesis, KTH, Sweden.
53. Jansson R. and Boström L. (2012), Determination of fire spalling of concrete – relevance of different test methods, Proceedings from the 7th International Conference on Structures in Fire, M. Fontana, A. Frangi, M. Knobloch (Eds.), Zurich, Switzerland, June 6-8, 2012.
54. Kalifa P., Chene G and Galle C. (2001), High-temperature behaviour of HPC with polypropylene fibres - From spalling to microstructure, Cement and Concrete Research, no 31 (2001) 1487–1499.
55. Kalifa P., Menneteau F.D. and Quenard D. (2000), Spalling and pore pressure in HPC at high temperatures, Cement and Concrete Research, 2000. 30(12): p. 1915-1927.
56. Khaliq W. and Kodur V. K. (2011), Effect of High Temperature on Tensile Strength of Different Types of High-Strength Concrete, Aci Materials Journal, 2011. 108(4): p. 394-402.
57. Khoury G. (2000), Effect of fire on concrete and concrete structures, Progress in Structural Engineering and Materials Volume 2, Issue 4, pp 429–447.
58. Khoury G. (2005), Spalling Review- Types, Assessment and Prevention, UPTUN report WP 4, Project GRD1-2001-40739, 5th Framework Programme of the European Union Competitive and Sustainable Growth.
59. Khoury G. (2008), Polypropylene fibres in heated concrete. Part 2: Pressure relief mechanisms and modelling criteria, Magazine of Concrete Research,Vol 60, No. 3, April, pp.189–204.
60. Klimentos T., Harouaka A., Mtawaa B. and Saner S. (1998), Experimental Determination of the Biot Elastic Constant: Applications in Formation Evaluation, SPE Reservoir Evaluation & Engineering, 01, SPE-30593-PA.
61. Klingsch E., Frangi A. and Fontana M. (2011), Fire Protection of Concrete Structures, in Proceedings of the third international workshop on performance, protection and strengthening of structures under extreme loading, PROTECT 2011, Lugano, Switzerland.

62. Klingsch E. (2014), Explosive spalling of concrete in fire, PhD thesis, ETH Zürich, Zürich, Switzerland.
63. Klingsch E., Frangi A. and Fontana M. (2011), High- and Ultrahigh-Performance Concrete: A systematic experimental analysis on spalling ACI Materials Journal, 2011(SP 279).
64. Klingsch E., Frangi A. and Fontana M. (2013), Explosive spalling of concrete in fire, Test report. IBK Tests report No. 352. 2013: Institute of Structural Engineering (IBK), ETH Zurich, Switzerland.
65. Klingsch E., Lu F., Käßmann R. and Tan K. H. (2015), Tests on the hot and residual permeability of concrete at high temperatures, 4th International RILEM Workshop on Concrete spalling due to fire exposure (IWCS), Leipzig, Germany.
66. Kodur V. K. (1998), Performance of high strength concrete-filled steel columns exposed to fire. Canadian Journal of Civil Engineering, 1998. 25(6): p. 975-981.
67. Kodur V. K. and Phan L. (2007), Critical factors governing the fire performance of high strength concrete systems. Fire Safety Journal, 2007. 42(6-7): p. 482-488.
68. Kodur V. K. (2014), Properties of Concrete at Elevated Temperatures, ISRN Civil Engineering, vol. 2014, Article ID 468510.
69. Kodur V. K. (2010), Spalling in High Strength Concrete Exposed to Fire - Concerns, Causes, Critical Parameters and Cures. ASCE.
70. Kodur V. K, Khaliq W. and Raut N. (2013), An approach to account for tie configuration in predicting fire resistance of reinforced concrete columns. Engineering Structures, 2013. 56(0): p. 1976-1985.
71. Kodur V. K and McGrath R. (2006), Effect of silica fume and lateral confinement on fire endurance of high strength concrete columns. Canadian Journal of Civil Engineering, 2006. 33(1): p. 93-102.
72. Lennon T. (2004), Fire safety of concrete structures: Background to BS 8110 fire design, BRE Report 468.
73. Li M., Qian C. and Sun W. (2004), Mechanical properties of high-strength concrete after fire, Cement and Concrete research 34 (2004), p. 1001-1005.
74. Lu F. and Fontana M. (2015), A thermo-hydro model for predicting spalling and evaluating the protective methods, 4th International RILEM Workshop on Concrete spalling due to fire exposure (IWCS), Leipzig, Germany.
75. Lu F. and Fontana M. (2015), Promatect-H plate against explosive spalling of HPC in fire - Test report, IBK Tests report No.Fo-2015-001, Institute of Structural Engineering (IBK), ETH Zurich, Zürich, Switzerland.
76. Lu F., Klingsch E., Fontana M. and Fernando D. (2014), Improved Permeability Model For Concrete At High Temperature, 8th International Conference on Structures in Fire Shanghai, China, June 11-13.
77. Lu F., Klingsch E. and Fontana M. (2015), Protection methods against the explosive spalling of concrete, PROTECT 2015—Fifth International Workshop on Performance, Protection & Strengthening of Structures under Extreme Loading, East Lansing, MI, USA, June 28-30.
78. Malhotra H. L. (1974), Determination of flame spread and fire resistance, Building Research Establishment, CP 72/74, July 1974, United Kingdom.
79. Malhotra H. L. (1984), Spalling of concrete in fires, Technical note 118, CIRA, London, UK.
80. Meyer-Ottens C. (1972), Zur Frage der Abplatzungen an Betonbauteilen aus Normalbeton bei Brandbeanspruchung, PhD thesis, Braunshweig, Germany.
81. Mindeguia J. C., Pimienta P., Noumowe A.and Kanema M. (2010), Temperature, pore pressure and mass variation of concrete subjected to high temperature – Experimental and numerical discussion on spalling risk, Cement and Concrete Research 40, 2010, 477-487.

82. Noumowe A., Clastres P., Debicki G. and Costaz J. (1996). Transient heating effect on high strength concrete. Nuclear engineering and design, 166(1), pp.99–108.
83. Sahota M.S. and Pagni P.J. (1979), Heat and Mass Transfer in Porous Media Subject to Fires, Int. Journal of Heat Mass Transfer, Vol. 22, pp 1069-1081.
84. Saito, H. (1965), Explosive spalling of prestressed concrete in fire, Occasonal report No. 22. Building Research Institute, Japan.
85. Schneider U. (1988), Concrete at High-Temperatures - A General-Review. Fire Safety Journal, 1988. 13(1): p. 55-68.
86. Schneider U. (1982), Verhalten von Beton bei hohen Temperaturen Deutscher Ausschuss für Stahlbeton, ed., Ernst & Sohn.
87. Schneider U. and Herbst H.-J. (1989), Permeabilität und Porosität von Beton bei hohen Temperaturen. Deutscher Ausschuss für Stahlbeton, 1989. Heft 403.
88. Sertmehemetoglu Y. (1977), On a mechanism of spalling of concrete under fire conditions, PhD thesis, University of London, King's Collage, United Kingdom.
89. Shorter G. W. and Harmathy T. Z. (1961) Discussion on the article "The fire resistance of concrete beams" by Ashton and Bate, Proceedings, Institute of Civil Engineers, Vol. 20, p. 313.
90. Shuttleworth (1997), Fire performance of concrete for tunnel linings, Channel Tunnel Rail Link Technical Report, Arup as cited in the report Arup Group Ltd, Fire resistance of concrete enclosures, Work Package 2: Spalling categories, report for the Nuclear Safety Directorate of the Health and Safety Executive, October 2005.
91. Skempton A. W. (1960). Effective stress in soils, concrete and rocks. In. Pore Pressure and Suction in Soils 4-16, London: Butterworths.
92. Sönnerberg S. (1952), The fight against fire (in Swedish), A book published by Berneces Förlag AB, Malmö, Sweden.
93. Sundius N. (1931), Investigation of fire exposed concrete by microscopy, Betong, No 2, 1931, (in Swedish).
94. Tait & Höj (1996), Storebaelt Eastern Railway Tunnel: Dania Tunnel Boring Machine Fire-Analysis and Recovery, Proceedings of the Institution of Civil Engineers, Supplement to Civil Engineering, Vol 114, Special issue 1.
95. Terzaghi C. (1925), Principles of Soil Mechanics. Engineering News-Record, 95(19-27).
96. Thelandersson S. (1974), Mechanical Behavior of Concrete Under Torsional Loading at Transient, High-Temperature Conditions, Bulletin 46, University of Lund, Lund, Sweden.
97. Torrent R., Frenzer G., Holderbank Management and Beratung Materialtechnische Abteilung, Methoden zur Messung und Beurteilung der Kennwerte des Ueberdeckungsbetons auf der Baustelle, 1995, Bundesamt für Strassenbau. 106 S.
98. Trafikministeriet (1995), Sikerhet ved Transport gennom Storebealtstunnelen, Official report from Trafikministeriet, Denmark, (in Danish).
99. Ulm F. J., Constantinides G. and Heukamp F. H. (2004), Is concrete a poromechanics materials? - A multiscale investigation of poroelastic properties, Materials and structures 37 (1), 43-58.
100. West bridge approach of Wu Bridge (2015) – Fire disaster report, Jiangsu Transportation Research Institute Company Limited, Jiangsu, China.
101. Woolson I. (1918), Fire in a reinforced concrete warehouse at Far Rockaway, New York, U.S.A, RED BOOKS of the British Fire Prevention Committee, No. 21.
102. Yermak N., Pliya P., Beaucour A. L., Noumowe A. and Simon A. (2015), Influence of polypropylene and steel fibers in concrete subjected to high temperature, Protect 2015, East lansing, MI, USA.

103. Zhang B. and Bicanic N. (2001), Fracture energy of high performance concrete at temperatures up to 450°C, Fracture Mechanics of Concrete Structures, de Borst et al, 2001 Swets & Zeitlinger.
104. Zhang B. and Bicanic N. (2002), Residual fracture toughness of normal-and high-strength gravel concrete after heating to 600°C, Materials Journal 99 (3), 217-226.
105. Zheng W.Z., Hou X.M., Shi D.S. and Xu, M.X.(2010), Experimental study on concrete spalling in pre-stressed slabs subjected to fire, Fire Safety Journal 45(2010)283–297.
106. Zhukov V. (1994), Forecast of a brittle failure of concrete by fire. Scientific Research Institute for Concrete and Reinforced Concrete, Moscow.
107. Zhukov V. (1976), Reasons of Explosive Spalling of Concrete by Fire, Beton Zhelezobeton (Concrete and Reinforcement Concrete), No. 3, 1976.

Curriculum vitae

Fangxia Lu

Date of birth:	22th June 1984
Place of birth:	Jinzhou, Liaoning, P. R. China
Nationality:	P.R. China

Since 2011	research assistant and PhD student
	ETH-Zurich – Institute of Structural Engineering (IBK), Zurich, Switzerland
	in the group of Prof. Dr. M. Fontana
2008 – 2011	Postgraduate, Master's degree
	Tongji University - Institute of Civil Engineering, Shanghai, P. R. China
2003 – 2008	Undergraduate, Bachelor's degree
	Tongji University - Institute of Civil Engineering, Shanghai, P. R. China
2000 - 2003	Secondary school, High school diploma
	Jinzhou No. 1 Tielu high school, Jinzhou, Liaoning, P. R. China